DEVELOPMENT OF A COOPERATIVE RANGE-BASED UNDERWATER NAVIGATION SYSTEM

SANTIAGO RÚA PÉREZ

UNIVERSIDAD PONTIFICIA BOLIVARIANA
ESCUELA DE INGENIERÍAS
DOCTORADO EN INGENIERÍA
MEDELLÍN
2020

DEVELOPMENT OF A COOPERATIVE RANGE-BASED UNDERWATER NAVIGATION SYSTEM

SANTIAGO RÚA PÉREZ

Dissertation presented to the School of Engineering in partial fulfillment of the requirements for the degree of PhD in Engineering (Doctor en Ingeniería)

Advisor
Rafael Esteban Vásquez Moncayo, Ph.D.
Antonio Manuel dos Santos Pascoal, Ph.D.

UNIVERSIDAD PONTIFICIA BOLIVARIANA
ESCUELA DE INGENIERÍAS
DOCTORADO EN INGENIERÍA
MEDELLÍN
2020

Nota de aceptación

_____

_____

_____

_____

Firma
Nombre:
Presidente del jurado

_____

Firma
Nombre:
Jurado

_____

Firma
Nombre:
Jurado

Medellín, May 26, 2020

DECLARACIÓN DE ORIGINALIDAD

"Declaro que esta tesis (o trabajo de grado) no ha sido presentada para optar a un título, ya sea en igual forma o con variaciones, en ésta o cualquier otra universidad". Art. 82 Régimen Discente de Formación Avanzada, Universidad Pontificia Bolivariana.

Firma Autor:

Santiago Ruía P.

This thesis is dedicated to my beloved MGC.

ACKNOWLEDGMENTS

First of all, I would like to thank the two people who introduced me to the world of underwater robotics, my advisor Rafael Vásquez, and professor Carlos Alejandro Zuluaga. This trip started when they hired me 6 years ago as a professional associated with the underwater robotics program, allowing me to complete my master's thesis and then to continue with my PhD. If I hadn't accepted this offer so many years ago, I probably wouldn't be delivering my thesis on these topics today.

I would like to say thanks to my advisor Rafael Vásquez for guiding me both in the development of my master's degree and in generating the motivation to continue with the development and completion of my PhD. Additionally, I want to thank all the professors and students associated with the underwater robotics program because from each one I have learned something important for my professional development.

During the development of my PhD, I participated in an international internship at the Instituto Superior Técnico de Lisboa, specifically I was at the Laboratory of Robotics and Engineering Systems LARSyS. I want to thank my advisor Antonio for receiving me and introducing me to the topic on which my thesis is based. Thank you very much for everything, I have learned so much in the short time I was there. Additionally, I met great people like Nandeesh, Hung Tuan, Francisco Rego, Vahid Hassani, and my great friend Naveen. Thank you very much Naveen for having the patience to teach me and explain so much about observability; I really learned a lot during my stay.

I also want to thank my family for the unconditional support I had during the development of my doctoral studies.

Finally, but not least, the love of my life Manuela Gamboa. She motivated me to start this path and supported me during all phases of it. During the most stressful moments, you were always there, encouraging me to finish and move it forward. I think it would not have been possible without you.

This thesis has been developed with the financing of Colciencias through the call for national doctorates 647 of 2015. Additionally, some parts of the research related to this work were funded by the Fondo Nacional de Financiamiento para la Ciencia, la Tecnología y la Innovación, Francisco José de Caldas; Ecopetrol; the Universidad Pontificia Bolivariana; and the Universidad Nacional de Colombia; project 1210-531-30550.

CONTENTS

Pág.

LIST OF FIGURES

LIST OF TABLES

Pág.

NOMENCLATURE

${}^{\mathcal{B}}\mathbf{v}(t)$	Linear velocity of the vehicle w.r.t $\{\mathcal{I}\}$, and expressed in $\{\mathcal{B}\}$
$\boldsymbol{\eta}$	Orientation of the vehicle
χ	Angular position of the manipulator
${}^{\mathcal{I}}\mathbf{b}(t)$	Position of the beacon
${}^{\mathcal{I}}\mathbf{d}(t)$	Range vector from the beacon to vehicle
${}^{\mathcal{I}}\mathbf{p}(t)$	Position of the vehicle w.r.t inertial frame
${}^{\mathcal{I}}\mathbf{v}_c(t)$	Ocean current w.r.t $\{\mathcal{I}\}$
$\ker(\cdot)$	Kernel of a matrix or null-space
$\mathbb{E}\{\cdot\}$	Expected value
$\mathcal{I}(\mathbf{x}_0)$	Set of all indistinguishable initial conditions from $\mathbf{x}_0$)
$\mathcal{O}$	Observability Matrix
$\mathcal{SO}(n)$	Orthogonal group in dimension n
$\mathcal{S}^n$	n-sphere space
ω_m	Angular velocity of the manipulator
$\perp$	Perpendicular
$\mathbf{w}(\cdot), \mathbf{w}^{\perp}(\cdot)$	Orthonormal vectors
$d(t)$	Range measurement
l_m	Manipulator's length
$S(\cdot)$	Skew-symmetric matrix
$\mathbf{e}_i \in \mathbb{R}^n$	The i^{th} columnn of the $n \times n$ identity matrix
$\boldsymbol{\omega}_v(t)$	Angular velocity of the vehicle
${}^{\mathcal{I}}_{\mathcal{B}}\mathcal{R}(t)$	Rotation matrix from $\{\mathcal{B}\}$ to $\{\mathcal{I}\}$
$\{\mathcal{B}\}$	Body-fixed frame
$\{\mathcal{I}\}$	Inertial frame
AHRS	Attitude and Heading References Systems
ASV	Autonomous Surface Vehicle
AUV	Autonomous Underwater Vehicle
CI	Confidence Interval
CTD	Conductivity, Temperature, and Depth sensor

DR	Dead-reckoning
DVL	Doppler Velocity Log
EKF	Extended Kalman Filter
FIM	Fisher Information Matrix
GINS	Gimbaled Inertial Navigation System
GNC	Guidance, Navigation and Control
GPS	Global Positioning System
INS	Inertial Navigation System
ISE	Integral of the Square Error
LBL	Long Base-Line
LEL	Least Entropy-Like
LKF	Linearized Kalman Filter
LQE	Linear Quadratic Estimator
LTI	Linear Time Invariant System
LTV	Linear Time Varying System
MAE	Mean Absolute Error
ROV	Remotely Operated Vehicle
SBL	Short Base-Line
SINS	Strapdown Inertial Navigation System
SLAM	Simultaneous Localization and Mapping
UAV	Unmanned Aerial Vehicle
USBL	Ultra Short Base-Line
VCBN	Vehicle moving in Circles, and the Beacon does Not move
VCBR	Vehicle moving in Circles, and the Beacon Rotating
VLBN	Vehicle moving in straight Lines, and the Beacon does Not move
VLBR	Vehicle moving in straight Lines, and the Beacon Rotating
VNBN	Neither Vehicle nor the beacon Move
VNBR	Vehicle does Not move, and the Beacon Rotating
XKF	eXogenous Kalman Filter

ABSTRACT

The motivation for improving underwater navigation systems arises from the need to increase the quality of the estimation of position, velocity and orientation of the vehicle. The development of an underwater navigation system is not trivial since traditional methods used for aerial, ground or water surface vehicles, that rely on satellite systems, cannot be used underwater. Therefore, a lot of effort has been made during the last decades to develop new methodologies to locate an underwater vehicle by using acoustic positioning systems. Within these acoustic systems, underwater navigation based on single-range measurements has appeared as a less expensive solution, which is simple to calibrate, deploy and recover. However, the implementation of such navigation systems require caution when a filter to estimate the position is developed, since it suffers from observability issues under certain scenarios.

This work addresses the development of a new methodology for the navigation system of an underwater vehicle based on single beacon measurements. By moving a cooperative mobile beacon attached under the surface vessel or platform, the system will be able to estimate the position of the vehicle. In order to achieve this, a model that describes the relative motion between the vehicle and the beacon is defined first, and then, observability conditions for the system are established. We define three types of maneuvers for the vehicle: moving in circles, straight lines, and without any motion. We found that, knowing beacon's initial position, it was possible to ensure observability for the vehicle's maneuvers. Additionally, in the worst case scenario, where neither the beacon or vehicle's initial positions are known, we found that the system is not observable just in the case when the vehicle remains in the same position.

Once these conditions are known, two state observers are implemented: an Extended Kalman Filter and the Exogenous Kalman Filter. We evaluated both observers by running Monte Carlo simulations. We used two metrics to evaluate the performance: the Mean Absolute Error and the Integral of the Square of the Error. Both observers presented good performance, but we prove global convergence for the XKF.

Finally, knowing which trajectories are better to increase the accuracy of the position estimation, a trajectory planner is implemented. We used the Fisher Information Matrix to define an index to be optimized in order to increase the accuracy in the state estimation. All the observability analyses and the estimation of the position are developed from a theoretical point of view and validated through simulations in Matlab.

KEYWORDS:

Marine system navigation, guidance and control; underwater navigation; single-range navigation; cooperative mobile beacon; observability.

1. INTRODUCTION

Offshore exploration requires highly reliable and precise systems in order to guarantee safety of people and ecosystems; such exploration systems allow one to obtain information from areas of interest [1–4]. Consequently, several researchers have focused their interests on the construction of underwater vehicles that allow the exploration of the ocean from a surface station. The most used underwater systems to perform such tasks include Autonomous Underwater Vehicles (AUVs) and Remotely Operated Vehicles (ROVs). These vehicles comprise mechanical and electronic components, and instruments such as multibeam echosounders, side scan sonars, cameras, sampling systems, among others [5–7].

Regardless if they are operated by cable (ROVs) or autonomous (AUVs), it is necessary to develop control strategies to achieve the desired movements [8,9], and navigation algorithms to localize the vehicle under the surface. Figure 1 shows a three-level hierarchical Guidance, Navigation, and Control (GNC) structure for an underwater vehicle [10, 11].

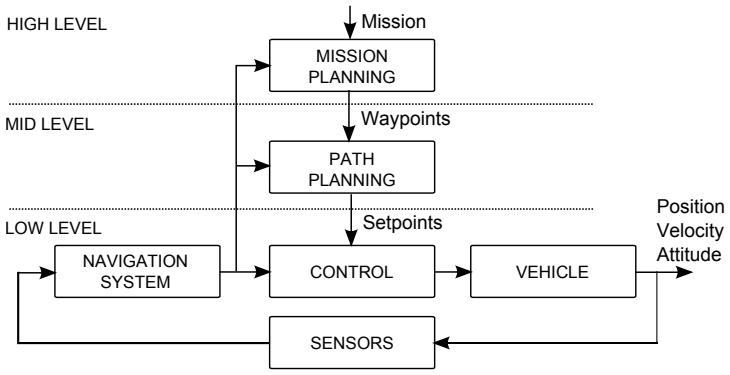

Figure 1: Navigation, guidance and control structure. In a typical GNC structure for an ROV the control and navigation systems are implemented in the vehicle, while the mission and path planning in the support vessel. Taken from [11].

.

The GNC system for an underwater vehicle can be developed with different degrees of

sophistication, depending on the type of operation that is to be performed, and the autonomy levels that need to be achieved [8, 12–14]. One of the main elements included in the GNC is the navigation system. It allows estimating the position, velocity, and attitude of the vehicle with respect to a system located on the surface control station, from measurements made with different sensors: Attitude and Heading Reference System (AHRS); Conductivity, Temperature, and Depth (CTD) sensor; pressure meter; acoustic positioning system; Global Positioning System (GPS); altimeter; and sonar; among others. Given the characteristics of water, the development of underwater localization systems is not trivial and presents a number of challenges [15–17]. Traditional methods that rely on GPS cannot be used underwater, due to the attenuation of the electromagnetic signals. Therefore, for certain operating depths, knowing the vehicle's position is not a simple issue, and this should be taken into account from the design stage in order to achieve a synchronized operation between the surface station (usually located on a vessel) and the underwater vehicle [18, 19]. To solve the navigation problem, technologies that rely acoustic signals are used since they can be propagated through water. Hence, arrays of sensors are used to determine the range and bearing to the vehicle.

This work is being developed within the Strategic Program for the Development of Robotic Technology for Offshore Exploration of the Colombian Seabed, project 1210-531-30550, contract 0265 - 2013, which is funded by the Fondo Nacional de Financiamiento para la Ciencia, la Tecnología y la Innovación, Francisco José de Caldas; the Colombian Petroleum company, ECOPETROL; the Universidad Pontificia Bolivariana - Sede Medellín, UPB; and the Universidad Nacional de Colombia - Sede Medellín, UNALMED.

1.1. LITERATURE REVIEW

The motivation for developing an underwater navigation system arises from the need to estimate the position, velocity, and orientation of the vehicle all the time. A wide range of navigation methods and sensor suites have been developed to solve the problem:

- **Inertial Navigation System (INS)**: these methods are based on accelerometers and gyroscopes mounted on the vehicle to estimate the position, velocity, and orientation via dead-reckoning. Knowing its current position, speed and course, the algorithm is able to calculate the new position at a given time [20, 21].

  There are two main design methods for an INS: Gimbaled type (GINS), where the inertial sensors are mounted on a stable platform which is isolated from the movement of the vehicle; and Strapdown (SINS), where the sensors are mounted rigidly to the structure of the vehicle. Because of their smaller size, lighter weight and easy manufacture, SINS are more suitable for underwater robotic applications [22, 23]. Some disadvantages of a SINS are: the initial alignment of the sensors can be difficult; estimation drift due to noise integration and bias; and expensive for more precise sensors [24–27].
- **Geophysical Map-based Navigation (GMN)**: the objective is to use bathymetric, geomagnetic, and gravitational information to estimate position, velocity, and orientation of the vehicle. As stated by Leonard and Bahr [28], these approaches are based on matching sensor data with an a priori environment map, under the assumption that there is sufficient spatial variation in the parameter(s) being measured to permit accurate localization. One of the main advantages of these techniques is to avoid the deployment of other sensors such as beacons to navigate within a different environment. Nevertheless, the method requires an a priori knowledge of the map, which can be expensive to be generated [29]. To get more information, see for instance Melo and Matos [30] and the references therein for a complete survey on advances on terrain based navigation for underwater vehicles.
- **Acoustic based navigation**: these systems comprise a transceiver/transponder set, and the measurements depend on the time of flight of acoustic signals within the water. The transceiver sends a signal that is received by the transponder, who answers sending back a response signal; the relative position between the transceiver and the transponder is computed by considering the speed of sound in the water. Within the acoustic positioning systems, single range-based navigation has appeared as an alternative solution for the location of underwater vehicles since it can reduce the infrastructure [15]. This navigation method only uses the range between the vehicle and the beacon; therefore, the state estimation of the vehicle involves many challenges [31, 32]. This type of navigation for underwater vehicles has been considered in recent years as a less expensive solution, simple to calibrate, to deploy and recover.

One of the first ideas using single beacon localization for underwater vehicles, appeared in 1995 with the work of Scherbatyuk [33]. He proposed a navigation system, based on an LBL system, with a single transponder, and onboard sensors to estimate the position of the vehicle and the current velocity. The proposed algorithm assumed that the vehicle moves in a straight-line path, therefore, some ambiguities were presented in the estimation of the initial position. By that time, the work of Scherbatyuk [33] showed the potential of using single transponder navigation with some observability drawbacks that should be solved.

Four years later, Song [34] gave necessary and sufficient conditions for local observability for 2D target tracking with single-range measurements. Using the Fisher Information Matrix (FIM), he established that if the target relative motion is moving with constant velocity or acceleration, the system was not observable. After those works, the research around single-range navigation grew up exponentially in the last two decades [31,35–50]. For instance, Larsen [31] proposed a navigation system based on dead-reckoning (DR), acoustic range, and range rate measurement to a single source. His concept, called Synthetic LBL, used temporal diversity of range measurement from a single stationary source and an accurate DR navigation system to estimate the position of the vehicle. In [37], Gadre and Stiwell presented a local observability analysis of the single range navigation system around some vehicle trajectories and in [38], they presented the same analysis in the presence of unknown currents. Hartsfield [39] tested the concept of Larsen [31] during sea trials with the REMUS 6000, an AUV capable of diving up to 6000 m.

Some researchers have been focused on developing algorithms to solve problems related to single beacon localization. To solve the problem of localization (indistinguishability of states), Dandach et al. [45,51] presented a continuous-time adaptive-source localization algorithm, which used a mobile agent to estimate the location of a stationary source. Saúde and Aguiar [52] proposed a solution to estimate the underwater vehicle position in the presence of unknown ocean currents based on the combination of DR with multiple range measurements taken at different instants of time. Huang et al. [46,50] presented a bank of maximum a posteriori estimators for single beacon localization. Clark et al. [53] proposed a Gaussian mixture filter which generated Gaussian mixture approximations to the conditional densities. Mandić et al. [54] presented a mobile beacon control algorithm that ensures observability in single-range measurement.

Observability analysis

As it was mentioned before, the observability analysis for single-beacon navigation is not a simple task. The theoretical foundation on observability for nonlinear system is based on the milestone paper from Hermann and Krener [55], where the fundamental notions about indistinguishability, local weak observability, and rank test were described.

Regarding the observability analysis for the single-beacon localization problem, Antonelli et al. [56] focused on the observability analysis of the relative localization of two AUV. Assuming that the vehicles were equipped with depth sensors, linear/angular velocity sensors, and communication devices with range measurements, they found conditions that ensure observability of the linearized model and locally observability conditions for the nonlinear system. Nevertheless, the scope of this work does not go into a deeper analysis in which trajectories should execute one vehicle to ensure the observability of the other. By using state augmentation and transforming the nonlinear system into a linear time-varying system, Batista et al. [57] found necessary and sufficient conditions on the observability of the nonlinear system. Inspired by this work, Bayat and Aguiar [58] addressed the single and multiple observability analysis of the Simultaneous Localization and Mapping (SLAM) for AUV navigation using range measurements to stationary beacons. Crasta et al. [59] investigated the observability for two classes of maneuvers in 2D and in [60,61], they extended the approach for 3D and trimming trajectories. All observability analyses carried out on the previous works assume that the beacon is fixed, therefore the vehicle should execute excited maneuvers to ensure observability on the system.

Practical considerations

The performance of the navigation system for an underwater vehicle can be degraded by communication losses, multipath effects, noise, and bandwidth limitation. Therefore, some researchers have developed special interests in robust methods, which guarantee performance over several scenarios. Olson et al. [62] proposed an outlier rejection algorithm to improve the performance of an EKF; the method was based on the representation of range data as graph and applied graph partitioning algorithms. Indiveri et al. [63] proposed an outlier rejection algorithm for single-beacon navigation based on the least entropy-like (LEL) [64]. Lekkas et al. [65] proposed a simple χ^2 statistics test in order to evaluate every new measurement and discard those which gave large residuals com-

pared to the predicted value of an EKF. More recently, Emami and Taban [66] proposed an H-infinity algorithm for underwater navigation, which decreased the effects of the outliers data.

Optimal and cooperative navigation perspectives

Knowing that the trajectories of the vehicle affect the observability of the system, two lines of work started being developed: first, cooperative localization between AUVs [67]; and second, the design of optimal trajectories, which maximize the information provided by sensors [68].

Regarding cooperative localization, Rui and Chitre [69] presented a cooperative positioning system between two AUVs. The idea was to use one vehicle to localize, while the other one was executing a lawnmower path over the survey area. Fallon [70] developed an algorithm for cooperative AUV navigation with an autonomous surface craft. By developing a path planning algorithm for the surface vehicle, the AUV was able to localize with respect to the surface vehicle. Webster et al. [71] reported a decentralized extended information filter for single-beacon cooperative navigation between vehicles. Using ranges and state information from a single reference, the other vehicles were able to improve their localization. Parlangeli and Indiveri [72, 73] described the single range observability issues related to cooperative underactuated underwater vehicles. They described all possible unobservable motions for the vehicles given the initial conditions and the velocity commands. Tan et al. [49] explored the use of a single-beacon vehicle for range only localization to support other AUVs. They developed a cooperative path-planning algorithm for the beacon based on dynamic programming and Markov decision formulation. Mandić et al. [54] developed a mobile beacon control algorithm that ensure observability for single-range navigation. Using a cost function based on the rank condition, the goal of the algorithm was to reduce this cost as much as possible.

Despite of the previous work, the trajectories that the vehicle or the beacon should execute only guarantee the observability of the system, but not how good is the information provided by the range measurements [68]. To tackle this problem, Moreno-Salinas et al. [74] found an optimal geometric configuration of a sensor network which maximized the range information available for the vehicles. Pedro et al. [75] developed a single-beacon localization algorithm based on the maximization of the information for localization, at the same time reducing energy consumption. Moreno-Salinas et al. [76]

developed an integrated motion planning, control, and estimation algorithm for range-based positioning, and Crasta et al. [77] extended the techniques proposed in [76] to deal with the presence of unknown disturbances represented by ocean currents.

1.2. PROBLEM STATEMENT

In spite of the progress made in range-based navigation, cooperative navigation for underwater vehicles remains as a promising field for the underwater robotic community. For instance, the Innovative Training Network on Autonomous Unmanned Aerial Systems for Marine and Coastal Monitoring (MarineUAS, http://marineuas.eu) is a doctoral program to strengthen research on Autonomous Unmanned Aerial Systems for Marine and Coastal Monitoring [78, 79]. One of the main focus of the program is to develop strategies of cooperative navigation between autonomous unmanned aerial vehicles (UAVs), autonomous surface vehicles (ASVs), and autonomous underwater vehicles (AUVs).

Most of the above solutions rely on the deployment of another vehicle (which can be expensive) or to execute (persistent) exciting manoeuvres (which can imply a deviation from the real mission) to ensure observability. Therefore, this dissertation is aimed at developing a new methodology for the navigation system of an underwater vehicle, based on the range measurement from the vehicle to a simple cooperative mobile beacon (cooperative in the sense that it is going to help in the observability of the system and simple in the sense that the use of another vehicle is not required) attached to a static support vessel or a fixed platform, which allows the vehicle to execute its mission without the need to perform manoeuvres to ensure observability. The main research questions which are addressed are:

- Will it be possible to develop a motion strategy for a cooperative mobile beacon, attached to a static surface vehicle or platform, which guarantees the observability of any given vehicle's trajectory?
- Based on the trajectories that should execute the beacon, in order to guarantee observability, will it be possible to propose a mechanism for the movement of the beacon?

- Will it be possible to quantify how good is the observed measurement for any given trajectory of the vehicle and the beacon?

1.3. CONTRIBUTION

The key novel contributions that emerge from this doctoral thesis are:

Chapter 2:

- Unlike the methods we found in the literature, we propose a simple mechanism attached to a surface vessel or platform, which can help to localize the vehicle underwater by using single-range measurement.
- We derive observability conditions for the combination of movement of the vehicle and the beacon. This conditions allow one to design control strategies for the beacon to guarantee observability of the whole system.
- We study the observability conditions in two scenarios: when it possible to know the beacon's initial position a priori and when it is not. This problem can be seen as an SLAM problem, where we are also interested in the location of the beacon.

Chapter 3:

- We developed and implemented a nonlinear filter based on the Extended Kalman Filter for the vehicle's and beacon's position. The filter was implemented with and without taking into account ocean currents.
- We implemented an improved a version of the EKF called Exogenous Kalman Filter for the vehicle's and beacon's position. Unlike the EKF, the XKF has global observability properties, and at the same time it shows good noise-rejection properties.

Chapter 4:

- We tackled the observability problem of single range navigation from a optimization point of view. For this, we maximized the Fisher Information Matrix in order to find trajectories that improve the observability of the system.

- Additionally, we included another cost function, which accounted for the energy used to move the beacon. Using the multi-objective toolbox from Matlab, we found the Pareto front, which shows that no matter how much we increase the energy of the beacon there will be a point where the FIM of the system will not be improved.

Additionally, the following contribution are for the research group are:

- This thesis strengthens the research group's lines: Control Theory and Mechatronics.
- The academic products associated with the thesis (conferences and journal papers) are reported to the research group, which enhances its position within the Colombian Science, Technology and Innovation System.
- During the Ph.D. several master student were advised in topics related with navigation and control of underwater vehicles.

1.4. PRODUCTS

During the PhD, different products were accomplished:

- Dissertataion document
- Articles:
  - **Rúa, S.**, Crasta, N., Vásquez, R.E., and Pascoal, A.M. 2020. Enhanced cooperative single-range underwater navigation based on optimal trajectories. *IFAC-PapersOnLine*, Accepted.
  - **Rúa, S.**, Crasta, N., Vásquez, R.E., Betancur, M.J., and Pascoal, A.M. 2019. Cooperative range-based navigation using a beacon with circular motion installed on board the support platform. *IFAC-PapersOnLine*, **52**(21). pp. 390–395. doi: 10.1016/j.ifacol.2019.12.338.
  - Vásquez, R.E., Castrillón, F., Posada, N.L., **Rúa, S.** and Zuluaga, C. 2019. Curriculum change for graduate-level control engineering education at the Universidad Pontificia Bolivariana. *IFAC-PapersOnLine*, **52**(9). pp. 306–311. doi: 10.1016/j.ifacol.2019.08.225.
  - **Rúa, S.**, Zuluaga, C.A., Posada, N.L., Castrillón, F. and Vásquez, R.E.

2016. Development of the Supervision/Control Software for a Multipurpose Three-Tank System. *IFAC-PapersOnLine*, **49**(6). pp. 156–161. doi: 10.1016/j.ifacol.2016.07.170

- **Rúa, S.** and Vásquez, R.E. 2016. Development of a Low-Level Control System for the ROV Visor3. *International Journal of Navigation and Observation*, **2016**. pp. 1–12. doi: 10.1155/2016/8029124
- Ramírez-Macías, J.A., Brongers, P., **Rúa, S.** and Vásquez, R.E. 2016. Hydrodynamic Modelling for the Remotely Operated Vehicle Visor3 Using CFD. *IFAC-PapersOnLine*, **49**(23). pp. 187–192. doi: 10.1016/j.ifacol.2016.10.341
- Aristizábal, L.M., **Rúa, S.**, Gaviria, C.E., Osorio, S.P., Zuluaga, C.A., Posada, N.L., and Vásquez, R.E. 2016. Design of an Open-Source Based Control Platform for an Underwater Remotely Operated Vehicle. *DYNA*, **83**(195). pp. 198–205. doi: 10.15446/dyna.v83n195.49828

- Software suite in Matlab with all the simulation presented in this work.

1.5. THESIS STRUCTURE

This thesis is organized as follows: Chapter 2. focuses on the observability analysis of the cooperative range-based navigation system. To this end, we first introduce the model of the vehicle and beacon. Then, we describe some definitions of observability for linear and nonlinear systems, which are going to be used in the following sections. Then, the observability properties of the system are studied with and without tanking into account ocean currents. Chapter 3. focuses on the implementation of the nonlinear filter for the beacon and vehicle's position estimation problem. First we introduce the model taking into account ocean currents and noise. Then, we implement an Extended Kalman Filter which is based on the linearization of the model around the current state estimation. Since the EKF does not have global stability properties, an variation called Exogenous Kalman Filter is implemented. Chapter 4. is focused on finding optimal trajectories which maximizes range information to localize the vehicle under the water. Chapter 5. presents some conclusions and future work related with underwater navigation.

2. OBSERVABILITY ANALYSIS

2.1. INTRODUCTION

The observability analysis is an important task while designing a state observer for a dynamical system. In particular, this chapter presents the observability analysis of a cooperative system; it is shown under which different combination of trajectories is the system observable.

2.2. SYSTEM MODELLING

To analyze the motion of the vehicle and the beacon, two coordinate frames are defined: an inertial Earth-fixed frame (this frame is considered as the North, East, Down frame NED $\{\mathcal{N}\}$; attached to a port facility or a stationary support vessel), where the motion of the vehicle is described, and a body-fixed frame $\{\mathcal{B}\}$, which is conveniently fixed to the vehicle and moves with it. Additionally, to define the mathematical model, two different scenarios are taken into account: first, the motion of the vehicle only depends on its velocity; and second, the motion is affected by ocean currents. Figure 2 shows the setup used in this work.

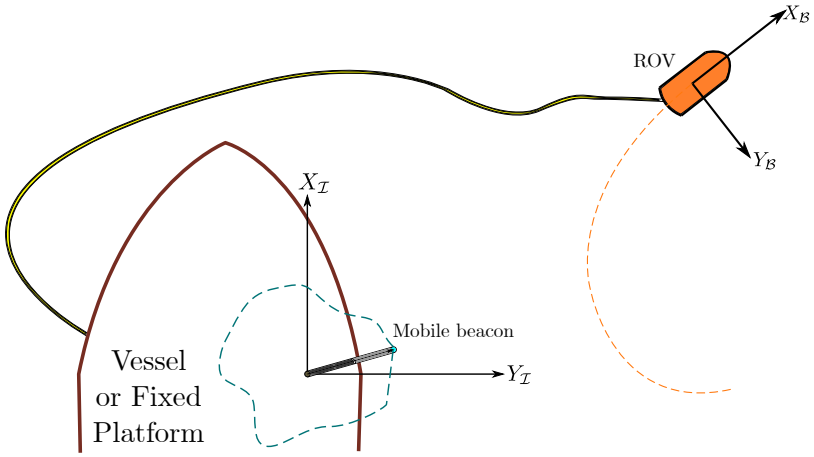

Figure 2: Setup configuration in 2D space. The orange dotted lines represent the trajectory executed by the vehicle, while the blue one the beacons trajectory.

2.2.1. Vehicle motion without ocean current

The kinematics (motion) of the vehicle (without being affected by ocean currents) can be described as

$$^{\mathcal{I}}\dot{\mathbf{p}}(t) = {}^{\mathcal{I}}_{\mathcal{B}}\mathcal{R}(t)\,{}^{\mathcal{B}}\mathbf{v}(t), \tag{2.1}$$

where $^{\mathcal{I}}\mathbf{p}(t) = [x_v, y_v, z_v]^\top \in \mathbb{R}^3$ denotes the position of the vehicle with respect to the inertial frame $\{\mathcal{I}\}$, $^{\mathcal{B}}\mathbf{v}(t) = [u_v, v_v, w_v]^\top \in \mathbb{R}^3$ is the linear velocity of the vehicle with respect to $\{\mathcal{I}\}$ and expressed in $\{\mathcal{B}\}$, and ${}^{\mathcal{I}}_{\mathcal{B}}\mathcal{R}(t) \in \mathcal{SO}(3)$ is the rotation matrix from $\{\mathcal{B}\}$ to $\{\mathcal{I}\}$. The orientation of the vehicle can be parameterized using Euler angles $\boldsymbol{\eta} = [\phi, \theta, \psi]^\top$, then the rotation matrix can be written as

$${}^{\mathcal{I}}_{\mathcal{B}}\mathcal{R}(t) = \begin{bmatrix} \mathrm{c}\psi\mathrm{c}\theta & -\mathrm{s}\psi\mathrm{c}\phi + \mathrm{c}\psi\mathrm{s}\theta\mathrm{s}\phi & \mathrm{s}\psi\mathrm{s}\phi + \mathrm{c}\psi\mathrm{s}\theta\mathrm{c}\phi \\ \mathrm{s}\psi\mathrm{c}\theta & \mathrm{c}\psi\mathrm{c}\phi + \mathrm{s}\psi\mathrm{s}\theta\mathrm{s}\phi & -\mathrm{c}\psi\mathrm{s}\phi + \mathrm{s}\psi\mathrm{s}\theta\mathrm{c}\phi \\ -\mathrm{s}\theta & \mathrm{c}\theta\mathrm{s}\phi & \mathrm{c}\theta\mathrm{c}\phi \end{bmatrix}, \tag{2.2}$$

where $\mathrm{s}\cdot = \sin(\cdot)$ and $\mathrm{c}\cdot = \cos(\cdot)$. Recall that the rotation matrix satisfies

$${}^{\mathcal{I}}_{\mathcal{B}}\dot{\mathcal{R}}(t) = {}^{\mathcal{I}}_{\mathcal{B}}\mathcal{R}(t)S(\boldsymbol{\omega}_v(t)), \tag{2.3}$$

where $\boldsymbol{\omega}_v(t) = [p, q, r]^\top \in \mathbb{R}^3$ denotes the angular velocity of the vehicle, and $S(\cdot)$ is the skew-symmetric matrix defined as

$$S(\mathbf{a}) := \begin{bmatrix} 0 & -a_3 & a_2 \\ a_3 & 0 & -a_1 \\ -a_2 & a_1 & 0 \end{bmatrix}, \tag{2.4}$$

for every $\mathbf{a} = [a_1, a_2, a_3]^\top \in \mathbb{R}^3$.

Assumption 1. *The roll and pitch motions of the vehicle are small, that is* $\phi \approx \theta \approx 0$.

Assumption 1 implies that the angular velocity in roll and pitch will be zero, that is $p = q = 0$. Additionally, it encompasses a wide range of vehicles such as ROVs and AUVs [19, 68, 80], which are designed to have stability in roll and pitch, or have no control over those motions.

Let $\mathbf{w}(\zeta) = [\cos(\zeta)\ \sin(\zeta)\ 0]^\top$ and $\mathbf{w}^\perp(\zeta) = [-\sin(\zeta)\ \cos(\zeta)\ 0]^\top$ be orthonormal vectors and $\mathbf{e}_i \in \mathbb{R}^3$, $i \in \{1, 2, 3\}$ the i^{th} column of the 3×3 identity matrix. Then, taking into account Assumption 1, the rotation matrix ${}^{\mathcal{I}}_{\mathcal{B}}\mathcal{R}(t)$ can be written as ${}^{\mathcal{I}}_{\mathcal{B}}\mathcal{R}(\psi(t)) = [\mathbf{w}(\psi(t))\ \ \mathbf{w}^\perp(\psi(t))\ \ \mathbf{e}_3]$. Using this fact and the equation (2.1), the motion of the vehicle can be written as

$$\left.\begin{aligned} \dot{x}_v &= u_v \cos\psi - v_v \sin\psi \\ \dot{y}_v &= u_v \sin\psi + v_v \cos\psi \\ \dot{z}_v &= w_v \end{aligned}\right\} \tag{2.5}$$

2.2.2. Vehicle motion with ocean current

In the previous section, the motion of the vehicle was formulated without considering the effects of the ocean current. Now, the idea is to model the motion of the vehicle being affected by ocean currents under certain assumptions:

Assumption 2. *Ocean currents are constant and irrotational.*

The kinematics (motion) of the vehicle affected by a constant ocean current is given by

$$\left.\begin{aligned} {}^{\mathcal{I}}\dot{\mathbf{p}}(t) &= {}^{\mathcal{I}}_{\mathcal{B}}\mathcal{R}(t)\,{}^{\mathcal{B}}\mathbf{v}(t) + {}^{\mathcal{I}}\mathbf{v}_c(t) \\ {}^{\mathcal{I}}\dot{\mathbf{v}}_c(t) &= 0 \end{aligned}\right\} \tag{2.6}$$

where ${}^{\mathcal{I}}\mathbf{v}_c(t) = [v_{c_x}, v_{c_y}, v_{c_z}]^\top \in \mathbb{R}^3$ is the unknown ocean current. Then, expanding (2.6) and using Assumption 1, the motion of the vehicle is given by

$$\left.\begin{aligned} \dot{x}_v &= u_v \cos\psi - v_v \sin\psi + v_{c_x} \\ \dot{y}_v &= u_v \sin\psi + v_v \cos\psi + v_{c_x} \\ \dot{z}_v &= w_v + v_{c_z} \\ \dot{v}_{c_x} &= \dot{v}_{c_y} = \dot{v}_{c_z} = 0 \end{aligned}\right\} \tag{2.7}$$

2.2.3. Beacon Motion

Consider now a support vessel or a fixed platform (where the inertial frame is fixed), which has a mobile beacon attached. This beacon sends an acoustic signal to the vehicle, and by measuring the time of flight it is possible to measure the range to the vehicle. Typically this beacon is assumed to be static [32, 57–61, 63, 64, 77, 81–85] or mobile by using another vehicle [54, 72, 73]. The proposed mechanism consists in a manipulator arm with 2-DoF (a revolute and a prismatic joint), which has the beacon attached at the tip (see Figure 3). The key idea is that the prismatic joint will be compensating the perturbations generated by the waves in the vessel (to regulate the depth of the beacon), while the revolute joint will be used for observability purposes.

Assumption 3. *The depth of the manipulator arm is known and maintained to a constant value.*

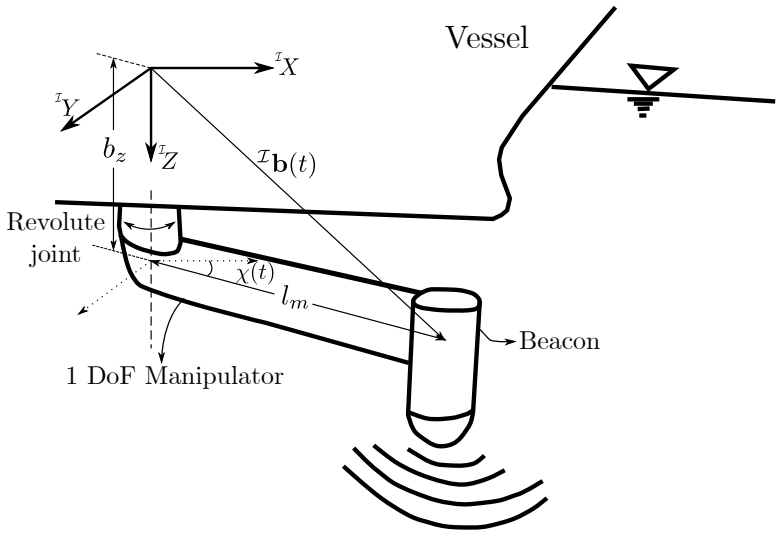

Figure 3: Manipulator arm with the beacon at the tip. The longitudinal axis will be used to compensate for the ocean wave and regulate the depth of the arm, while the rotational movement to ensure observability in the system.

Let $^{\mathcal{I}}\mathbf{b}(t) = [b_x, b_y, b_z]^\top \in \mathbb{R}^3$ denote the position of the beacon with respect to the inertial frame. The motion of this beacon is given by

$$\left.\begin{aligned} {}^{\mathcal{I}}\dot{\mathbf{b}}(t) &= l_m \omega_m \mathbf{w}^{\perp}\left(\chi(t)\right), \\ \dot{\chi}(t) &= \omega_m, \end{aligned}\right\} \tag{2.8}$$

where $l_m \in \mathbb{R}$ is the manipulator's length, $\omega_m \in \mathbb{R}$ is the angular velocity of the

manipulator, and $\chi \in [0, 2\pi)$ is the angular position of the manipulator in the xy plane. Notice that the motion of this manipulator is only in the xy-plane.

Since the beacon is fixed to a vessel or a platform, Assumption 3 implies that the manipulator should have a regulator to control the depth at a specific value. Let ${}^{\mathcal{I}}\mathbf{d}(t) = [d_x, d_y, d_z]^\top \in \mathbb{R}^3$ denote the range vector from the beacon to vehicle and given by ${}^{\mathcal{I}}\mathbf{d}(t) = {}^{\mathcal{I}}\mathbf{b}(t) - {}^{\mathcal{I}}\mathbf{p}(t)$. Then, the range measurement $d(t)$ is given by

$$d(t) = ||{}^{\mathcal{I}}\mathbf{d}(t)|| = ||{}^{\mathcal{I}}\mathbf{b}(t) - {}^{\mathcal{I}}\mathbf{p}(t)||, \tag{2.9}$$

where $||\cdot||$ denotes the Euclidean norm in $\mathbb{R}^n$.

2.3. PROBLEM STATEMENT

Now that the model of the vehicle and the beacon were defined, the problem to be solved can be stated. For the motion of the vehicle there are two scenarios: whether or not the vehicle is being affected by ocean current. Further, it is assumed that the depth of the beacon (b_z) and the vehicle (p_z) are known or measured. The 3D kinematic model of the vehicle and the beacon for the two scenarios (see Figure 4) are given by

- Without ocean current:

$$\left.\begin{aligned} {}^{\mathcal{I}}\dot{\mathbf{p}}(t) &= {}^{\mathcal{I}}_{\mathcal{B}}\mathcal{R}(\psi(t)){}^{\mathcal{B}}\mathbf{v}(t) \\ {}^{\mathcal{I}}\dot{\mathbf{b}}(t) &= l_m\omega_m\mathbf{w}^{\perp}(\chi(t)) \\ \dot{\chi}(t) &= \omega_m \\ d(t) &= ||{}^{\mathcal{I}}\mathbf{b}(t) - {}^{\mathcal{I}}\mathbf{p}(t)|| \\ p_z(t) &= {}^{\mathcal{I}}\mathbf{p}(t)^\top\mathbf{e}_3 \\ b_z(t) &= {}^{\mathcal{I}}\mathbf{b}(t)^\top\mathbf{e}_3 \end{aligned}\right\} \tag{2.10}$$

- With ocean current:

$$\left.\begin{aligned}
{}^{\mathcal{I}}\dot{\mathbf{p}}(t) &= {}^{\mathcal{I}}_{\mathcal{B}}\mathcal{R}(\psi(t)){}^{\mathcal{B}}\mathbf{v}(t) + {}^{\mathcal{I}}\mathbf{v}_c(t) \\
{}^{\mathcal{I}}\dot{\mathbf{v}}_c(t) &= 0 \\
{}^{\mathcal{I}}\dot{\mathbf{b}}(t) &= l_m\omega_m\mathbf{w}^{\perp}\left(\chi(t)\right) \\
\dot{\chi}(t) &= \omega_m \\
d(t) &= ||{}^{\mathcal{I}}\mathbf{b}(t) - {}^{\mathcal{I}}\mathbf{p}(t)|| \\
p_z(t) &= {}^{\mathcal{I}}\mathbf{p}(t)^{\top}\mathbf{e}_3 \\
b_z(t) &= {}^{\mathcal{I}}\mathbf{b}(t)^{\top}\mathbf{e}_3
\end{aligned}\right\}, \tag{2.11}$$

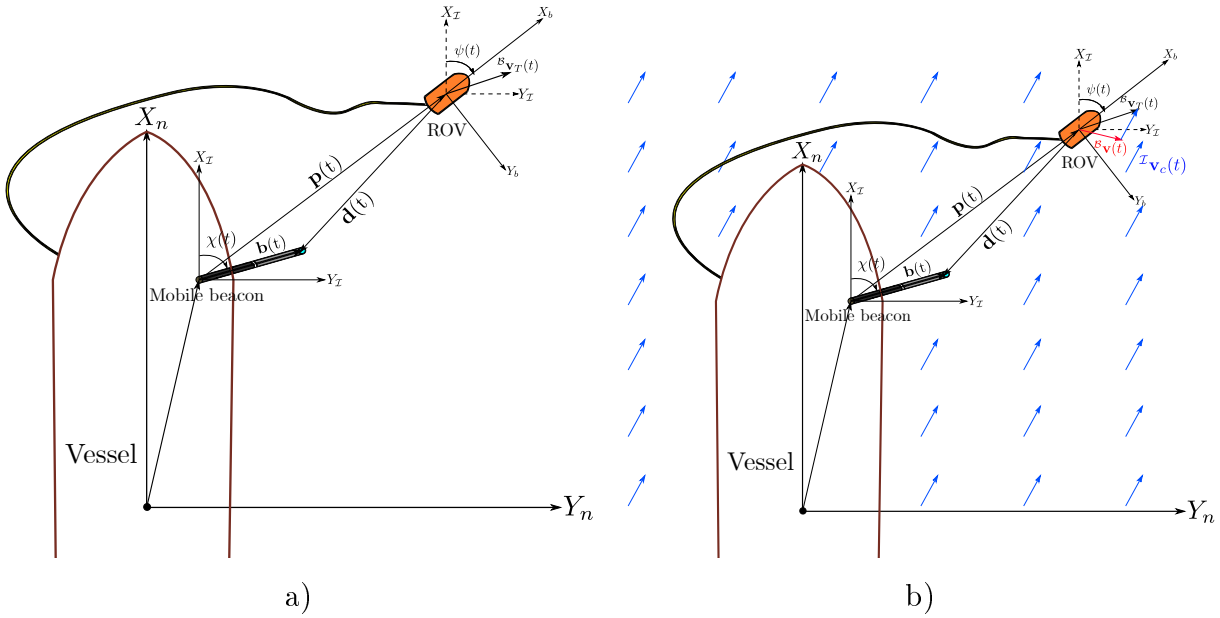

Figure 4: Illustration of the proposed setup with the vehicle and the beacon. In a) without taking into account the current, and in b) with ocean currents.

Throughout this work, the velocity and the orientation of the vehicle, and the angular velocity of the manipulator are assumed as inputs to the system. These variables can be available from an Attitude Heading Reference System (AHRS) for the orientation, a Doppler Velocity Log (DVL) for the velocity, and a Rotary Encoder (for the angular velocity of the manipulator). The problem addressed here is to study whether or not it is possible to estimate the initial position of the vehicle and the beacon given the time histories of the inputs (linear velocity and rotation of the vehicle, and rotation of the beacon), and the time histories of the outputs (depths and range from the beacon to the

vehicle). Notice that the solution of the problem is not trivial since the observability is going to change depending on the trajectories executed by the vehicle and the beacon.

To solve this problem, the following section introduces some definitions needed to carry out the observability analysis of the system (2.10) (respectively (2.11) with ocean currents).

2.4. OBSERVABILITY DEFINITIONS

In the following, some necessary definitions are introduced for observability analysis of the system (2.11) ((2.10) resp.). The definitions for linear and nonlinear system are presented.

Nonlinear Systems

Consider a general nonlinear system

$$\left.\begin{aligned} \dot{\mathbf{x}} &= \boldsymbol{f}(\mathbf{x}, \mathbf{u}) \\ \boldsymbol{y} &= \boldsymbol{h}(\mathbf{x}) \end{aligned}\right\} \tag{2.12}$$

defined on $\mathbb{R}^n$, where $\boldsymbol{f}$ is a smooth and complete vector field on $\mathbb{R}^n$, the input vector $\mathbf{u} = [u_1 \cdots u_p]^{\mathrm{T}}$ takes values in a compact subset Ω of $\mathbb{R}^r$ containing zero in its interior, and the output function $\boldsymbol{h}\colon \mathbb{R}^n \to \mathbb{R}^m$ has smooth components $h_1, \ldots, h_q$.

Two states $\mathbf{x}_1, \mathbf{x}_2 \in \mathbb{R}^n$ are *indistinguishable* for the system (2.12) if, for every admissible input $\mathbf{u} \in \Omega$, the solutions of (2.12) satisfying the initial conditions $\mathbf{x}(0) = \mathbf{x}_1$ and $\mathbf{x}(0) = \mathbf{x}_2$ produce identical output-time histories. In other words, $\mathbf{x}_1, \mathbf{x}_2 \in \mathbb{R}^n$ are indistinguishable for the system (2.12), if and only if

$$\boldsymbol{h}\left(\Phi_{\mathbf{u}}\left(t, \mathbf{x}_1\right)\right) = \boldsymbol{h}\left(\Phi_{\mathbf{u}}\left(t, \mathbf{x}_2\right)\right) \tag{2.13}$$

for every $t \geq 0$ and input $\mathbf{u}$, where $\Phi_{\mathbf{u}}(t, \mathbf{x_0})$ denotes the solution of the system (2.12) at time t for the initial condition $\mathbf{x}_0$ and the input $\mathbf{u}$. Given $\mathbf{x}_0 \in \mathbb{R}^n$, let us denote $\mathcal{I}(\mathbf{x}_0) \subseteq \mathbb{R}^n$ as the set of all points that are indistinguishable from $\mathbf{x}_0$ with respect to the system (2.7). Recall that the indistinguishability is an equivalence relation on $\mathbb{R}^n$.

The following definitions from [55] are used. The system (2.12) is *observable at* $\mathbf{x}_0 \in \mathbb{R}^n$ if $\mathcal{I}(\mathbf{x}_0) = \{\mathbf{x}_0\}$, and is *observable* if $\mathcal{I}(\mathbf{x}_0) = \{\mathbf{x}_0\}$ for every $\mathbf{x}_0$. The system (2.12) is

weakly observable at $\mathbf{x}_0 \in \mathbb{R}^n$ if $\mathbf{x}_0$ is an isolated point of $\mathcal{I}(\mathbf{x}_0)$. The system (2.12) is *weakly observable* if it is weakly observable at every $\mathbf{x}_0 \in \mathbb{R}^n$. Clearly, observability implies weak observability.

Linear Time Varying Systems

Consider a general LTV system

$$\left.\begin{aligned} \dot{\mathbf{x}} &= A(t)\mathbf{x}(t) + B(t)\mathbf{u}(t) \\ \boldsymbol{y} &= C(t)\mathbf{x}(t) \\ \mathbf{x}(t_0) &= \mathbf{x}_0 \end{aligned}\right\} \tag{2.14}$$

defined on $\mathbb{R}^n$, where $\mathbf{x} \in \mathbb{R}^n$ is the state vector, $\mathbf{u} \in \mathbb{R}^r$ is the input vector, $\boldsymbol{y} \in \mathbb{R}^m$ is the output vector, $A(t), B(t), C(t), D(t)$ are matrices with appropriate dimensions, and $\mathbf{x}_0 \in \mathbb{R}^n$ is the initial condition of the system. The solution for the equation (2.14) is given by

$$\left.\begin{aligned} \mathbf{x}(t) &= \Phi(t, t_0)\mathbf{x}_0 + \int_{t_0}^{t} \Phi(t, \tau)B(\tau)\mathbf{u}(\tau)d\tau \\ \boldsymbol{y}(t) &= C(t)\Phi(t, t_0)\mathbf{x}_0 + \int_{t_0}^{t} C(t)\Phi(t, \tau)B(\tau)\mathbf{u}(\tau)d\tau \end{aligned}\right\} \tag{2.15}$$

where $\Phi(t, t_0) \in \mathbb{R}^{n\times n}$ is the state transition matrix, and is given by the Peano-Baker series

$$\Phi(t, t_0) = I + \int_{t_0}^{t} A(\sigma_1)d\sigma_1 + \int_{t_0}^{t} A(\sigma_1)\int_{t_0}^{\sigma_1} A(\sigma_2)d\sigma_2 d\sigma_1 + ... \tag{2.16}$$

Recall that observability is referred to whether is possible or not to estimate the initial condition of the system given the time history of the input and output. Then, from the output equation in (2.15), the observability can be determined by analyzing when we can find a solution for the equation

$$\begin{aligned} \tilde{\boldsymbol{y}}(t) &= \boldsymbol{y}(t) - \int_{t_0}^{t} C(t)\Phi(t, \tau)B(\tau)\mathbf{u}(\tau)d\tau \\ &= C(t)\Phi(t, t_0)\mathbf{x}_0 \end{aligned} \tag{2.17}$$

for the unknown $\mathbf{x}_0 \in \mathbb{R}^n$. The following definitions are borrowed from [86]. Given two times $t_1 > t_0 > 0$, the unobservable subspace on $[t_0, t_1]$ denoted as $\mathcal{UO}[t_0, t_1]$ from the system (2.14) consists of all states $\mathbf{x}_0 \in \mathbb{R}^n$ for which $C(t)\Phi(t, t_0)\mathbf{x}_0 = \mathbf{0}, \forall t \in [t_0, t_1]$. The system (2.14) is observable if and only if $\mathcal{UO}[t_0, t_1] = \{\mathbf{0}\}$. From this last definition,

the relationship between indistinguishable initial conditions and the unobservable space can be derived. Given a input/output pair $\{\mathbf{u}(t), \boldsymbol{y}(t)\}$ with $t \in [t_0, t_1]$ associated with the initial condition $\mathbf{x}_0 \in \mathbb{R}^n$ of system (2.14). Then $\mathcal{I}(\mathbf{x}_0) = \{\mathbf{x}_0 + \mathbf{x}_u : \mathbf{x}_u \in \mathcal{UO}[t_0, t_1]\}$ is the set of all indistinguishable initial conditions on $[t_0, t_1]$ from system (2.14).

Additionally, the unobservable space can be analyzed by computing the kernel of the observability matrix from system (2.14), which is given by

$$\mathcal{O} = \begin{bmatrix} N_0(t,_t 0) \\ N_1(t,_t 0) \\ \vdots \\ N_{k-1}(t, t_0) \end{bmatrix}$$

where

$$N_i(t, t_0) := \frac{\mathrm{d}^i C(t)\Phi(t, t_0)}{\mathrm{d}t^i}, i \in \{0, 1, ..., k-1\}$$

2.5. OBSERVABILITY ANALYSIS WITHOUT OCEAN CURRENT

Up to this point, only the kinematic model of the vehicle and beacon have been defined. Note that the system (2.10) is nonlinear since the time evolution of the state and the output depend on a nonlinear function of the state.

To perform the observability analysis of model (2.10), first the model is transformed to the reference frame $\{\mathcal{B}\}$. Subsequently, inspired by the approach [32,57], an state space augmentation is applied to convert the nonlinear system into a LTV system. Taking into account that this new system is equivalent* and by using linear system tools, the observability of the system is analyzed. Figure 5 shows a summary of this procedure.

Additionally, since the information of the depth is available for the vehicle and the beacon, the whole observability analysis will be carried out in the horizontal plane. Even though the range measurement is acquired in a three dimensional space, the range in 2D can be obtained by applying Pythagorean theorem as $d_{xy} = \sqrt{(d^2 - \Delta z^2)}$,

*Equivalent in the sense that the state trajectories of the linear varying system have one-to-one correspondence to the state trajectories of the nonlinear system. In other words, the transformation is injective.

where $\Delta z = p_z - b_z$ is the difference between two depths (vehicle and beacon), and d_{xy} denotes the range measurement in the xy-plane. Then, for the sake of completeness, the system (2.10) in a two dimensional space can be rewritten as

$$\left.\begin{aligned} {}^{\mathcal{I}}\dot{\mathbf{p}}(t) &= {}^{\mathcal{I}}_{\mathcal{B}}\mathcal{R}(\psi(t)){}^{\mathcal{B}}\mathbf{v}(t) \\ {}^{\mathcal{I}}\dot{\mathbf{b}}(t) &= l_m\omega_m\mathbf{w}^{\perp}(\chi(t)) \\ \dot{\chi}(t) &= \omega_m \\ d_{xy}(t) &= ||{}^{\mathcal{I}}\mathbf{b}(t) - {}^{\mathcal{I}}\mathbf{p}(t)|| \end{aligned}\right\} \tag{2.18}$$

where ${}^{\mathcal{I}}\mathbf{p}$, ${}^{\mathcal{B}}\mathbf{v}$, ${}^{\mathcal{I}}\mathbf{b} \in \mathbb{R}^2$, ${}^{\mathcal{I}}_{\mathcal{B}}\mathcal{R} \in \mathcal{SO}(2)$, and the vectors $\mathbf{w}(\cdot)$ and $\mathbf{w}^{\perp}(\cdot)$ are properly redefined in $\mathbb{R}^2$.

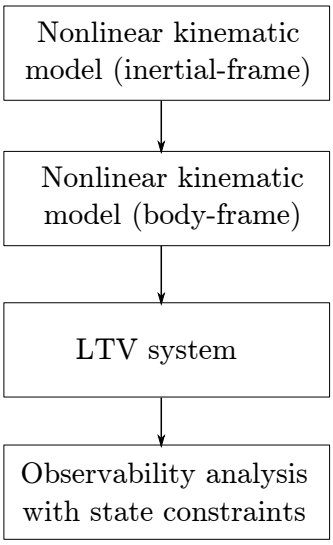

Figure 5: Observability analysis procedure for the underwater navigation system. Notice that the state from the LTV system has constraints, since it comes from a similarity transformation done to a nonlinear system.

Recall that the system (2.18) is expressed with respect to the $\{\mathcal{I}\}$ frame and the state is given by the position of the vehicle and the beacon. The key idea here is to express the model (2.18) in the frame $\{\mathcal{B}\}$ and to use the range vector ${}^{\mathcal{B}}\mathbf{d}(t)$ and the manipulator angle $\chi(t)$ as new state variable of the system. With these two variables it is possible to describe the motion of the system (2.18). From this part of the document, explicit dependence of time (t) will be omitted for sake of simplicity. Further, since Assumption 1 implies rotation only in the z-axis, let $\mathcal{R}_\alpha := \mathcal{R}(\alpha)$ denote the rotation matrix that rotates vectors by an angle $\alpha \in [0, 2\pi)$ about the z-axis. Since $\psi(t)$ represents the

rotation from $\{\mathcal{B}\}$ to $\{\mathcal{I}\}$, then ${}^{\mathcal{I}}_{\mathcal{B}}\mathcal{R}(\psi(t)) := \mathcal{R}_\psi$ Let us rewrite the range vector in the $\{\mathcal{B}\}$ frame, that is

$$ {}^{\mathcal{B}}\mathbf{d} = \mathcal{R}_\psi^\top({}^{\mathcal{I}}\mathbf{b} - {}^{\mathcal{I}}\mathbf{p}). \tag{2.19} $$

Using the time derivatives of the vehicle and beacon positions (2.18) and the equation (2.3), it follows that

$$ \begin{aligned} {}^{\mathcal{B}}\dot{\mathbf{d}} &= \dot{\mathcal{R}}_\psi^\top({}^{\mathcal{I}}\mathbf{b} - {}^{\mathcal{I}}\mathbf{p}) + \mathcal{R}_\psi^\top({}^{\mathcal{I}}\dot{\mathbf{b}} - {}^{\mathcal{I}}\dot{\mathbf{p}}) \\ &= -S(r)\mathcal{R}_\psi^\top({}^{\mathcal{I}}\mathbf{b} - {}^{\mathcal{I}}\mathbf{p}) + \mathcal{R}_\psi^\top(l_m\omega_m\mathbf{w}^\perp(\chi) - {}^{\mathcal{I}}_{\mathcal{B}}\mathcal{R}_\psi\,{}^{\mathcal{B}}\mathbf{v}) \\ &= -S(r){}^{\mathcal{B}}\mathbf{d} - {}^{\mathcal{B}}\mathbf{v} + l_m\omega_m\mathcal{R}_\psi^\top\mathbf{w}^\perp(\chi) \end{aligned} \tag{2.20} $$

To get a state-space realization of the system, let us define the state vector as $\mathbf{x} = [\mathbf{x}_1, x_2]^\top \stackrel{\text{def}}{=} [{}^{\mathcal{B}}\mathbf{d}, \chi] \in \mathbb{R}^2 \times [0, 2\pi)$, and recall that $r \in \mathbb{R}$ the angular velocity of the vehicle, $\omega_m \in \mathbb{R}$ the angular velocity of the beacon, ${}^{\mathcal{B}}\mathbf{v} \in \mathbb{R}^2$ the linear velocity of the vehicle, and $\mathcal{R}_\psi \in \mathcal{SO}(2)$ are inputs to the system. Then, the state-space realization can be written as

$$ \left.\begin{aligned} \dot{\mathbf{x}}_1 &= -S(r)\mathbf{x}_1 - {}^{\mathcal{B}}\mathbf{v} + l_m\omega_m\mathcal{R}_\psi^\top\mathbf{w}^\perp(x_2) \\ \dot{x}_2 &= \omega_m \end{aligned}\right\} \tag{2.21} $$

From (2.18) and (2.19), and by using the square range measurement instead of the usual range measurement, it is possible to rewrite the output equation as

$$ \begin{aligned} d_{xy}^2 &= ||{}^{\mathcal{I}}\mathbf{b} - {}^{\mathcal{I}}\mathbf{p}||^2 \\ &= {}^{\mathcal{B}}\mathbf{d}^\top{}^{\mathcal{B}}\mathbf{d} \\ &= \mathbf{x}_1^\top\mathbf{x}_1 \end{aligned} \tag{2.22} $$

At this point, it is important to point out that square range measurement is used for observability purpose, and that the conclusions obtained with this measurement does not change [59]. The following remark summarizes this statement.

Remark 1. *The system (2.10) (respectively (2.11)) with range squared measurement is observable if and only if the system (2.10) (respectively (2.11)) with range measurement is observable.*

Proof. Suppose that the system (2.10) (respectively (2.11)) with range squared measurement is observable. Thus, for every different pair of initial conditions $\mathbf{x}_0$ and $\mathbf{z}_0$, there

exists a time $t^* \in [0, t^*]$, and an input $\mathbf{u}^*$ such that $\boldsymbol{h}\left(\Phi_{\mathbf{u}^*}\left(t^*, \mathbf{x}_0\right)\right)^2 \neq \boldsymbol{h}\left(\Phi_{\mathbf{u}^*}\left(t^*, \mathbf{z}_0\right)\right)^2$. Then, it also follows that $\boldsymbol{h}\left(\Phi_{\mathbf{u}^*}\left(t^*, \mathbf{x}_0\right)\right) \neq \boldsymbol{h}\left(\Phi_{\mathbf{u}^*}\left(t^*, \mathbf{z}_0\right)\right)$, which means that the system (2.10) (respectively (2.11)) with range measurement is observable. The reverse can be concluded in the same way. This completes the proof. □

Now that the system is expressed in the $\{\mathcal{B}\}$ frame, a state augmentation is applied to make the system linear with respect to the state variables. Notice that the nonlinearities in the state variables come from the output equation (2.22) and the term $\mathbf{w}^{\perp}\left(x_2\right)$ in (2.21). Inspired by the same ideas presented in [81], let us define the following state-space augmentation $\mathbf{z} := [\mathbf{z}_1, \mathbf{z}_2, \mathbf{z}_3, z_4, z_5, z_6] := [\mathbf{x}_1, \mathcal{R}_{\psi}^{\top}\mathbf{w}^{\perp}\left(x_2\right), \mathcal{R}_{\pi/2}^{\top}\mathbf{z}_2,\ \mathbf{z}_1^{\top}\mathbf{z}_1,\ \mathbf{z}_1^{\top}\mathbf{z}_2, \mathbf{z}_1^{\top}\mathbf{z}_3]$. Then, the system (2.21) with the previous state augmentation described, can be rewritten in linear form (for a detailed step by step of this procedure, see Appendix A.1.) with state variable $\mathbf{z} \in \mathbb{R}^9$, input vector $\mathbf{u} = [{}^{\mathcal{B}}\mathbf{v}^{\top},\ \omega_m,\ r]^{\top} \in \mathbb{R}^4$, and output $y \in \mathbb{R}$ as

$$\left.\begin{aligned} \dot{\mathbf{z}} &= A(\mathbf{u})\mathbf{z} + B\mathbf{u} \\ y &= C\mathbf{z} \end{aligned}\right\} \tag{2.23}$$

where

$$A(\mathbf{u}) = \begin{bmatrix} -S(r) & l_m\omega_m I_2 & \mathbf{0} & \mathbf{0} & \mathbf{0} & \mathbf{0} \\ \mathbf{0} & -S(r) & -\omega_m I_2 & \mathbf{0} & \mathbf{0} & \mathbf{0} \\ \mathbf{0} & (\omega_m - r)I_2 & \mathbf{0} & \mathbf{0} & \mathbf{0} & \mathbf{0} \\ -2{}^{\mathcal{B}}\mathbf{v}^{\top} & \mathbf{0} & \mathbf{0} & 0 & 2l_m\omega_m & 0 \\ \mathbf{0} & -{}^{\mathcal{B}}\mathbf{v}^{\top} & \mathbf{0} & 0 & 0 & -\omega_m \\ \mathbf{0} & \mathbf{0} & -{}^{\mathcal{B}}\mathbf{v}^{\top} & 0 & \omega_m & 0 \end{bmatrix},$$

$$B = \begin{bmatrix} -I_2 & \mathbf{0} & \mathbf{0} \\ \mathbf{0} & \mathbf{0} & \mathbf{0} \\ \mathbf{0} & \mathbf{0} & \mathbf{0} \\ \mathbf{0} & 0 & 0 \\ \mathbf{0} & l_m & 0 \\ \mathbf{0} & 0 & 0 \end{bmatrix},$$

$$C = \begin{bmatrix} \mathbf{0} & \mathbf{0} & \mathbf{0} & 1 & 0 & 0 \end{bmatrix},$$

and the initial conditions satisfying

$$\begin{bmatrix} \mathbf{z}_1(0) \\ \mathbf{z}_2(0) \\ \mathbf{z}_3(0) \\ z_4(0) \\ z_5(0) \\ z_6(0) \end{bmatrix} := \begin{bmatrix} \mathbf{x}_1(0) \\ \mathcal{R}_{\psi_0}^{\top} \mathbf{w}^{\perp}\left(x_2(0)\right) \\ \mathcal{R}_{\pi/2}^{\top} \mathbf{z}_2(0) \\ \mathbf{z}_1(0)^{\top} \mathbf{z}_1(0) \\ \mathbf{z}_1(0)^{\top} \mathbf{z}_2(0) \\ \mathbf{z}_1(0)^{\top} \mathbf{z}_3(0) \end{bmatrix} \tag{2.24}$$

It is important to explain that the constraints imposed in the initial conditions (2.24) are important for the observability analysis. These constraints guarantee one-to-one correspondence between the original nonlinear system (2.21) and the LTV system described by (2.23).

Now that the system is LTV, one way to solve this problem is to find the Observability Gramian and test if it is nonsingular for any $t > 0$. Nevertheless, this is not a simple task, mainly due to the state transition matrix given by the Peano-Baker series in (2.16). Instead, the set of admissible inputs $\mathbf{u}$ to the system is redefined. The motion of the vehicle and the beacon are restricted to trim trajectories. Along these trajectories the velocities measured in the body frame and the control inputs $\mathbf{u}$ are constant [87].

Assumption 4. *The vehicle and beacon are executing trim trajectories, that is,* $\dot{\mathbf{u}} = 0$.

Notice that Assumption 4 implies that the system (2.23) can be seen as an LTI system, since $A(\mathbf{u})$ is constant and known. Then, the observability analysis of the system can be carried out by just analyzing the observability matrix. Further, the class of maneuvers executed by the vehicle and beacon can be summarized as:

- vehicle
  - staying at the same point: $||^{\mathcal{B}}\mathbf{v}|| = 0$.
  - moving in straight lines: $||^{\mathcal{B}}\mathbf{v}|| \neq 0$ and $r = 0$.
  - moving in circles: $||^{\mathcal{B}}\mathbf{v}|| \neq 0$ and $r \neq 0$.
- beacon
  - without movement: $\omega_m = 0$
  - rotating: $\omega_m \neq 0$.

Based on these maneuvers, the observability analysis is carried out for the system (2.23).

Proposition 1. *Consider system* (2.23) *with* $\mathbf{u} \in \mathbb{R}^4$ *fulfilling assumption 4. Further,*

suppose that the vehicle moves in circles, that is,

$$||^{\mathcal{B}}\mathbf{v}|| \neq 0, r \neq 0, \tag{2.25}$$

and the beacon rotates with angular rate

$$\omega_m \neq 0 \neq \pm r \neq 2r \neq \frac{1}{2}r. \tag{2.26}$$

Then, the system (2.23) is observable.

Proof. Consider the initial condition $\mathbf{z}(0) \in \mathbb{R}^9$ and let $\mathbf{u} \in \mathbb{R}^4$ be constant. Since the input is known and constant, (2.23) is an LTI system. The observability matrix associated with the system (2.23) is defined by $\mathcal{O} = [C, CA, ..., CA^{n-1}]^\top$ with $n \in \{1, 2, .., 9\}$. Then the observability matrix is given by

$$\mathcal{O} = 2\begin{bmatrix}
\mathbf{0} & \mathbf{0} & \mathbf{0} & 1 & 0 & 0 & \\
-{}^{\mathcal{B}}\mathbf{v}^\top & \mathbf{0} & \mathbf{0} & 0 & l_m\omega_m & 0 & \\
-r\ {}^{\mathcal{B}}\mathbf{v}^{\perp^\top} & -2l_m\omega_m\,{}^{\mathcal{B}}\mathbf{v}^\top & \mathbf{0} & 0 & 0 & -l_m\omega_m^2 & \\
r^2\ {}^{\mathcal{B}}\mathbf{v}^\top & -3l_mr\omega_m\,{}^{\mathcal{B}}\mathbf{v}^{\perp^\top} & 3l_m\omega_m^2\,{}^{\mathcal{B}}\mathbf{v}^\top & 0 & -l_m\omega_m^3 & 0 & \\
r^3\ {}^{\mathcal{B}}\mathbf{v}^{\perp^\top} & l_m\omega_m\,{}^{\mathcal{B}}\mathbf{v}^\top g_1(r,\omega_m) & 3l_mr\omega_m^2\,{}^{\mathcal{B}}\mathbf{v}^{\perp^\top} & 0 & 0 & l_m\omega_m^4 & \\
-r^4\ {}^{\mathcal{B}}\mathbf{v}^\top & l_mr\omega_m\,{}^{\mathcal{B}}\mathbf{v}^{\perp^\top} g_2(r,\omega_m) & l_m\omega_m^2\,{}^{\mathcal{B}}\mathbf{v}^\top g_3(r,\omega_m) & 0 & l_m\omega_m^5 & 0 & \\
-r^5\ {}^{\mathcal{B}}\mathbf{v}^{\perp^\top} & -l_m\omega_m\,{}^{\mathcal{B}}\mathbf{v}^\top g_4(r,\omega_m) & -l_mr\omega_m^2\,{}^{\mathcal{B}}\mathbf{v}^{\perp^\top} g_2(r,\omega_m) & 0 & 0 & -l_m\omega_m^6 & \\
r^6\ {}^{\mathcal{B}}\mathbf{v}^\top & -l_mr\omega_m\,{}^{\mathcal{B}}\mathbf{v}^{\perp^\top} g_5(r,\omega_m) & l_m\omega_m^2\,{}^{\mathcal{B}}\mathbf{v}^\top g_6(r,\omega_m) & 0 & -l_m\omega_m^7 & 0 & \\
r^7\ {}^{\mathcal{B}}\mathbf{v}^{\perp^\top} & l_m\omega_m\,{}^{\mathcal{B}}\mathbf{v}^\top g_7(r,\omega_m) & l_mr\omega_m^2\,{}^{\mathcal{B}}\mathbf{v}^{\perp^\top} g_5(r,\omega_m) & 0 & 0 & l_m\omega_m^8 & 0
\end{bmatrix} \tag{2.27}$$

where ${}^{\mathcal{B}}\mathbf{v}^\perp = \mathcal{R}_{\pi/2}{}^{\mathcal{B}}\mathbf{v}$, and $g_i : \mathbb{R}^2 \mapsto \mathbb{R}$ with $i \in \{1, 2, ..., 7\}$, are functions of ω_m and r given by

$$\begin{aligned}
g_1(r,\omega_m) &= 4r^2 - 3r\omega_m + 4\omega_m^2,\\
g_2(r,\omega_m) &= 5r^2 - 6r\omega_m + 7\omega_m^2,\\
g_3(r,\omega_m) &= 4r^2 - 3r\omega_m + 5\omega_m^2,\\
g_4(r,\omega_m) &= 3r^4 - 5r^3\omega_m + 7r^2\omega_m^2 - 4r\omega_m^3 + 3\omega_m^4,\\
g_5(r,\omega_m) &= 7r^4 - 15r^3\omega_m + 25r^2\omega_m^2 - 21r\omega_m^3 + 13\omega_m^4,\\
g_6(r,\omega_m) &= 6r^4 - 10r^3\omega_m + 14r^2\omega_m^2 - 8r\omega_m^3 + 7\omega_m^4,\\
g_7(r,\omega_m) &= 8r^6 - 21r^5\omega_m + 41r^4\omega_m^2 - 45r^3\omega_m^3 + 35r^2\omega_m^4 - 15r\omega_m^5 + 8\omega_m^6.
\end{aligned}$$

The determinant of (2.27) is given by

$$\det(\mathcal{O}) = -256r^3\omega_m^{10}l_m^6||^{\mathcal{B}}\mathbf{v}||^6(r-\omega_m)^7(2r-\omega_m)^2(2\omega_m-r)^4(\omega_m+r)^4.$$

Note that if (2.25) and (2.26) hold, then $\det(\mathcal{O}) \neq 0$, which implies that the observability matrix is full rank and therefore system (2.23) is observable. This completes the proof. □

Nevertheless, since the state-augmented system (2.23) is not a minimal realization of the original nonlinear system [88, 89], it is important to analyze the observability of the system when (2.25) and (2.26) do not hold. Therefore, the following scenarios are analyzed:

1. **V**ehicle moving in **C**ircles, and the **B**eacon **R**otating (**VCBR**).
2. **V**ehicle moving in **C**ircles, and the **B**eacon does **N**ot move (**VCBN**).
3. **V**ehicle moving in straight **L**ines, and the **B**eacon **R**otating (**VLBR**).
4. **V**ehicle moving in straight **L**ines, and the **B**eacon does **N**ot move (**VLBN**).
5. **V**ehicle does **N**ot move, and the **B**eacon **R**otating (**VNBR**).
6. Neither the vehicle nor the beacon move (**VNBN**).

Two additional scenarios for each of these cases are analyzed: when the beacon's initial position is known a priori, and when it is not known.

2.5.1. Vehicle moving in circles

Here, the observability of the system is analyzed assuming that the vehicle is moving in circles, that is, $r \neq 0$ and $||^{\mathcal{B}}\mathbf{v}|| \neq 0$, while the beacon can be rotating or not. In Proposition 1 the case in which the beacon was rotating was analyzed. Now consider that the beacon does not move ($\omega_m = 0$); hence, the following proposition establishes the observability properties of the system given a stationary beacon.

Proposition 2 (VCBN). *Consider system (2.23) with $\mathbf{u} \in \mathbb{R}^4$ fulfilling assumption 4. Further, suppose that the vehicle moves in circles ((2.25) holds) and the beacon does not move, that is,*

$$\omega_m = 0. \tag{2.28}$$

Then, the system (2.23) with the constraints in the initial conditions (2.24) is not weakly observable. Moreover, for every $\mathbf{z}(0) \in \mathbb{R}^9$, the set of all indistinguishable initial

conditions denoted by $\mathcal{I}(\mathbf{z}(0))$ *is given by*

$$\mathcal{I}(\mathbf{z}(0)) = \left\{ \mathbf{z}(0), \begin{bmatrix} \mathbf{z}_1(0) \\ \mathbf{s}_\beta \\ \mathbf{s}_\beta^\perp \\ z_4(0) \\ \mathbf{z}_1^\top(0)\mathbf{s}_\beta \\ \mathbf{z}_1^\top(0)\mathbf{s}_\beta^\perp \end{bmatrix} \right\}, \tag{2.29}$$

where $\mathbf{s}_\beta : [0, 2\pi) \mapsto \mathcal{S}^1$ *is the map described by* $\mathbf{s}_\beta := [\cos\beta \ \ \sin\beta]^\top$ *and* $\mathbf{s}_\beta^\perp := \mathcal{R}_{\pi/2}^\top \mathbf{s}_\beta$.

Proof. Consider the initial condition $\mathbf{z}(0) \in \mathbb{R}^9$ and let $\mathbf{u} \in \mathbb{R}^4$ be constant. Since the input is known and constant, (2.23) is an LTI system. Taking into account (2.28), the first three rows of the observability matrix associated with the system (2.23) are calculated by

$$\mathcal{O} = \begin{bmatrix} \mathbf{0} & \mathbf{0} & \mathbf{0} & 1 & 0 & 0 \\ -2^{\mathcal{B}}\mathbf{v}^\top & \mathbf{0} & \mathbf{0} & 0 & 0 & 0 \\ -2r^{\mathcal{B}}\mathbf{v}^{\perp\top} & \mathbf{0} & \mathbf{0} & 0 & 0 & 0 \end{bmatrix} \tag{2.30}$$

and the following rows can be computed as $CA^j = -r^2(CA^{j-2})$ for $j \in \{3, 4, 5, ...\}$. Since the rank of (2.30) is 3, then the kernel of $\mathcal{O}$ is given by

$$\ker(\mathcal{O}) = \begin{bmatrix} \mathbf{0} & \mathbf{0} & \mathbf{0} & \mathbf{0} & \mathbf{0} & \mathbf{0} \\ \mathbf{e}_x & \mathbf{e}_y & \mathbf{0} & \mathbf{0} & \mathbf{0} & \mathbf{0} \\ \mathbf{0} & \mathbf{0} & \mathbf{e}_x & \mathbf{e}_y & \mathbf{0} & \mathbf{0} \\ 0 & 0 & 0 & 0 & 0 & 0 \\ 0 & 0 & 0 & 0 & 1 & 0 \\ 0 & 0 & 0 & 0 & 0 & 1 \end{bmatrix}. \tag{2.31}$$

Recall that the unobservable space is given by all initial conditions that generate the same input-output map. Therefore, all initial conditions of the form $\bar{\mathbf{z}}(0) = \mathbf{z}(0) + \ker(\mathcal{O})\boldsymbol{\alpha}$ with $\boldsymbol{\alpha} = [\alpha_1, \alpha_2, \alpha_3, \alpha_4, \alpha_5, \alpha_6]^\top \in \mathbb{R}^6$, are indistinguishable from $\mathbf{z}_0$. Then

$$\begin{bmatrix} \bar{\mathbf{z}}_1(0) \\ \bar{\mathbf{z}}_2(0) \\ \bar{\mathbf{z}}_3(0) \\ \bar{z}_4(0) \\ \bar{z}_5(0) \\ \bar{z}_6(0) \end{bmatrix} = \begin{bmatrix} \mathbf{z}_1(0) \\ \mathbf{z}_2(0) + \boldsymbol{\alpha}_a \\ \mathbf{z}_3(0) + \boldsymbol{\alpha}_b \\ z_4(0) \\ z_5(0) + \alpha_5 \\ z_6(0) + \alpha_6 \end{bmatrix}, \tag{2.32}$$

where $\boldsymbol{\alpha}_a = [\alpha_1, \alpha_2]^\top$ and $\boldsymbol{\alpha}_b = [\alpha_3, \alpha_4]^\top$. Recall that the initial conditions should satisfy the constraints given by (2.24). Since $\mathbf{z}_2 := \mathcal{R}_\psi^\top \mathbf{w}^\perp(x_2)$, then

$$\begin{aligned} \bar{\mathbf{z}}_2^\top(0)\bar{\mathbf{z}}_2(0) &= 1, \\ (\mathbf{z}_2(0) + \boldsymbol{\alpha}_a)^\top (\mathbf{z}_2(0) + \boldsymbol{\alpha}_a) &= 1, \\ ||\boldsymbol{\alpha}_a + \mathbf{z}_2(0)||^2 &= 1, \\ \boldsymbol{\alpha}_a &= -\mathbf{z}_2(0) + \mathbf{s}_\beta, \end{aligned} \tag{2.33}$$

where $\mathbf{s}_\beta := [\cos\beta, \sin\beta]^\top$ with $\beta \in [0, 2\pi)$. From the relation between $\mathbf{z}_2(0)$ and $\mathbf{z}_3(0)$ in (2.24) and using (2.32), it can be concluded that

$$\begin{aligned} \bar{\mathbf{z}}_3(0) &= \mathcal{R}_{\pi/2}^\top \bar{\mathbf{z}}_2(0), \\ \mathbf{z}_3(0) + \boldsymbol{\alpha}_b &= \mathcal{R}_{\pi/2}^\top (\mathbf{z}_2(0) + \boldsymbol{\alpha}_a), \\ \boldsymbol{\alpha}_b &= \mathcal{R}_{\pi/2}^\top \boldsymbol{\alpha}_a. \end{aligned} \tag{2.34}$$

Moreover, it is possible to obtain α_5 and α_6 from the relation of z_5 and z_6 in (2.24), thus

$$\begin{aligned} \bar{z}_5(0) &= z_5(0) + \alpha_5, \\ \bar{\mathbf{z}}_1^\top(0)\bar{\mathbf{z}}_2(0) &= \mathbf{z}_1^\top(0)\mathbf{z}_2(0) + \alpha_5, \\ \mathbf{z}_1^\top(0)(\mathbf{z}_2(0) + \boldsymbol{\alpha}_a) &= \mathbf{z}_1^\top(0)\mathbf{z}_2(0) + \alpha_5, \\ \alpha_5 &= \mathbf{z}_1^\top(0)\boldsymbol{\alpha}_a \end{aligned} \tag{2.35}$$

and

$$\begin{aligned} \bar{z}_6(0) &= z_6(0) + \alpha_6, \\ \bar{\mathbf{z}}_1^\top(0)\bar{\mathbf{z}}_3(0) &= \mathbf{z}_1^\top(0)\mathbf{z}_3(0) + \alpha_6, \\ \mathbf{z}_1^\top(0)(\mathbf{z}_3(0) + \boldsymbol{\alpha}_b) &= \mathbf{z}_1^\top(0)\mathbf{z}_3(0) + \alpha_6, \\ \alpha_6 &= \mathbf{z}_1^\top(0)\boldsymbol{\alpha}_b. \end{aligned} \tag{2.36}$$

Then, the set of indistinguishable initial conditions are given by

$$\begin{bmatrix} \bar{\mathbf{z}}_1(0) \\ \bar{\mathbf{z}}_2(0) \\ \bar{\mathbf{z}}_3(0) \\ \bar{z}_4(0) \\ \bar{z}_5(0) \\ \bar{z}_6(0) \end{bmatrix} = \begin{bmatrix} \mathbf{z}_1(0) \\ \mathbf{s}_\beta \\ \mathbf{s}_\beta^\perp \\ z_4(0) \\ \mathbf{z}_1^\top(0)\mathbf{s}_\beta \\ \mathbf{z}_1^\top(0)\mathbf{s}_\beta^\perp \end{bmatrix}$$

This implies that the set of indistinguishable initial conditions from $\mathbf{z}(0) \in \mathbb{R}^9$ is a continuous of points parametrized by a free parameter β and described by (2.29). Thus the system is not weakly observable. This completes the proof. □

To give a psychical meaning of the set (2.29), the initial condition $\mathbf{z}(0)$ needs to be transformed to the original coordinate system. Using (2.24) and (2.19), it can be shown that the initial beacon's position in the $\{\mathcal{I}\}$ frame is related by ${}^{\mathcal{I}}\mathbf{b}(0) = l_m \mathcal{R}_{\pi/2}^{\top} \mathcal{R}_{\psi_0} \mathbf{z}_2(0)$. Additionally, the initial vehicle's position is given by ${}^{\mathcal{I}}\mathbf{p}(0) = {}^{\mathcal{I}}\mathbf{b}(0) - {}^{\mathcal{I}}\mathbf{d}(0)$, which implies ${}^{\mathcal{I}}\mathbf{p}(0) = \mathcal{R}_{\psi_0} \left(l_m \mathcal{R}_{\pi/2}^{\top} \mathbf{z}_2(0) - \mathbf{z}_1(0) \right)$. Then, the indistinguishable initial condition in the beacon's position is given by

$$\begin{aligned} {}^{\mathcal{I}}\bar{\mathbf{b}}(0) &= l_m \mathcal{R}_{\pi/2}^{\top} \mathcal{R}_{\psi_0} \bar{\mathbf{z}}_2(0), \\ &= l_m \mathcal{R}_{\pi/2}^{\top} \mathcal{R}_{\psi_0} \mathbf{s}_{\beta}, \\ &= l_m \mathbf{s}_{\gamma}, \end{aligned} \tag{2.37}$$

where $\mathbf{s}_{\gamma} = \mathcal{R}_{\pi/2}^{\top} \mathcal{R}_{\psi_0} \mathbf{s}_{\beta}$ with $\gamma := \beta + \psi_0 + \pi/2$ and $\gamma \in [0, 2\pi)$. And for the position

$$\begin{aligned} {}^{\mathcal{I}}\bar{\mathbf{p}}(0) &= \mathcal{R}_{\psi_0} \left(l_m \mathcal{R}_{\pi/2}^{\top} \bar{\mathbf{z}}_2(0) - \bar{\mathbf{z}}_1(0) \right), \\ &= l_m \mathbf{s}_{\gamma} - \mathcal{R}_{\psi_0} \mathbf{z}_1(0), \\ &= l_m \mathbf{s}_{\gamma} - {}^{\mathcal{I}}\mathbf{d}(0), \\ &= {}^{\mathcal{I}}\mathbf{p}(0) - \left({}^{\mathcal{I}}\mathbf{b}(0) - l_m \mathbf{s}_{\gamma} \right). \end{aligned} \tag{2.38}$$

Figure 6 shows the geometrical interpretation of the set (2.29).

The observability conditions given by the proposition 2, establish the set of indistinguishable initial conditions when the beacon and vehicle initial positions are unknown. The following corollary states the observability properties when it is possible to known the beacon's initial position.

Corollary 1. *Suppose that the initial condition of the beacon is known. Then the system is observable.*

Proof. Suppose that the initial conditions of the beacon are known, that is, ${}^{\mathcal{I}}\bar{\mathbf{b}}(0) = {}^{\mathcal{I}}\mathbf{b}(0)$. Using this in (2.38) implies that ${}^{\mathcal{I}}\bar{\mathbf{p}}(0) = {}^{\mathcal{I}}\mathbf{p}(0)$. Consequently, $\mathcal{I}(\mathbf{p}(\mathbf{0})) = \{\mathbf{p}(0)\}$ and the system is observable. This completes the proof. □

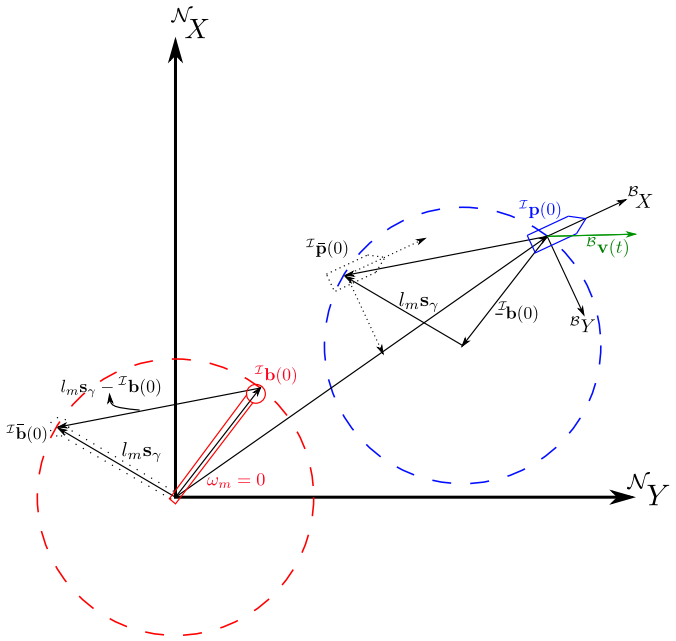

Figure 6: Geometric interpretation of indistinguishable initial conditions for the VCBN condition without taking into account ocean currents. Notice that the set of the indistinguishable initial conditions for the vehicle's position is given by a circle centered in $^{\mathcal{I}}\mathbf{p}(0) - {}^{\mathcal{I}}\mathbf{b}(0)$.

2.5.2. Vehicle moving in straight lines

In the previous sections, the observability analysis was carried out assuming that the vehicle was moving forward and rotating at the same time. Here, the observability of the system is analyzed assuming that the vehicle is moving in straight lines, that is, $r = 0$ and $||^{\mathcal{B}}\mathbf{v}|| \neq 0$, while beacon can be rotating or not.

First, we analyze the observability conditions when the beacon is not moving. The following proposition states the observability properties of the system assuming that the beacon does not move and the vehicle is moving in straight lines.

Proposition 3 (VLBN). *Consider system (2.23) with $\mathbf{u} \in \mathbb{R}^4$ fulfilling assumption 4. Further, suppose that the vehicle moves in straight lines, that is,*

$$||^{\mathcal{B}}\mathbf{v}|| \neq 0 \text{ and } r = 0, \tag{2.39}$$

and the beacon does not move ((2.28) holds). Then, the system (2.23) with the constraints in the initial conditions (2.24) is not weakly observable. Moreover, for every

$\mathbf{z}(0) \in \mathbb{R}^9$, *the set of all indistinguishable initial conditions denoted by* $\mathcal{I}(\mathbf{z}(0))$ *is given by*

$$\mathcal{I}(\mathbf{z}(0)) = \left\{ \mathbf{z}(0), \begin{bmatrix} \mathbf{z}_1(0) + \gamma^{\mathcal{B}}\mathbf{v}^{\perp} \\ \mathbf{s}_\beta \\ \mathbf{s}_\beta^{\perp} \\ z_4(0) \\ \mathbf{z}_1^{\top}(0)\mathbf{s}_\beta + \gamma^{\mathcal{B}}\mathbf{v}^{\perp^{\top}}\mathbf{s}_\beta \\ \mathbf{z}_1^{\top}(0)\mathbf{s}_\beta^{\perp} + \gamma^{\mathcal{B}}\mathbf{v}^{\perp^{\top}}\mathbf{s}_\beta^{\perp} \end{bmatrix} \right\}, \tag{2.40}$$

where $\mathbf{s}_\beta : [0, 2\pi) \mapsto \mathcal{S}^1$ *is the map described by* $\mathbf{s}_\beta := [\cos\beta \ \ \sin\beta]^{\top}$, $\mathbf{s}_\beta^{\perp} := \mathcal{R}_{\pi/2}^{\top}\mathbf{s}_\beta$ *and* $\gamma \in \{0, -2\mathbf{z}_1(0)^{\top}{}^{\mathcal{B}}\mathbf{v}^{\perp}/||^{\mathcal{B}}\mathbf{v}||^2\}$.

Proof. Consider the initial condition $\mathbf{z}(0) \in \mathbb{R}^9$ and let $\mathbf{u} \in \mathbb{R}^4$ be such that is constant. Since the input is known and constant, (2.23) is an LTI system. Taking into account (2.28), the first two rows of the observability matrix associated with the system (2.23) are calculated by

$$\mathcal{O} = \begin{bmatrix} \mathbf{0} & \mathbf{0} & \mathbf{0} & 1 & 0 & 0 \\ -2^{\mathcal{B}}\mathbf{v}^{\top} & \mathbf{0} & \mathbf{0} & 0 & 0 & 0 \end{bmatrix} \tag{2.41}$$

and the following rows can be computed as $CA^j = \mathbf{0}$ for $j \in \{2, 3, ...\}$. Since the rank of (2.30) is 2, then the kernel of $\mathcal{O}$ is given by

$$\ker(\mathcal{O}) = \begin{bmatrix} {}^{\mathcal{B}}\mathbf{v}^{\perp} & \mathbf{0} & \mathbf{0} & \mathbf{0} & \mathbf{0} & \mathbf{0} & \mathbf{0} \\ \mathbf{0} & \mathbf{e}_x & \mathbf{e}_y & \mathbf{0} & \mathbf{0} & \mathbf{0} & \mathbf{0} \\ \mathbf{0} & \mathbf{0} & \mathbf{0} & \mathbf{e}_x & \mathbf{e}_y & \mathbf{0} & \mathbf{0} \\ 0 & 0 & 0 & 0 & 0 & 0 & 0 \\ 0 & 0 & 0 & 0 & 0 & 1 & 0 \\ 0 & 0 & 0 & 0 & 0 & 0 & 1 \end{bmatrix}. \tag{2.42}$$

Notice that the linear subspace generated by the $\ker(\mathcal{O})$ is of 7^{th} order and there are only five constraints in the initial conditions (2.24). Therefore, the unobservable subspace will depend on two free parameters, which implies that the set of indistinguishable initial conditions is given by a continuous of points and, hence, the system is not observable. To characterize this set, recall that all initial conditions of the form $\bar{\mathbf{z}}(0) = \mathbf{z}(0) + \ker(\mathcal{O})\boldsymbol{\alpha}$

with $\boldsymbol{\alpha} = [\alpha_1, \alpha_2, \alpha_3, \alpha_4, \alpha_5, \alpha_6, \alpha_7]^\top \in \mathbb{R}^7$, are indistinguishable from $\mathbf{z}_0$. Then

$$\begin{bmatrix} \bar{\mathbf{z}}_1(0) \\ \bar{\mathbf{z}}_2(0) \\ \bar{\mathbf{z}}_3(0) \\ \bar{z}_4(0) \\ \bar{z}_5(0) \\ \bar{z}_6(0) \end{bmatrix} = \begin{bmatrix} \mathbf{z}_1(0) + \alpha_1 {}^{\mathcal{B}}\mathbf{v}^{\perp} \\ \mathbf{z}_2(0) + \boldsymbol{\alpha}_a \\ \mathbf{z}_3(0) + \boldsymbol{\alpha}_b \\ z_4(0) \\ z_5(0) + \alpha_6 \\ z_6(0) + \alpha_7 \end{bmatrix}, \tag{2.43}$$

where $\boldsymbol{\alpha}_a = [\alpha_2, \alpha_3]^\top \in \mathbb{R}^2$ and $\boldsymbol{\alpha}_b = [\alpha_4, \alpha_5]^\top \in \mathbb{R}^2$. Recall that the initial conditions should satisfy the constraints given by (2.24). Since $\mathbf{z}_2 := \mathcal{R}_\psi^\top \mathbf{w}^\perp(x_2)$, then

$$\begin{aligned} \bar{\mathbf{z}}_2^\top(0)\bar{\mathbf{z}}_2(0) &= 1, \\ \boldsymbol{\alpha}_a &= -\mathbf{z}_2(0) + \mathbf{s}_\beta, \end{aligned} \tag{2.44}$$

where $\mathbf{s}_\beta = [\cos\beta, \sin\beta]^\top$ with $\beta \in [0, 2\pi)$. From the relation between $\mathbf{z}_2(0)$ and $\mathbf{z}_3(0)$ in (2.24) and using (2.32), it can be concluded that $\boldsymbol{\alpha}_b = \mathcal{R}_{\pi/2}^\top \boldsymbol{\alpha}_a$ Now, from (2.24)

$$\begin{aligned} \bar{z}_4(0) &= z_4(0), \\ \bar{\mathbf{z}}_1^\top(0)\bar{\mathbf{z}}_1(0) &= \mathbf{z}_1^\top(0)\mathbf{z}_1(0), \\ \left(\mathbf{z}_1(0) + \alpha_1 {}^{\mathcal{B}}\mathbf{v}^{\perp}\right)^\top \left(\mathbf{z}_1(0) + \alpha_1 {}^{\mathcal{B}}\mathbf{v}^{\perp}\right) &= \mathbf{z}_1^\top(0)\mathbf{z}_1(0), \\ \alpha_1(2\mathbf{z}_1^\top(0) {}^{\mathcal{B}}\mathbf{v}^{\perp} + \alpha_1 ||{}^{\mathcal{B}}\mathbf{v}||^2) &= 0. \end{aligned} \tag{2.45}$$

Here, either $\alpha_1 = 0$ or $\alpha_1 = -2\mathbf{z}_1^\top(0) {}^{\mathcal{B}}\mathbf{v}^{\perp} / ||{}^{\mathcal{B}}\mathbf{v}||^2$. Moreover, it is possible to obtain α_6 from the relation of $z_5(0)$ in (2.24) given by

$$\begin{aligned} \bar{z}_5(0) &= z_5(0) + \alpha_6, \\ \left(\mathbf{z}_1^\top(0) + \alpha_1 {}^{\mathcal{B}}\mathbf{v}^{\perp^\top}\right)\mathbf{s}_\beta &= z_5(0) + \alpha_6, \\ \alpha_6 &= -z_5(0) + \mathbf{z}_1^\top(0)\mathbf{s}_\beta + \alpha_1 {}^{\mathcal{B}}\mathbf{v}^{\perp^\top}\mathbf{s}_\beta. \end{aligned} \tag{2.46}$$

Following the same procedure for α_7, it follows that

$$\alpha_7 = -z_6(0) + \mathbf{z}_1^\top(0)\mathbf{s}_\beta^\perp + \alpha_1 {}^{\mathcal{B}}\mathbf{v}^{\perp^\top}\mathbf{s}_\beta^\perp. \tag{2.47}$$

Finally, the set of indistinguishable initial conditions is given by

$$\begin{bmatrix} \bar{\mathbf{z}}_1(0) \\ \bar{\mathbf{z}}_2(0) \\ \bar{\mathbf{z}}_3(0) \\ \bar{z}_4(0) \\ \bar{z}_5(0) \\ \bar{z}_6(0) \end{bmatrix} = \begin{bmatrix} \mathbf{z}_1(0) + \gamma {}^{\mathcal{B}}\mathbf{v}^{\perp} \\ \mathbf{s}_\beta \\ \mathbf{s}_\beta^\perp \\ z_4(0) \\ \mathbf{z}_1^\top(0)\mathbf{s}_\beta + \gamma {}^{\mathcal{B}}\mathbf{v}^{\perp^\top}\mathbf{s}_\beta \\ \mathbf{z}_1^\top(0)\mathbf{s}_\beta^\perp + \gamma {}^{\mathcal{B}}\mathbf{v}^{\perp^\top}\mathbf{s}_\beta^\perp \end{bmatrix},$$

with $\gamma \in \{0, -2\mathbf{z}_1^\top(0)^{\mathcal{B}}\mathbf{v}^\perp/||^{\mathcal{B}}\mathbf{v}||^2\}$. This completes the proof. □

The observability conditions given by the proposition 3, establish the set of indistinguishable initial conditions when the beacon and the vehicle are unknown. The following corollary states the observability properties when the information of the beacon's initial position is known.

Corollary 2. *Suppose that the initial condition of the beacon is known, then, the system is weakly observable.*

Proof. Since the beacon's initial position is known, that is ${}^{\mathcal{I}}\bar{\mathbf{b}}(0) = {}^{\mathcal{I}}\mathbf{b}(0)$, it implies that $\bar{\mathbf{z}}_2(0) = \mathbf{z}_2(0)$ and, hence, $\boldsymbol{\alpha}_a = \boldsymbol{\alpha}_b = \mathbf{0}$. Moreover, using the fact that $\bar{z}_4(0) = z_4(0)$, it can be obtained that $\alpha_1 \in \{0, -2\mathbf{z}_1^\top(0)^{\mathcal{B}}\mathbf{v}^\perp/||^{\mathcal{B}}\mathbf{v}||^2\}$. Additionally, it also implies that $\alpha_6 = \alpha_1 {}^{\mathcal{B}}\mathbf{v}^{\perp^\top}\mathbf{z}_2(0)$ and $\alpha_7 = \alpha_1 {}^{\mathcal{B}}\mathbf{v}^{\perp^\top}\mathbf{z}_3(0)$. Therefore, the set of indistinguishable initial conditions denoted by $\mathcal{I}(\mathbf{z}(0))$ is given by

$$\mathcal{I}(\mathbf{z}(0)) = \left\{ \mathbf{z}(0), \mathbf{z}(0) - 2\frac{\mathbf{z}_1^\top(0)^{\mathcal{B}}\mathbf{v}^\perp}{||^{\mathcal{B}}\mathbf{v}||^2} \begin{bmatrix} {}^{\mathcal{B}}\mathbf{v}^\perp \\ \mathbf{0} \\ \mathbf{0} \\ 0 \\ {}^{\mathcal{B}}\mathbf{v}^{\perp^\top}\mathbf{z}_2(0) \\ {}^{\mathcal{B}}\mathbf{v}^{\perp^\top}\mathbf{z}_3(0) \end{bmatrix} \right\}, \tag{2.48}$$

Notice that this set consists of only two isolated points, then it can be concluded that the system is weakly observable. This completes the proof. □

Notice that the observability properties stated in proposition 3 and corollary 2, both assume that the beacon does not move. While in the first, the set of indistinguishable initial conditions was a continuous of points, by knowing the initial conditions of the beacon, we could reduce it to just two points. It would be expected that by moving the beacon, a richer trajectory will be generated. Indeed, that is the case and the following proposition states the observability properties of the system assuming that the beacon rotates and the vehicle moves in straight lines.

Proposition 4 (VLBR). *Consider the system* (2.23) *with* $\mathbf{u} \in \mathbb{R}^4$ *fulfilling assumption 4. Further, suppose that the vehicle moves in straight lines (that is ,* (2.39) *holds) and the beacon rotates (that is,* (2.26) *holds). Then, the system* (2.23) *with the constraints in the initial conditions* (2.24) *is observable.*

Proof. Consider the initial condition $\mathbf{z}(0) \in \mathbb{R}^9$ and let $\mathbf{u} \in \mathbb{R}^4$ be constant. Since the input is known and constant, (2.23) is an LTI system. Taking into account (2.26) and (2.39), the first six rows of the observability matrix associated with the system (2.23) are given by

$$\mathcal{O} = \begin{bmatrix} \mathbf{0} & \mathbf{0} & \mathbf{0} & 1 & 0 & 0 \\ -2{}^{\mathcal{B}}\mathbf{v}^{\top} & \mathbf{0} & \mathbf{0} & 0 & 2l_m\omega_m & 0 \\ \mathbf{0} & -4l_m\omega_m{}^{\mathcal{B}}\mathbf{v}^{\top} & \mathbf{0} & 0 & 0 & -2l_m\omega_m^2 \\ \mathbf{0} & \mathbf{0} & 6l_m\omega_m^2{}^{\mathcal{B}}\mathbf{v}^{\top} & 0 & -2l_m\omega_m^3 & 0 \\ \mathbf{0} & 8l_m\omega_m{}^{\mathcal{B}}\mathbf{v}^{\top} & \mathbf{0} & 0 & 0 & 2l_m\omega_m^4 \\ \mathbf{0} & \mathbf{0} & -10l_m\omega_m^4{}^{\mathcal{B}}\mathbf{v}^{\top} & 0 & 2l_m\omega_m^5 & 0 \end{bmatrix} \tag{2.49}$$

and the following rows can be computed as $CA^j = -w_m^2(2CA^{j-2} + \omega_m^2 CA^{j-4})$ for $j \in \{6, 7, 8, ...\}$. Since the rank of (2.49) is 6, then the kernel $\mathcal{O}$ of the observability matrix is given by

$$\ker(\mathcal{O}) = \begin{bmatrix} {}^{\mathcal{B}}\mathbf{v}^{\perp} & \mathbf{0} & \mathbf{0} \\ \mathbf{0} & {}^{\mathcal{B}}\mathbf{v}^{\perp} & \mathbf{0} \\ \mathbf{0} & \mathbf{0} & {}^{\mathcal{B}}\mathbf{v}^{\perp} \\ 0 & 0 & 0 \\ 0 & 0 & 0 \\ 0 & 0 & 0 \end{bmatrix}. \tag{2.50}$$

Recall that unobservable space is given by all initial conditions of the form $\bar{\mathbf{z}}(0) = \mathbf{z}(0) + \ker(\mathcal{O})\boldsymbol{\alpha}$ with $\boldsymbol{\alpha} = [\alpha_1, \alpha_2, \alpha_3]^{\top} \in \mathbb{R}^3$, are indistinguishable from $\mathbf{z}_0$. Then

$$\begin{bmatrix} \bar{\mathbf{z}}_1(0) \\ \bar{\mathbf{z}}_2(0) \\ \bar{\mathbf{z}}_3(0) \\ \bar{z}_4(0) \\ \bar{z}_5(0) \\ \bar{z}_6(0) \end{bmatrix} = \begin{bmatrix} \mathbf{z}_1(0) + \alpha_1{}^{\mathcal{B}}\mathbf{v}^{\perp} \\ \mathbf{z}_2(0) + \alpha_2{}^{\mathcal{B}}\mathbf{v}^{\perp} \\ \mathbf{z}_3(0) + \alpha_3{}^{\mathcal{B}}\mathbf{v}^{\perp} \\ z_4(0) \\ z_5(0) \\ z_6(0) \end{bmatrix}. \tag{2.51}$$

Moreover, since the initial conditions should satisfy the constraint given by (2.24), then $\bar{\mathbf{z}}_3(0) = \mathcal{R}_{\pi/2}^{\top}\bar{\mathbf{z}}_2(0)$, implies that $\alpha_3{}^{\mathcal{B}}\mathbf{v}^{\perp} - \alpha_2{}^{\mathcal{B}}\mathbf{v} = \mathbf{0}$. Since both vectors (${}^{\mathcal{B}}\mathbf{v}^{\perp}$ and ${}^{\mathcal{B}}\mathbf{v}$)

are orthogonal, then $\alpha_2 = \alpha_3 = 0$. From the relation $\bar{z}_5(0) = z_5(0)$, it follows that

$$\begin{aligned}
\left(\mathbf{z}_1(0) + \alpha_1 {}^{\mathcal{B}}\mathbf{v}^{\perp}\right)^{\top} \mathbf{z}_2(0) &= \mathbf{z}_1^{\top}(0)\mathbf{z}_2(0), \\
\alpha_1 \mathbf{z}_2^{\top}(0) {}^{\mathcal{B}}\mathbf{v}^{\perp} &= 0, \\
\alpha_1 ||\mathbf{z}_2^{\top}(0)||\ ||{}^{\mathcal{B}}\mathbf{v}^{\perp}|| \cos\theta &= 0, \\
\alpha_1 \cos\theta &= 0,
\end{aligned} \tag{2.52}$$

where θ is the angle between $\mathbf{z}_2^{\top}(0)$ and ${}^{\mathcal{B}}\mathbf{v}^{\perp}$. Following the same procedure for $\bar{z}_6(0) = z_6(0)$, leads to the same equation (2.52). Then $\alpha_1 = 0$ or $\mathbf{z}_2^{\top}(0) \perp {}^{\mathcal{B}}\mathbf{v}^{\perp}$. Since $\alpha_1 = \alpha_2 = \alpha_3 = 0$, then $\bar{\mathbf{z}}(0) = \mathbf{z}(0)$ and the system is observable. This completes the proof.

□

Remark 2. *Notice, that if the system without the knowledge of the beacon's initial condition is observable, then the system will be observable with the additional information of the beacon's position.*

2.5.3. Vehicle does not move

In the previous sections, the observability analysis was carried out assuming that the vehicle was moving forward but without rotation. Here, the observability of the system will be analyzed assuming that the vehicle does not move, that is $||{}^{\mathcal{B}}\mathbf{v}|| = 0$, while beacon can be rotating or not.

The case when both are not moving is trivial. Since neither the vehicle nor the beacon are generating richer trajectories, the system will not be observable. Therefore the observability analysis in this section is carried out by assuming that the beacon rotates. For more information related with the observability analysis when the beacon is not rotating, see Appendix A.2. for more information.

The following proposition states the observability properties of the system assuming that the beacon rotates and the vehicle does not move.

Proposition 5 (VNBR). *Consider the system (2.23) with $\mathbf{u} \in \mathbb{R}^4$ fulfilling assumption 4. Further, suppose that the vehicle does not move, that is,*

$$||{}^{\mathcal{B}}\mathbf{v}|| = 0; \tag{2.53}$$

and the beacon rotates (that is, (2.26) hold). Then, the system (2.23) with the constraints in the initial conditions (2.24) is not observable. Moreover, for every $\mathbf{z}(0) \in \mathbb{R}^9$*, the set of all indistinguishable initial conditions, denoted as* $\mathcal{I}(\mathbf{z}(0))$*, is given by*

$$\mathcal{I}(\mathbf{z}(0)) = \left\{ \mathbf{z}(0), \begin{bmatrix} \frac{1}{2}||\mathbf{z}_1(0)+\mathbf{z}_2(0)||\mathbf{s}_\alpha + \frac{1}{2}||\mathbf{z}_1(0)-\mathbf{z}_2(0)||\mathbf{s}_\beta \\ \frac{1}{2}||\mathbf{z}_1(0)+\mathbf{z}_2(0)||\mathbf{s}_\alpha - \frac{1}{2}||\mathbf{z}_1(0)-\mathbf{z}_2(0)||\mathbf{s}_\beta \\ \frac{1}{2}||\mathbf{z}_1(0)+\mathbf{z}_2(0)||\mathbf{s}_\alpha^\perp - \frac{1}{2}||\mathbf{z}_1(0)-\mathbf{z}_2(0)||\mathbf{s}_\beta^\perp \\ z_4(0) \\ z_5(0) \\ z_6(0) \end{bmatrix} \right\}, \tag{2.54}$$

where $\mathbf{s}_\gamma : [0, 2\pi) \mapsto \mathcal{S}^1$ *is the map described by* $\mathbf{s}_\gamma := [\cos\gamma \ \ \sin\gamma]^\top$*,* $\mathbf{s}_\gamma^\perp := \mathcal{R}_{\pi/2}^\top \mathbf{s}_\gamma$*, and* $\alpha = \cos^{-1}\left(\left(\frac{\mathbf{z}_1(0)+\mathbf{z}_2(0)}{||\mathbf{z}_1(0)+\mathbf{z}_2(0)||}\right)^\top \left(\frac{\mathbf{z}_1(0)-\mathbf{z}_2(0)}{||\mathbf{z}_1(0)-\mathbf{z}_2(0)||}\right)\right) + \beta$ *.*

Proof. Consider the initial condition $\mathbf{z}(0) \in \mathbb{R}^9$ and let $\mathbf{u} \in \mathbb{R}^4$ be constant. Since the input is known and constant, (2.23) becomes in an LTI system. Moreover, since the vehicle does not move ($||^{\mathcal{B}}\mathbf{v}|| = 0$), the first three rows of the observability matrix associated with the system (2.23) are given by

$$\mathcal{O} = \begin{bmatrix} \mathbf{0} & \mathbf{0} & \mathbf{0} & 1 & 0 & 0 \\ \mathbf{0} & \mathbf{0} & \mathbf{0} & 0 & 2l_m\omega_m & 0 \\ \mathbf{0} & \mathbf{0} & \mathbf{0} & 0 & 0 & -2l_m\omega_m^2 \end{bmatrix} \tag{2.55}$$

and the following rows can be computed as $CA^j = -w_m^2(CA^{j-2})$ for $j \in \{3, 4, 5, ...\}$. Notice, that the rank of (2.55) is 3, then the kernel of the observability matrix $\mathcal{O}$ is given by

$$\ker(\mathcal{O}) = \begin{bmatrix} \mathbf{e}_x & \mathbf{e}_y & \mathbf{0} & \mathbf{0} & \mathbf{0} & \mathbf{0} \\ \mathbf{0} & \mathbf{0} & \mathbf{e}_x & \mathbf{e}_y & \mathbf{0} & \mathbf{0} \\ 0 & 0 & 0 & 0 & \mathbf{e}_x & \mathbf{e}_y \\ 0 & 0 & 0 & 0 & 0 & 0 \\ 0 & 0 & 0 & 0 & 0 & 0 \\ 0 & 0 & 0 & 0 & 0 & 0 \end{bmatrix}. \tag{2.56}$$

Recall that the unobservable space is given by all initial conditions of the form $\bar{\mathbf{z}}(0) = \mathbf{z}(0) + \ker(\mathcal{O})\boldsymbol{\alpha}$ with $\boldsymbol{\alpha} = [\alpha_1, \alpha_2, \alpha_3, \alpha_4, \alpha_5, \alpha_6]^\top \in \mathbb{R}^6$, which are indistinguishable from

$\mathbf{z}(0)$. Then

$$\begin{bmatrix} \bar{\mathbf{z}}_1(0) \\ \bar{\mathbf{z}}_2(0) \\ \bar{\mathbf{z}}_3(0) \\ \bar{z}_4(0) \\ \bar{z}_5(0) \\ \bar{z}_6(0) \end{bmatrix} = \begin{bmatrix} \mathbf{z}_1(0) + \boldsymbol{\alpha}_a \\ \mathbf{z}_2(0) + \boldsymbol{\alpha}_b \\ \mathbf{z}_3(0) + \boldsymbol{\alpha}_c \\ z_4(0) \\ z_5(0) \\ z_6(0) \end{bmatrix}, \tag{2.57}$$

where $\boldsymbol{\alpha}_a := [\alpha_1, \alpha_2]^\top$, $\boldsymbol{\alpha}_b := [\alpha_3, \alpha_4]^\top$, and $\boldsymbol{\alpha}_c := [\alpha_5, \alpha_6]^\top$. Recall that the initial conditions should satisfy the constraints given by (2.24). Since $\mathbf{z}_2 := \mathcal{R}_\psi^\top \mathbf{w}^\perp(x_2)$, then $\boldsymbol{\alpha}_b$ fulfills the equation $||\boldsymbol{\alpha}_b + \mathbf{z}_2(0)||^2 = 1$. From the relation between $\mathbf{z}_2(0)$ and $\mathbf{z}_3(0)$ in (2.24) and using (2.57), it can be concluded that $\boldsymbol{\alpha}_c = \mathcal{R}_{\pi/2}^\top \boldsymbol{\alpha}_b$. Further, since $\bar{z}_4(0) = z_4(0)$ and $\bar{z}_5(0) = z_5(0)$, it follows that $||\boldsymbol{\alpha}_a + \mathbf{z}_1(0)||^2 = ||\mathbf{z}_1(0)||^2$ and $\boldsymbol{\alpha}_a^\top \boldsymbol{\alpha}_b + \boldsymbol{\alpha}_a^\top \mathbf{z}_2(0) + \boldsymbol{\alpha}_b^\top \mathbf{z}_1(0) = 0$ respectively. Gathering all three equations, we have that

$$\left.\begin{aligned} ||\boldsymbol{\alpha}_a + \mathbf{z}_1(0)||^2 &= ||\mathbf{z}_1(0)||^2, \\ ||\boldsymbol{\alpha}_b + \mathbf{z}_2(0)||^2 &= 1, \\ \boldsymbol{\alpha}_a^\top \boldsymbol{\alpha}_b + \boldsymbol{\alpha}_a^\top \mathbf{z}_2(0) + \boldsymbol{\alpha}_b^\top \mathbf{z}_1(0) &= 0. \end{aligned}\right\} \tag{2.58}$$

Notice that the are four variables ($\boldsymbol{\alpha}_a$ and $\boldsymbol{\alpha}_b$) but just three equations, therefore the solution of (2.58) has one free parameter, which implies that the system is not observable. Moreover, the solution of (2.58) (To see the details in the procedure, go to Appendix A.3.) is given by

$$\left.\begin{aligned} \boldsymbol{\alpha}_a &= -\mathbf{z}_1(0) + \frac{1}{2}||\mathbf{z}_1(0) + \mathbf{z}_2(0)||\mathbf{s}_\alpha + \frac{1}{2}||\mathbf{z}_1(0) - \mathbf{z}_2(0)||\mathbf{s}_\beta, \\ \boldsymbol{\alpha}_b &= -\mathbf{z}_2(0) + \frac{1}{2}||\mathbf{z}_1(0) + \mathbf{z}_2(0)||\mathbf{s}_\alpha - \frac{1}{2}||\mathbf{z}_1(0) - \mathbf{z}_2(0)||\mathbf{s}_\beta, \end{aligned}\right\} \tag{2.59}$$

where $\beta \in [0, 2\pi)$ and $\alpha = \cos^{-1}\left(\left(\frac{\mathbf{z}_1(0)+\mathbf{z}_2(0)}{||\mathbf{z}_1(0)+\mathbf{z}_2(0)||}\right)^\top \left(\frac{\mathbf{z}_1(0)-\mathbf{z}_2(0)}{||\mathbf{z}_1(0)-\mathbf{z}_2(0)||}\right)\right) + \beta$.

Then, the set of indistinguishable initial conditions is described by

$$\begin{bmatrix} \bar{\mathbf{z}}_1(0) \\ \bar{\mathbf{z}}_2(0) \\ \bar{\mathbf{z}}_3(0) \\ \bar{z}_4(0) \\ \bar{z}_5(0) \\ \bar{z}_6(0) \end{bmatrix} = \begin{bmatrix} \frac{1}{2}||\mathbf{z}_1(0) + \mathbf{z}_2(0)||\mathbf{s}_\alpha + \frac{1}{2}||\mathbf{z}_1(0) - \mathbf{z}_2(0)||\mathbf{s}_\beta \\ \frac{1}{2}||\mathbf{z}_1(0) + \mathbf{z}_2(0)||\mathbf{s}_\alpha - \frac{1}{2}||\mathbf{z}_1(0) - \mathbf{z}_2(0)||\mathbf{s}_\beta \\ \frac{1}{2}||\mathbf{z}_1(0) + \mathbf{z}_2(0)||\mathbf{s}_\alpha^\perp - \frac{1}{2}||\mathbf{z}_1(0) - \mathbf{z}_2(0)||\mathbf{s}_\beta^\perp \\ z_4(0) \\ z_5(0) \\ z_6(0) \end{bmatrix},$$

with $\beta \in [0, 2\pi)$ and $\alpha = \cos^{-1}\left(\left(\frac{\mathbf{z}_1(0)+\mathbf{z}_2(0)}{||\mathbf{z}_1(0)+\mathbf{z}_2(0)||}\right)^\top \left(\frac{\mathbf{z}_1(0)-\mathbf{z}_2(0)}{||\mathbf{z}_1(0)-\mathbf{z}_2(0)||}\right)\right) + \beta$. This completes the proof. □

The observability conditions, given by the proposition 5, establish the set of indistinguishable initial conditions when the beacon and vehicle initial positions are unknown. The following corollary, states the observability properties when the initial position of the beacon is known a priori.

Corollary 3. *Suppose that the initial condition of the beacon is known. Then, the system is observable.*

Proof. Since the beacon's initial position is known, that is ${}^{\mathcal{I}}\bar{\mathbf{b}}(0) = {}^{\mathcal{I}}\mathbf{b}(0)$, it implies that $\bar{\mathbf{z}}_2(0) = \mathbf{z}_2(0)$ and $\bar{\mathbf{z}}_3(0) = \mathbf{z}_3(0)$; and hence $\boldsymbol{\alpha}_b = \boldsymbol{\alpha}_c = \mathbf{0}$. Since $\bar{z}_5(0) = z_5(0)$ and $\bar{z}_6(0) = z_6(0)$, it implies that $\boldsymbol{\alpha}_a^\top \mathbf{z}_2(0) = 0$ and $\boldsymbol{\alpha}_a^\top \mathbf{z}_3(0) = 0$. Since $\mathbf{z}_2(0) \perp \mathbf{z}_3(0)$, it implies that $\boldsymbol{\alpha}_a = \mathbf{0}$. Then, the set of indistinguishable initial conditions is given by $\mathcal{I}(\mathbf{z}(0)) = \{\mathbf{z}(0)\}$ and the system is observable. This completes the proof. □

2.5.4. Simulation Results

To illustrate the different sets of indistinguishable initial conditions, three examples have been implemented in Matlab$^{\text{TM}}$; which is a high-performance language developed by MathWorks. This section presents the simulations results for different conditions:

- *Scenario 1*: the vehicle moves in circles and the beacon does not move. This corresponds to Proposition 2. Notice that in this case, there is a continuous of points that are indistinguishable between them. The initial position and orientation of the vehicle are ${}^{\mathcal{I}}\mathbf{p}(0) = [10, 5]^\top$ m and $\psi(0) = \pi/4$, respectively. The manipulator's length is set to $l_m = 2$ m and the initial angle to $\chi(0) = \pi/3$, which implies that ${}^{\mathcal{I}}\mathbf{b}(0) = [1.00, 1.73]^\top$ m. The linear and angular velocity of the vehicle are given by ${}^{\mathcal{B}}\mathbf{v} = [2.1, 0.3]^\top$ m/s and $r = 0.2$ rad/s, respectively. The beacon does not move, that is, $\omega_m = 0$ rad/s. Recall that the set of indistinguishable initial conditions in the original coordinate frame is given by the equations (2.37) and (2.38). Then, by choosing for example $\gamma = \chi(0) + \pi/2$, a pair of indistinguishable initial conditions is given by ${}^{\mathcal{I}}\bar{\mathbf{b}}(0) = [-1.73, 1.00]^\top$ m and ${}^{\mathcal{I}}\bar{\mathbf{p}}(0) = [7.26, 4.26]^\top$ m.

  Simulation results are shown in Figure 7. Figure 7(a) shows two different

initial conditions that are indistinguishable. Although the initial conditions are different, the output trajectory is the same (see Figure 7(b)). Furthermore, once the beacon's position is known, the dashed black circle disappear and the system is observable (as it was proved in Corollary 1).

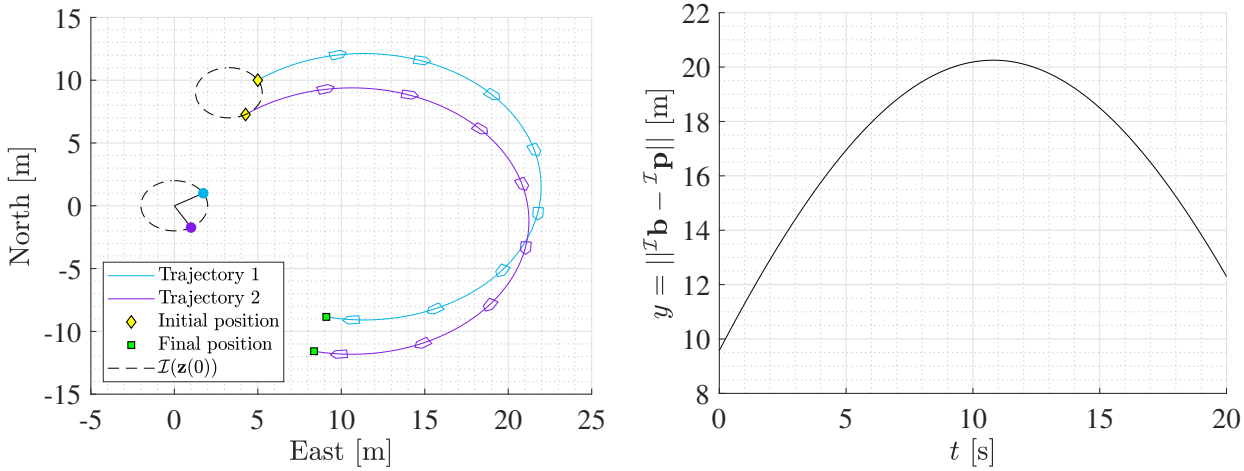

(a) (b)

Figure 7: Simulation results for two different initial conditions in VCBN scenario without taking into account ocean currents. Every initial condition in the black dashed line will be indistinguishable.

- *Scenario 2*: the vehicle moves in straight lines and the beacon does not rotate. Nevertheless, the beacon's position is known a priori. This corresponds to Corollary **??**. For this particular case, there are just two isolated points given by (2.48). Applying a state transformation to recover the state in the original coordinate frame, it yields

$$\begin{aligned} {}^{\mathcal{I}}\bar{\mathbf{p}}(0) &= {}^{\mathcal{I}}\mathbf{b}(0) - {}^{\mathcal{I}}\bar{\mathbf{d}}(0), \\ &= {}^{\mathcal{I}}\mathbf{b}(0) - \mathcal{R}_{\psi_0}\bar{\mathbf{z}}_1(0), \\ &= {}^{\mathcal{I}}\mathbf{b}(0) - \mathcal{R}_{\psi_0}\left(I_2 - 2\frac{{}^{\mathcal{B}}\mathbf{v}^{\perp}\ {}^{\mathcal{B}}\mathbf{v}^{\perp\top}}{||{}^{\mathcal{B}}\mathbf{v}||^2}\right)\mathbf{z}_1(0), \\ &= {}^{\mathcal{I}}\mathbf{b}(0) - \left(I_2 - 2\frac{{}^{\mathcal{B}}\mathbf{v}^{\perp}\ {}^{\mathcal{B}}\mathbf{v}^{\perp\top}}{||{}^{\mathcal{B}}\mathbf{v}||^2}\right){}^{\mathcal{I}}\mathbf{d}(0). \end{aligned} \tag{2.60}$$

In this case, the initial position and orientation of the vehicle are ${}^{\mathcal{I}}\mathbf{p}(0) = [5, 10]^{\top}$ m and $\psi(0) = 0$, respectively. The manipulator's length and initial angle

are the same that in the first scenario, which implies that ${}^{\mathcal{I}}\mathbf{b}(0) = [1.00, 1.73]^\top$. The linear velocity of the vehicle is given by ${}^{\mathcal{B}}\mathbf{v} = [2.1, 0]^\top$ m/s. The angular rate of the vehicle and beacon were set up to zero, that is, $r = 0$ and $w_m = 0$ rad/s. Once the velocity is set up, the other indistinguishable initial condition is given by ${}^{\mathcal{I}}\bar{\mathbf{p}}(0) = [5.00, -6.54]^\top$ m, which fulfills the condition (2.60). Simulation results are shown in Figure 8. Figure 7(a) shows two different initial conditions that are indistinguishable. Although the initial conditions are different, the output trajectory is the same (see Figure 8(b)). Since these point are isolated, the system is weakly observable.

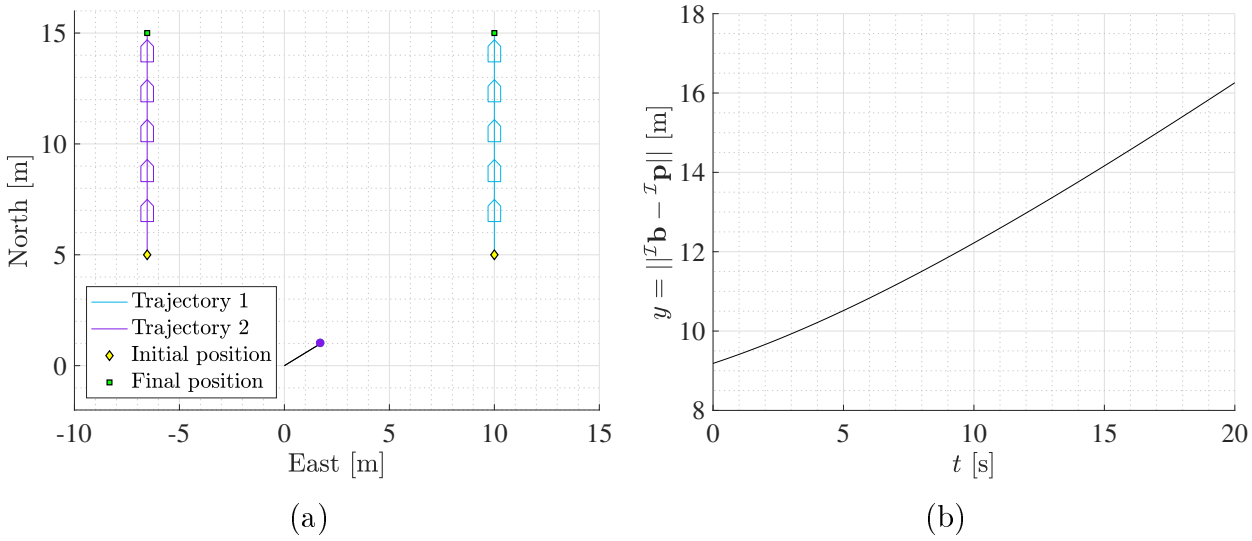

(a) (b)

Figure 8: Simulation results for two different initial conditions in VLBN scenario without taking into account ocean currents. The beacon's initial position is known, therefore there just two isolated indistinguishable initial conditions.

- *Scenario 3*: the vehicle moves in straight lines and the beacon does not move at the begining, with the same inputs and initial conditions of the previous scenario. At $t = 10$ s, the beacon starts moving with angular velocity $\omega_m = 0.3$ rad/s, while the vehicle does not change its trajectory. The key idea behind this example is to illustrate how by moving the beacon, the two indistinguishable trajectories go in different directions, allowing one to distinguish between both initial conditions.

  Simulation results are shown in Figure 9. Figure 9(a) shows two different initial conditions of the vehicle that are indistinguishable since the beacon is not moving. Once the beacon starts moving at $t = 10$ s, both trajectories become

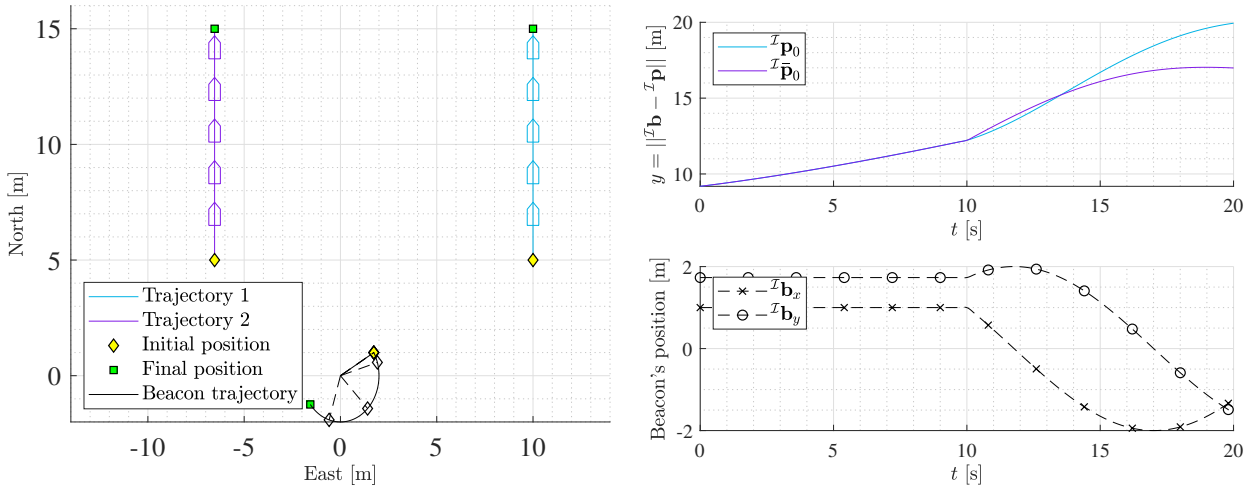

(a) (b)

Figure 9: Simulation results for a combination of trajectories without taking into account ocean currents. The beacon's initial position is known, therefore there just two isolated indistinguishable initial conditions. Once the beacon start moving both trajectories can be distinguish and hence the two initial conditions.

distinguishable between them (see Figure 9(b)).

2.6. OBSERVABILITY ANALYSIS WITH OCEAN CURRENT

Up to this point, the observability analysis was carried without taking into account a model for the ocean currents affecting the vehicle. Now, consider the system (2.11), and using the information of the depth for the vehicle and beacon, the system (2.11) can be rewritten in 2D as

$$\left.\begin{aligned} {}^{\mathcal{I}}\dot{\mathbf{p}}(t) &= {}^{\mathcal{I}}_{\mathcal{B}}\mathcal{R}(\psi(t)){}^{\mathcal{B}}\mathbf{v}(t) + {}^{\mathcal{I}}\mathbf{v}_c(t) \\ {}^{\mathcal{I}}\dot{\mathbf{v}}_c(t) &= 0 \\ {}^{\mathcal{I}}\dot{\mathbf{b}}(t) &= l_m\omega_m\mathbf{w}^{\perp}\left(\chi(t)\right) \\ \dot{\chi}(t) &= \omega_m \\ d_{r_{xy}}(t) &= ||{}^{\mathcal{I}}\mathbf{b}(t) - {}^{\mathcal{I}}\mathbf{p}(t)|| \end{aligned}\right\}, \tag{2.61}$$

where ${}^{\mathcal{I}}\mathbf{p}$, ${}^{\mathcal{B}}\mathbf{v}$, ${}^{\mathcal{I}}\mathbf{v}_c$, ${}^{\mathcal{I}}\mathbf{b} \in \mathbb{R}^2$, ${}^{\mathcal{I}}_{\mathcal{B}}\mathcal{R} \in \mathcal{SO}(2)$, and the vectors $\mathbf{w}(\cdot)$ and $\mathbf{w}^{\perp}(\cdot)$ are properly redefined in $\mathbb{R}^2$. Using the same approach described by Figure 5, first the system will be expressed in the $\mathcal{B}$-frame. Taking the time derivative of (2.19) and using the relations in (2.61), it is possible to describe the system in the $\{\mathcal{B}\}$ as follows

$$ {}^{\mathcal{B}}\dot{\mathbf{d}} = -S(r){}^{\mathcal{B}}\mathbf{d} - {}^{\mathcal{B}}\mathbf{v} + l_m\omega_m\mathcal{R}_{\psi}^{\top}\mathbf{w}^{\perp}(\chi) - {}^{\mathcal{B}}\mathbf{v}_c. \tag{2.62} $$

Additionally, since ${}^{\mathcal{B}}\mathbf{v}_c = \mathcal{R}_{\psi}^{\top}{}^{\mathcal{I}}\mathbf{v}_c$, then, the time derivative of the current is given by

$$ {}^{\mathcal{B}}\dot{\mathbf{v}}_c = -S(r){}^{\mathcal{B}}\mathbf{v}_c. \tag{2.63} $$

To summarize, the system is completely described in the $\{\mathcal{B}\}$-frame by the following set of equations

$$ \left.\begin{aligned} {}^{\mathcal{B}}\dot{\mathbf{d}} &= -S(r){}^{\mathcal{B}}\mathbf{d} - {}^{\mathcal{B}}\mathbf{v} + l_m\omega_m\mathcal{R}_{\psi}^{\top}\mathbf{w}^{\perp}(\chi) - {}^{\mathcal{B}}\mathbf{v}_c \\ {}^{\mathcal{B}}\dot{\mathbf{v}}_c &= -S(r){}^{\mathcal{B}}\mathbf{v}_c \\ \dot{\chi} &= \omega_m \end{aligned}\right\}, \tag{2.64} $$

with state variable $\mathbf{x} = [{}^{\mathcal{B}}\mathbf{d}, {}^{\mathcal{B}}\mathbf{v}_c, \chi]^{\top} \in \mathbb{R}^4 \times [0, 2\pi)$. The output equation is given by

$$ d_{r_{xy}}^2 = {}^{\mathcal{B}}\mathbf{d}^{\top}{}^{\mathcal{B}}\mathbf{d}. \tag{2.65} $$

Notice that the next step in Figure 5, is to apply a state augmentation to transform the system into a linear one with respect to the state variables. To that end, let us define the following state-space augmentation $\mathbf{z} := [\mathbf{z}_1, \mathbf{z}_2, \mathbf{z}_3, \mathbf{z}_4, z_5, z_6, z_7, z_8, z_9, z_{10}, z_{11}] := [{}^{\mathcal{B}}\mathbf{d}, {}^{\mathcal{B}}\mathbf{v}_c, \mathcal{R}_{\psi}^{\top}\mathbf{w}^{\perp}(\chi), \mathcal{R}_{\pi/2}^{\top}\mathbf{z}_3, \mathbf{z}_1^{\top}\mathbf{z}_1, \mathbf{z}_1^{\top}\mathbf{z}_2, \mathbf{z}_1^{\top}\mathbf{z}_3, \mathbf{z}_1^{\top}\mathbf{z}_4, \mathbf{z}_2^{\top}\mathbf{z}_2, \mathbf{z}_2^{\top}\mathbf{z}_3, \mathbf{z}_2^{\top}\mathbf{z}_4]$. Then, the system (2.64) can be transformed into a linear one (for a detailed step by step of this procedure, see Appendix A.4.) with state variable $\mathbf{z} \in \mathbb{R}^{15}$, input vector $\mathbf{u} = [{}^{\mathcal{B}}\mathbf{v}^{\top}, \omega_m, r] \in \mathbb{R}^4$, and output $y \in \mathbb{R}$ as

$$ \left.\begin{aligned} \dot{\mathbf{z}} &= A(\mathbf{u})\mathbf{z} + B\mathbf{u} \\ y &= C\mathbf{z} \end{aligned}\right\} \tag{2.66} $$

where

$$A(\mathbf{u}) = \begin{bmatrix} -S(r) & -I_2 & l_m\omega_m I_2 & \mathbf{0} & \mathbf{0} & \mathbf{0} & \mathbf{0} & \mathbf{0} & \mathbf{0} & \mathbf{0} & \mathbf{0} \\ \mathbf{0} & -S(r) & \mathbf{0} & \mathbf{0} & \mathbf{0} & \mathbf{0} & \mathbf{0} & \mathbf{0} & \mathbf{0} & \mathbf{0} & \mathbf{0} \\ \mathbf{0} & \mathbf{0} & -S(r) & -\omega_m I_2 & \mathbf{0} & \mathbf{0} & \mathbf{0} & \mathbf{0} & \mathbf{0} & \mathbf{0} & \mathbf{0} \\ \mathbf{0} & \mathbf{0} & \omega_m I_2 & -S(r) & \mathbf{0} & \mathbf{0} & \mathbf{0} & \mathbf{0} & \mathbf{0} & \mathbf{0} & \mathbf{0} \\ -2^{\mathcal{B}}\mathbf{v}^\top & \mathbf{0} & \mathbf{0} & \mathbf{0} & 0 & -2 & 2l_m\omega_m & 0 & 0 & 0 & 0 \\ \mathbf{0} & -^{\mathcal{B}}\mathbf{v}^\top & \mathbf{0} & \mathbf{0} & 0 & 0 & 0 & 0 & -1 & l_m\omega_m & 0 \\ \mathbf{0} & \mathbf{0} & -^{\mathcal{B}}\mathbf{v}^\top & \mathbf{0} & 0 & 0 & 0 & -\omega_m & 0 & -1 & 0 \\ \mathbf{0} & \mathbf{0} & \mathbf{0} & -^{\mathcal{B}}\mathbf{v}^\top & 0 & 0 & \omega_m & 0 & 0 & 0 & -1 \\ \mathbf{0} & \mathbf{0} & \mathbf{0} & \mathbf{0} & 0 & 0 & 0 & 0 & 0 & 0 & 0 \\ \mathbf{0} & \mathbf{0} & \mathbf{0} & \mathbf{0} & 0 & 0 & 0 & 0 & 0 & 0 & -\omega_m \\ \mathbf{0} & \mathbf{0} & \mathbf{0} & \mathbf{0} & 0 & 0 & 0 & 0 & 0 & \omega_m & 0 \end{bmatrix},$$

$$B = \begin{bmatrix} -I_2 & \mathbf{0} & \mathbf{0} \\ \mathbf{0} & \mathbf{0} & \mathbf{0} \\ \mathbf{0} & \mathbf{0} & \mathbf{0} \\ \mathbf{0} & \mathbf{0} & \mathbf{0} \\ \mathbf{0} & 0 & 0 \\ \mathbf{0} & 0 & 0 \\ \mathbf{0} & l_m & 0 \\ \mathbf{0} & 0 & 0 \\ \mathbf{0} & 0 & 0 \\ \mathbf{0} & 0 & 0 \\ \mathbf{0} & 0 & 0 \end{bmatrix},$$

$$C = \begin{bmatrix} \mathbf{0} & \mathbf{0} & \mathbf{0} & \mathbf{0} & 1 & 0 & 0 & 0 & 0 & 0 & 0 \end{bmatrix},$$

and the initial conditions satisfying

$$\begin{bmatrix} \mathbf{z}_1(0) \\ \mathbf{z}_2(0) \\ \mathbf{z}_3(0) \\ \mathbf{z}_4(0) \\ z_5(0) \\ z_6(0) \\ z_7(0) \\ z_8(0) \\ z_9(0) \\ z_{10}(0) \\ z_{11}(0) \end{bmatrix} := \begin{bmatrix} {}^{\mathcal{B}}\mathbf{d}(0) \\ {}^{\mathcal{B}}\mathbf{v}_c(0) \\ \mathcal{R}_{\psi_0}^{\top}\mathbf{w}^{\perp}(\chi(0)) \\ \mathcal{R}_{\pi/2}^{\top}\mathbf{z}_3(0) \\ \mathbf{z}_1(0)^{\top}\mathbf{z}_1(0) \\ \mathbf{z}_1(0)^{\top}\mathbf{z}_2(0) \\ \mathbf{z}_1(0)^{\top}\mathbf{z}_3(0) \\ \mathbf{z}_1(0)^{\top}\mathbf{z}_4(0) \\ \mathbf{z}_2(0)^{\top}\mathbf{z}_2(0) \\ \mathbf{z}_2(0)^{\top}\mathbf{z}_3(0) \\ \mathbf{z}_2(0)^{\top}\mathbf{z}_4(0) \end{bmatrix} \tag{2.67}$$

Based on assumption 4, system (2.66) can be analyzed as an LTI system, since $A(\mathbf{u})$ is constant and known. Further, recall that the observability analysis is carried out for the class of maneuvers generated by assumption 4.

2.6.1. Vehicle moving in circles

Here, the observability of the system is analyzed assuming that the vehicle is moving in circles, that is, $r \neq 0$ and $||{}^{\mathcal{B}}\mathbf{v}|| \neq 0$, while the beacon can be rotating or not. First, we will establish the observability properties of the system (2.66) given that the beacon is rotating.

Proposition 6. *Consider system* (2.66) *with* $\mathbf{u} \in \mathbb{R}^4$ *fulfilling assumption 4. Further, suppose that the vehicle moves in circles, that is,*

$$||{}^{\mathcal{B}}\mathbf{v}|| \neq 0, r \neq 0, \tag{2.68}$$

and the beacon rotates with angular rate

$$\omega_m \neq 0 \neq \pm r \neq \pm 2r \neq \pm\frac{1}{2}r. \tag{2.69}$$

Then, the system (2.66) *is observable.*

Proof. Consider the initial condition $\mathbf{z}(0) \in \mathbb{R}^{15}$ and let $\mathbf{u} \in \mathbb{R}^4$ be constant. Since the input is known and constant, (2.66) is an LTI system. The observability matrix

associated with the system (2.66) is defined by $\mathcal{O} = [C, CA, ..., CA^{n-1}]^\top$ with $n \in \{1, 2, .., 15\}$ and the determinant is given by

$$\det(\mathcal{O}) = -1048576 r^{18} \omega_m^{26} l_m^8 ||^{\mathcal{B}}\mathbf{v}||^6 (r^2 - \omega_m^2)^{15} (r^2 - 4\omega_m^2)^4 (4r^2 - \omega_m^2)^4.$$

Note that if (2.68) and (2.69) hold, then $\det(\mathcal{O}) \neq 0$, which implies that the observability matrix is full rank and therefore system (2.66) is observable. This completes the proof. □

Notice that by rotating the beacon and moving the vehicle in circles, the system is observable. Now, since there are constraints in the initial conditions, it is important to analyze the observability properties of the system given (2.68) or (2.69) do not hold. For instance, the following proposition establishes it when the beacon is not rotating, that is, $\omega_m = 0$.

Proposition 7. *Consider system (2.66) with $\mathbf{u} \in \mathbb{R}^4$ fulfilling assumption 4. Further, suppose that the vehicle moves in circles ((2.68) holds) and the beacon does not move, that is,*

$$\omega_m = 0. \tag{2.70}$$

Then, the system (2.66) with the constraints in the initial conditions (2.67) is not observable. Moreover, for every $\mathbf{z}(0) \in \mathbb{R}^{15}$, the set of all indistinguishable initial conditions denoted by $\mathcal{I}(\mathbf{z}(0))$ is given by

$$\mathcal{I}(\mathbf{z}(0)) = \left\{ \mathbf{z}(0), \begin{bmatrix} \mathbf{z}_1(0) \\ \mathbf{z}_2(0) \\ \mathbf{s}_\beta \\ \mathbf{s}_\beta^\perp \\ z_5(0) \\ z_6(0) \\ \mathbf{z}_1^\top(0)\mathbf{s}_\beta \\ \mathbf{z}_1^\top(0)\mathbf{s}_\beta^\perp \\ z_9(0) \\ \mathbf{z}_2^\top(0)\mathbf{s}_\beta \\ \mathbf{z}_2^\top(0)\mathbf{s}_\beta^\perp \end{bmatrix} \right\}, \tag{2.71}$$

where $\mathbf{s}_\beta : [0, 2\pi) \mapsto \mathcal{S}^1$ is the map described by $\mathbf{s}_\beta := [\cos\beta \ \ \sin\beta]^\top$ and $\mathbf{s}_\beta^\perp := \mathcal{R}_{\pi/2}^\top \mathbf{s}_\beta$.

Proof. Consider the initial condition $\mathbf{z}(0) \in \mathbb{R}^{15}$ and let $\mathbf{u} \in \mathbb{R}^4$ be constant. Since the input is known and constant, (2.66) is an LTI system. Taking into account (2.70),

the first seven rows of the observability matrix associated with the system (2.66) is calculated as

$$\mathcal{O} = -2\begin{bmatrix} \mathbf{0} & \mathbf{0} & \mathbf{0} & \mathbf{0} & -0.5 & 0 & 0 & 0 & 0 & 0 & 0 \\ {}^{\mathcal{B}}\mathbf{v}^{\top} & \mathbf{0} & \mathbf{0} & \mathbf{0} & 0 & 1 & 0 & 0 & 0 & 0 & 0 \\ r\ {}^{\mathcal{B}}\mathbf{v}^{\perp\top} & -2\ {}^{\mathcal{B}}\mathbf{v}^{\top} & \mathbf{0} & \mathbf{0} & 0 & 0 & 0 & 0 & -1 & 0 & 0 \\ -r^2\ {}^{\mathcal{B}}\mathbf{v}^{\top} & -3r\ {}^{\mathcal{B}}\mathbf{v}^{\perp\top} & \mathbf{0} & \mathbf{0} & 0 & 0 & 0 & 0 & 0 & 0 & 0 \\ -r^3\ {}^{\mathcal{B}}\mathbf{v}^{\perp\top} & 4r^2\ {}^{\mathcal{B}}\mathbf{v}^{\top} & \mathbf{0} & \mathbf{0} & 0 & 0 & 0 & 0 & 0 & 0 & 0 \\ r^4\ {}^{\mathcal{B}}\mathbf{v}^{\top} & 5r^3\ {}^{\mathcal{B}}\mathbf{v}^{\perp\top} & \mathbf{0} & \mathbf{0} & 0 & 0 & 0 & 0 & 0 & 0 & 0 \\ r^5\ {}^{\mathcal{B}}\mathbf{v}^{\perp\top} & -6r^4\ {}^{\mathcal{B}}\mathbf{v}^{\top} & \mathbf{0} & \mathbf{0} & 0 & 0 & 0 & 0 & 0 & 0 & 0 \end{bmatrix} \tag{2.72}$$

and the following rows can be computed as $CA^j = -r^2\left(2CA^{j-2} - r^2CA^{j-4}\right)$ for $j \in \{7, 8, 9, ...\}$. Since the rank of (2.30) is 7, then the kernel of $\mathcal{O}$ is given by

$$\ker(\mathcal{O}) = \begin{bmatrix} \mathbf{0} & \mathbf{0} & \mathbf{0} & \mathbf{0} & \mathbf{0} & \mathbf{0} & \mathbf{0} & \mathbf{0} \\ \mathbf{0} & \mathbf{0} & \mathbf{0} & \mathbf{0} & \mathbf{0} & \mathbf{0} & \mathbf{0} & \mathbf{0} \\ \mathbf{e}_x & \mathbf{e}_y & \mathbf{0} & \mathbf{0} & \mathbf{0} & \mathbf{0} & \mathbf{0} & \mathbf{0} \\ \mathbf{0} & \mathbf{0} & \mathbf{e}_x & \mathbf{e}_y & \mathbf{0} & \mathbf{0} & \mathbf{0} & \mathbf{0} \\ 0 & 0 & 0 & 0 & 0 & 0 & 0 & 0 \\ 0 & 0 & 0 & 0 & 0 & 0 & 0 & 0 \\ 0 & 0 & 0 & 0 & 1 & 0 & 0 & 0 \\ 0 & 0 & 0 & 0 & 0 & 1 & 0 & 0 \\ 0 & 0 & 0 & 0 & 0 & 0 & 0 & 0 \\ 0 & 0 & 0 & 0 & 0 & 0 & 1 & 0 \\ 0 & 0 & 0 & 0 & 0 & 0 & 0 & 1 \end{bmatrix} \tag{2.73}$$

Recall that the unobservable space is given by all initial conditions that generate the same input-output map. Therefore, all initial conditions of the form $\bar{\mathbf{z}}(0) = \mathbf{z}(0) +$

$\ker(\mathcal{O})\boldsymbol{\alpha}$ with $\boldsymbol{\alpha} = [\alpha_1, ..., \alpha_8]^\top \in \mathbb{R}^8$, are indistinguishable from $\mathbf{z}_0$. Then

$$\begin{bmatrix} \bar{\mathbf{z}}_1(0) \\ \bar{\mathbf{z}}_2(0) \\ \bar{\mathbf{z}}_3(0) \\ \bar{\mathbf{z}}_4(0) \\ \bar{z}_5(0) \\ \bar{z}_6(0) \\ \bar{z}_7(0) \\ \bar{z}_8(0) \\ \bar{z}_9(0) \\ \bar{z}_{10}(0) \\ \bar{z}_{11}(0) \end{bmatrix} = \begin{bmatrix} \mathbf{z}_1(0) \\ \mathbf{z}_2(0) \\ \mathbf{z}_3(0) + \boldsymbol{\alpha}_a \\ \mathbf{z}_4(0) + \boldsymbol{\alpha}_b \\ z_5(0) \\ z_6(0) \\ z_7(0) + \alpha_5 \\ z_8(0) + \alpha_6 \\ z_9(0) \\ z_{10}(0) + \alpha_7 \\ z_{11}(0) + \alpha_8 \end{bmatrix}, \tag{2.74}$$

where $\boldsymbol{\alpha}_a = [\alpha_1, \alpha_2]^\top$ and $\boldsymbol{\alpha}_b = [\alpha_3, \alpha_4]^\top$. Recall that the initial conditions should satisfy the constraints given by (2.67). Since $\mathbf{z}_3 := \mathcal{R}_\psi^\top \mathbf{w}^\perp(\chi)$, then

$$\begin{aligned} \bar{\mathbf{z}}_3^\top(0)\bar{\mathbf{z}}_3(0) &= 1, \\ ||\boldsymbol{\alpha}_a + \mathbf{z}_3(0)||^2 &= 1, \\ \boldsymbol{\alpha}_a &= -\mathbf{z}_3(0) + \mathbf{s}_\beta, \end{aligned} \tag{2.75}$$

where $\mathbf{s}_\beta := [\cos\beta, \sin\beta]^\top$ with $\beta \in [0, 2\pi)$. From the relation between $\mathbf{z}_3(0)$ and $\mathbf{z}_4(0)$ in (2.67) and using (2.74), it can be concluded that

$$\begin{aligned} \bar{\mathbf{z}}_4(0) &= \mathcal{R}_{\pi/2}^\top \bar{\mathbf{z}}_3(0), \\ \mathbf{z}_4(0) + \boldsymbol{\alpha}_b &= \mathcal{R}_{\pi/2}^\top \left(\mathbf{z}_3(0) + \boldsymbol{\alpha}_a\right), \\ \boldsymbol{\alpha}_b &= \mathcal{R}_{\pi/2}^\top \boldsymbol{\alpha}_a. \end{aligned} \tag{2.76}$$

Moreover, using the fact that $\mathbf{z}_7(0) := \mathbf{z}_1(0)^\top \mathbf{z}_3(0)$ and $\mathbf{z}_8(0) := \mathbf{z}_1(0)^\top \mathbf{z}_4(0)$ in (2.74), it is possible to obtain α_5 and α_6, thus

$$\begin{aligned} \bar{\mathbf{z}}_1^\top(0)\bar{\mathbf{z}}_3(0) &= \mathbf{z}_1^\top(0)\mathbf{z}_3(0) + \alpha_5, \\ \mathbf{z}_1^\top(0)\left(\mathbf{z}_3(0) + \boldsymbol{\alpha}_a\right) &= \mathbf{z}_1^\top(0)\mathbf{z}_3(0) + \alpha_5, \\ \alpha_5 &= \mathbf{z}_1^\top(0)\boldsymbol{\alpha}_a, \end{aligned} \tag{2.77}$$

and

$$\begin{aligned} \bar{\mathbf{z}}_1^\top(0)\bar{\mathbf{z}}_4(0) &= \mathbf{z}_1^\top(0)\mathbf{z}_4(0) + \alpha_6, \\ \mathbf{z}_1^\top(0)\left(\mathbf{z}_4(0) + \boldsymbol{\alpha}_b\right) &= \mathbf{z}_1^\top(0)\mathbf{z}_4(0) + \alpha_6, \\ \alpha_6 &= \mathbf{z}_1^\top(0)\boldsymbol{\alpha}_b. \end{aligned} \tag{2.78}$$

Following the same procedure, and the relations $\mathbf{z}_{10}(0) := \mathbf{z}_2(0)^\top \mathbf{z}_3(0)$ and $\mathbf{z}_{11}(0) := \mathbf{z}_2(0)^\top \mathbf{z}_4(0)$ in (2.74), it implies that $\alpha_7 = \mathbf{z}_2^\top(0)\boldsymbol{\alpha}_a$ and $\alpha_8 = \mathbf{z}_2^\top(0)\boldsymbol{\alpha}_b$. Hence, the set of indistinguishable initial conditions are given by

$$\begin{bmatrix} \bar{\mathbf{z}}_1(0) \\ \bar{\mathbf{z}}_2(0) \\ \bar{\mathbf{z}}_3(0) \\ \bar{\mathbf{z}}_4(0) \\ \bar{z}_5(0) \\ \bar{z}_6(0) \\ \bar{z}_7(0) \\ \bar{z}_8(0) \\ \bar{z}_9(0) \\ \bar{z}_{10}(0) \\ \bar{z}_{11}(0) \end{bmatrix} = \begin{bmatrix} \mathbf{z}_1(0) \\ \mathbf{z}_2(0) \\ \mathbf{s}_\beta \\ \mathbf{s}_\beta^\perp \\ z_5(0) \\ z_6(0) \\ \mathbf{z}_1^\top(0)\mathbf{s}_\beta \\ \mathbf{z}_1^\top(0)\mathbf{s}_\beta^\perp \\ z_9(0) \\ \mathbf{z}_2^\top(0)\mathbf{s}_\beta \\ \mathbf{z}_2^\top(0)\mathbf{s}_\beta^\perp \end{bmatrix}.$$

This implies that the set of indistinguishable initial conditions from $\mathbf{z}(0) \in \mathbb{R}^{15}$ is a continuous of points parametrized by a free parameter β and described by (2.71). Thus the system is not observable. This completes the proof. □

Corollary 4. *Suppose that the initial condition of the beacon is known. Then the system is observable.*

Proof. Suppose that the initial condition of the beacon is known, that is, ${}^{\mathcal{I}}\bar{\mathbf{b}}(0) = {}^{\mathcal{I}}\mathbf{b}(0)$. which implies that $\bar{\mathbf{z}}_2(0) = \mathbf{z}_2(0)$ and $\bar{\mathbf{z}}_3(0) = \mathbf{z}_3(0)$. The last conditions imply that $\boldsymbol{\alpha}_a = 0$ and $\boldsymbol{\alpha}_b = 0$, and therefore $\alpha_5 = \alpha_6 = \alpha_7 = \alpha_8 = 0$. Consequently, $\mathcal{I}(\mathbf{z}(0)) = \{\mathbf{z}(0)\}$ and the system is observable. This completes the proof. □

2.6.2. Vehicle moving in straight lines

In the previous sections, the observability analysis was carried out assuming that the vehicle was moving forward and rotating at the same time. Here, the observability of the system will be analyzed assuming that the vehicle is moving in straight lines, that is, $r = 0$ and $||{}^{\mathcal{B}}\mathbf{v}|| \neq 0$.

Based on the results of the previous sections, when the observability properties were

established for the system without currents, we are only interested in knowing if the observability properties are maintained with the inclusion of the new state (ocean current velocity). In the case when the beacon is not rotating, it is expected that the system will not be observable (without knowing the initial position of the beacon) or weakly observable (knowing the initial position of the beacon). Additionally, for the rest of the analysis, it is assumed that the initial position of the beacon is known.

Therefore, the following proposition states the observability properties of the system assuming that the beacon rotates and the vehicle is going in straight lines.

Proposition 8. *Consider the system* (2.66) *with* $\mathbf{u} \in \mathbb{R}^4$ *fulfilling assumption 4. Further, suppose that the vehicle moves in straight lines (that is , $r = 0$ and $||^{\mathcal{B}}\mathbf{v}|| \neq 0$) and the beacon rotates (that is, $\omega_m \neq 0$). Additionally, that the initial beacon's position is known. Then, the system* (2.66) *with the constraints in the initial conditions* (2.67) *is observable.*

Proof. Consider the initial condition $\mathbf{z}(0) \in \mathbb{R}^{15}$ and let $\mathbf{u} \in \mathbb{R}^4$ be constant. Since the input is known and constant, (2.66) is an LTI system. Then, the first seven rows of the observability matrix are given by

$$\mathcal{O} = -2\begin{bmatrix} \mathbf{0} & \mathbf{0} & \mathbf{0} & \mathbf{0} & -0.5 & 0 \\ {}^{\mathcal{B}}\mathbf{v}^\top & \mathbf{0} & \mathbf{0} & \mathbf{0} & 0 & 1 \\ \mathbf{0} & -2\,{}^{\mathcal{B}}\mathbf{v}^\top & 2l_m\omega_m\,{}^{\mathcal{B}}\mathbf{v}^\top & \mathbf{0} & 0 & 0 \\ \mathbf{0} & \mathbf{0} & \mathbf{0} & -3l_m\omega_m^2\,{}^{\mathcal{B}}\mathbf{v}^\top & 0 & 0 \\ \mathbf{0} & \mathbf{0} & -4l_m\omega_m^3\,{}^{\mathcal{B}}\mathbf{v}^\top & \mathbf{0} & 0 & 0 \\ \mathbf{0} & \mathbf{0} & \mathbf{0} & 5l_m\omega_m^4\,{}^{\mathcal{B}}\mathbf{v}^\top & 0 & 0 \\ \mathbf{0} & \mathbf{0} & 6l_m\omega_m^5\,{}^{\mathcal{B}}\mathbf{v}^\top & \mathbf{0} & 0 & 0 \end{bmatrix} \begin{bmatrix} 0 & 0 & 0 & 0 & 0 \\ -l_m\omega_m & 0 & 0 & 0 & 0 \\ 0 & l_m\omega_m^2 & -1 & 2l_m\omega_m & 0 \\ l_m\omega_m^3 & 0 & 0 & 0 & -3l_m\omega_m^2 \\ 0 & -l_m\omega_m^4 & 0 & -4l_m\omega_m^3 & 0 \\ -l_m\omega_m^5 & 0 & 0 & 0 & 5l_m\omega_m^4 \\ 0 & l_m\omega_m^6 & 0 & -6l_m\omega_m^5 & 0 \end{bmatrix} \tag{2.79}$$

and the following rows can be computed as $CA^j = -\omega_m^2\left(2CA^{j-2} - \omega_m^2 CA^{j-4}\right)$ for

$j \in \{7, 8, 9, ...\}$. Since the rank of (2.79) is 7, then the kernel of $\mathcal{O}$ is given by

$$\ker(\mathcal{O}) = \begin{bmatrix} {}^{\mathcal{B}}\mathbf{v}^{\perp} & \mathbf{0} & \mathbf{0} & \mathbf{0} & -\mathbf{e}_x & \mathbf{0} & \mathbf{0} & \mathbf{0} \\ \mathbf{0} & {}^{\mathcal{B}}\mathbf{v}^{\perp} & \mathbf{0} & \mathbf{0} & \mathbf{0} & -\mathbf{e}_x & \mathbf{0} & \mathbf{0} \\ \mathbf{0} & \mathbf{0} & {}^{\mathcal{B}}\mathbf{v}^{\perp} & \mathbf{0} & \mathbf{0} & \mathbf{0} & -\mathbf{e}_x & \mathbf{0} \\ \mathbf{0} & \mathbf{0} & \mathbf{0} & {}^{\mathcal{B}}\mathbf{v}^{\perp} & \mathbf{0} & \mathbf{0} & \mathbf{0} & -\mathbf{e}_x \\ 0 & 0 & 0 & 0 & 0 & 0 & 0 & 0 \\ 0 & 0 & 0 & 0 & {}^{\mathcal{B}}\mathbf{v}^{\top}\mathbf{e}_x & 0 & 0 & 0 \\ 0 & 0 & 0 & 0 & 0 & 0 & 0 & 0 \\ 0 & 0 & 0 & 0 & 0 & 0 & 0 & 0 \\ 0 & 0 & 0 & 0 & 0 & 2{}^{\mathcal{B}}\mathbf{v}^{\top}\mathbf{e}_x & 0 & 0 \\ 0 & 0 & 0 & 0 & 0 & 0 & {}^{\mathcal{B}}\mathbf{v}^{\top}\mathbf{e}_x & 0 \\ 0 & 0 & 0 & 0 & 0 & 0 & 0 & {}^{\mathcal{B}}\mathbf{v}^{\top}\mathbf{e}_x \end{bmatrix} \tag{2.80}$$

Recall that the unobservable space is given by all initial conditions that generate the same input-output map. Therefore, all initial conditions of the form $\bar{\mathbf{z}}(0) = \mathbf{z}(0) + \ker(\mathcal{O})\boldsymbol{\alpha}$ with $\boldsymbol{\alpha} = [\alpha_1, ..., \alpha_8]^{\top} \in \mathbb{R}^8$, are indistinguishable from $\mathbf{z}_0$. Then

$$\begin{bmatrix} \bar{\mathbf{z}}_1(0) \\ \bar{\mathbf{z}}_2(0) \\ \bar{\mathbf{z}}_3(0) \\ \bar{\mathbf{z}}_4(0) \\ \bar{z}_5(0) \\ \bar{z}_6(0) \\ \bar{z}_7(0) \\ \bar{z}_8(0) \\ \bar{z}_9(0) \\ \bar{z}_{10}(0) \\ \bar{z}_{11}(0) \end{bmatrix} = \begin{bmatrix} \mathbf{z}_1(0) + \alpha_1{}^{\mathcal{B}}\mathbf{v}^{\perp} - \alpha_5\mathbf{e}_x \\ \mathbf{z}_2(0) + \alpha_2{}^{\mathcal{B}}\mathbf{v}^{\perp} - \alpha_6\mathbf{e}_x \\ \mathbf{z}_3(0) + \alpha_3{}^{\mathcal{B}}\mathbf{v}^{\perp} - \alpha_7\mathbf{e}_x \\ \mathbf{z}_4(0) + \alpha_4{}^{\mathcal{B}}\mathbf{v}^{\perp} - \alpha_8\mathbf{e}_x \\ z_5(0) \\ z_6(0) + \alpha_5{}^{\mathcal{B}}\mathbf{v}^{\top}\mathbf{e}_x \\ z_7(0) \\ z_8(0) \\ z_9(0) + 2\alpha_6{}^{\mathcal{B}}\mathbf{v}^{\top}\mathbf{e}_x \\ z_{10}(0) + \alpha_7{}^{\mathcal{B}}\mathbf{v}^{\top}\mathbf{e}_x \\ z_{11}(0) + \alpha_8{}^{\mathcal{B}}\mathbf{v}^{\top}\mathbf{e}_x \end{bmatrix}. \tag{2.81}$$

Notice that the initial conditions should satisfy the constraints given by (2.67). Since the initial beacon's position is known, then $\bar{\mathbf{z}}_3(0) = \mathbf{z}_3(0)$ and $\bar{\mathbf{z}}_2(0) = \mathbf{z}_2(0)$. Using the fact that $\mathbf{z}_5(0) := \mathbf{z}_1^{\top}(0)\mathbf{z}_1(0)$ and defining $\boldsymbol{\alpha}_a := \alpha_1{}^{\mathcal{B}}\mathbf{v}^{\perp} - \alpha_5\mathbf{e}_x$, then it is possible to obtain a relation for $\boldsymbol{\alpha}_a$ given by

$$\begin{aligned} \bar{\mathbf{z}}_1^{\top}(0)\bar{\mathbf{z}}_1(0) &= \mathbf{z}_5(0), \\ ||\boldsymbol{\alpha}_a + \mathbf{z}_1(0)||^2 &= ||\mathbf{z}_1(0)||^2, \\ \boldsymbol{\alpha}_a &= -\mathbf{z}_1(0) + ||\mathbf{z}_1(0)||\mathbf{s}_{\beta}, \end{aligned} \tag{2.82}$$

where $\mathbf{s}_\beta := [\cos\beta, \sin\beta]^\top$ with $\beta \in [0, 2\pi)$. Moreover, using the relation $\mathbf{z}_7(0) := \mathbf{z}_1^\top(0)\mathbf{z}_3(0)$ and the value of $\boldsymbol{\alpha}_a$ in (2.81), it leads to

$$\begin{aligned} \mathbf{z}_7(0) &= \bar{\mathbf{z}}_1^\top(0)\bar{\mathbf{z}}_3(0), \\ \mathbf{z}_7(0) &= (\mathbf{z}_1(0) + \boldsymbol{\alpha}_a)^\top \mathbf{z}_3(0), \\ (-\mathbf{z}_1(0) + ||\mathbf{z}_1(0)||\mathbf{s}_\beta)^\top \mathbf{z}_3(0) &= 0, \\ \mathbf{z}_1(0)^\top \mathbf{z}_3(0) &= ||\mathbf{z}_1(0)||\mathbf{s}_\beta^\top \mathbf{z}_3(0), \end{aligned} \tag{2.83}$$

which implies that $\beta = \angle\mathbf{z}_1(0)$. Since β has the same angle as $\mathbf{z}_1(0)$, then equation (2.82) implies that $\boldsymbol{\alpha}_a = \mathbf{0}$. Hence $\bar{\mathbf{z}}_1(0) = \mathbf{z}_1(0)$. Recall that ${}^{\mathcal{B}}\mathbf{v}^\perp = \mathcal{R}_{\pi/2}{}^{\mathcal{B}}\mathbf{v} = [-v_v, u_v]^\top$.

- First, suppose that $u_v = 0$. Then, equation (2.81) implies that $\bar{z}_6(0) = z_6(0)$, $\bar{z}_9(0) = z_9(0)$, $\bar{z}_{10}(0) = z_{10}(0)$, and $\bar{z}_{11}(0) = z_{11}(0)$.
- Now, suppose that $u_v \neq 0$. Since $\boldsymbol{\alpha}_a = \mathbf{0}$, it implies that $\alpha_1 {}^{\mathcal{B}}\mathbf{v}^\perp = \alpha_5 \mathbf{e}_x$, which in turn implies $\alpha_1 = \alpha_5 = 0$ and $\bar{z}_6(0) = z_6(0)$. Further, $\bar{\mathbf{z}}_3(0) = \mathbf{z}_3(0)$ and $\bar{\mathbf{z}}_4(0) = \mathbf{z}_4(0)$ implies $\alpha_3 = \alpha_4 = \alpha_7 = \alpha_8 = 0$, which further implies that $\bar{z}_{10}(0) = z_{10}(0)$ and $\bar{z}_{11}(0) = z_{11}(0)$.

Defining $\boldsymbol{\alpha}_b := \alpha_2 {}^{\mathcal{B}}\mathbf{v}^\perp - \alpha_6 \mathbf{e}_x$ and using $\bar{z}_{10}(0) = z_{10}(0)$ and $\bar{z}_{11}(0) = z_{11}(0)$, it implies $\boldsymbol{\alpha}_b^\top \mathbf{z}_3(0) = 0$ and $\boldsymbol{\alpha}_b^\top \mathbf{z}_4(0) = 0$, respectively. Since $\mathbf{z}_3(0) \perp \mathbf{z}_4(0)$, then $\boldsymbol{\alpha}_b = \mathbf{0}$, which implies $\bar{\mathbf{z}}_2(0) = \mathbf{z}_2(0)$. In other words, $\mathcal{I}(\mathbf{z}(0)) = \{\mathbf{z}(0)\}$ and hence the system is observable. □

2.6.3. Vehicle does not move

In the previous sections, the observability analysis was carried out assuming that the vehicle was moving forward but without rotation. Here, the observability of the system will be analyzed assuming that the vehicle does not move, that is $||{}^{\mathcal{B}}\mathbf{v}|| = 0$. From the observability analysis carried out in the previous sections, where the currents were not taken into account, the only case where the system was observable was when the beacon rotates and its initial position was known (Corollary 3).

Therefore, the following proposition states the observability properties of the system assuming that the beacon rotates and the vehicle is not moving.

Proposition 9. *Consider the system (2.66) with $\mathbf{u} \in \mathbb{R}^4$ fulfilling assumption 4. Further, suppose that the vehicle does not move (that is $||{}^{\mathcal{B}}\mathbf{v}|| = 0$), the beacon rotates (that*

is $\omega_m \neq 0$) and the initial beacon's position is known. Then, the system (2.66) with the constraints in the initial conditions (2.67) is observable.

Proof. Consider the initial condition $\mathbf{z}(0) \in \mathbb{R}^{15}$ and let $\mathbf{u} \in \mathbb{R}^4$ be constant. Since the input is known and constant, (2.66) is an LTI system. Then, the first seven rows of the observability matrix are given by

$$\mathcal{O} = -2\begin{bmatrix} \mathbf{0} & \mathbf{0} & \mathbf{0} & \mathbf{0} & -0.5 & 0 & 0 & 0 & 0 & 0 & 0 \\ \mathbf{0} & \mathbf{0} & \mathbf{0} & \mathbf{0} & 0 & 1 & -l_m\omega_m & 0 & 0 & 0 & 0 \\ \mathbf{0} & \mathbf{0} & \mathbf{0} & \mathbf{0} & 0 & 0 & 0 & l_m\omega_m^2 & -1 & 2l_m\omega_m & 0 \\ \mathbf{0} & \mathbf{0} & \mathbf{0} & \mathbf{0} & 0 & 0 & l_m\omega_m^3 & 0 & 0 & 0 & -3l_m\omega_m^2 \\ \mathbf{0} & \mathbf{0} & \mathbf{0} & \mathbf{0} & 0 & 0 & 0 & -l_m\omega_m^4 & 0 & -4l_m\omega_m^3 & 0 \\ \mathbf{0} & \mathbf{0} & \mathbf{0} & \mathbf{0} & 0 & 0 & -l_m\omega_m^5 & 0 & 0 & 0 & 5l_m\omega_m^4 \\ \mathbf{0} & \mathbf{0} & \mathbf{0} & \mathbf{0} & 0 & 0 & 0 & l_m\omega_m^6 & 0 & 6l_m\omega_m^5 & 0 \end{bmatrix} \tag{2.84}$$

and the following rows can be computed as $CA^j = -\omega_m^2\left(2CA^{j-2} - \omega_m^2 CA^{j-4}\right)$ for $j \in \{7, 8, 9, ...\}$. Since the rank of (2.84) is 7, then the kernel of $\mathcal{O}$ is given by

$$\ker(\mathcal{O}) = \begin{bmatrix} \mathbf{e}_x & \mathbf{e}_x & \mathbf{0} & \mathbf{0} & \mathbf{0} & \mathbf{0} & \mathbf{0} & \mathbf{0} \\ \mathbf{0} & \mathbf{0} & \mathbf{e}_x & \mathbf{e}_x & \mathbf{0} & \mathbf{0} & \mathbf{0} & \mathbf{0} \\ \mathbf{0} & \mathbf{0} & \mathbf{0} & \mathbf{0} & \mathbf{e}_x & \mathbf{e}_x & \mathbf{0} & \mathbf{0} \\ \mathbf{0} & \mathbf{0} & \mathbf{0} & \mathbf{0} & \mathbf{0} & \mathbf{0} & \mathbf{e}_x & \mathbf{e}_x \\ 0 & 0 & 0 & 0 & 0 & 0 & 0 & 0 \\ 0 & 0 & 0 & 0 & 0 & 0 & 0 & 0 \\ 0 & 0 & 0 & 0 & 0 & 0 & 0 & 0 \\ 0 & 0 & 0 & 0 & 0 & 0 & 0 & 0 \\ 0 & 0 & 0 & 0 & 0 & 0 & 0 & 0 \\ 0 & 0 & 0 & 0 & 0 & 0 & 0 & 0 \\ 0 & 0 & 0 & 0 & 0 & 0 & 0 & 0 \end{bmatrix} \tag{2.85}$$

Recall that the unobservable space is given by all initial conditions that generate the same input-output map. Therefore, all initial conditions of the form $\bar{\mathbf{z}}(0) = \mathbf{z}(0) +$

$\ker(\mathcal{O})\boldsymbol{\alpha}$ with $\boldsymbol{\alpha} = [\alpha_1, ..., \alpha_8]^\top \in \mathbb{R}^8$, are indistinguishable from $\mathbf{z}_0$. Then

$$\begin{bmatrix} \bar{\mathbf{z}}_1(0) \\ \bar{\mathbf{z}}_2(0) \\ \bar{\mathbf{z}}_3(0) \\ \bar{\mathbf{z}}_4(0) \\ \bar{z}_5(0) \\ \bar{z}_6(0) \\ \bar{z}_7(0) \\ \bar{z}_8(0) \\ \bar{z}_9(0) \\ \bar{z}_{10}(0) \\ \bar{z}_{11}(0) \end{bmatrix} = \begin{bmatrix} \mathbf{z}_1(0) + \boldsymbol{\alpha}_a \\ \mathbf{z}_2(0) + \boldsymbol{\alpha}_b \\ \mathbf{z}_3(0) + \boldsymbol{\alpha}_c \\ \mathbf{z}_4(0) + \boldsymbol{\alpha}_d \\ z_5(0) \\ z_6(0) \\ z_7(0) \\ z_8(0) \\ z_9(0) \\ z_{10}(0) \\ z_{11}(0) \end{bmatrix}, \tag{2.86}$$

where $\boldsymbol{\alpha}_a = [\alpha_1, \alpha_2]^\top$, $\boldsymbol{\alpha}_b = [\alpha_3, \alpha_4]^\top$, $\boldsymbol{\alpha}_c = [\alpha_5, \alpha_6]^\top$, and $\boldsymbol{\alpha}_d = [\alpha_7, \alpha_8]^\top$. Since the initial beacon's position is known, then $\bar{\mathbf{z}}_3(0) = \mathbf{z}_3(0)$ and $\bar{\mathbf{z}}_4(0) = \mathbf{z}_4(0)$, which implies that $\boldsymbol{\alpha}_c = \boldsymbol{\alpha}_d = \mathbf{0}$. Using $z_7(0) = \mathbf{z}_1^\top(0)\mathbf{z}_3(0)$ and $z_8(0) = \mathbf{z}_1^\top(0)\mathbf{z}_4(0)$ in (2.86), it implies $\boldsymbol{\alpha}_a^\top \mathbf{z}_3(0) = 0$ and $\boldsymbol{\alpha}_a^\top \mathbf{z}_4(0) = 0$, respectively. Since $\mathbf{z}_3(0) \perp \mathbf{z}_4(0)$, then $\boldsymbol{\alpha}_a = \mathbf{0}$. Consequently, the same analysis can be applied to $z_{10}(0)$ and $z_{11}(0)$, and find that $\boldsymbol{\alpha}_b = \mathbf{0}$. Hence, $\bar{\mathbf{z}}_1(0) = \mathbf{z}_1(0)$ and $\bar{\mathbf{z}}_2(0) = \mathbf{z}_2(0)$. In other words, $\mathcal{I}(\mathbf{z}(0)) = \{\mathbf{z}(0)\}$ and hence the system is observable. □

2.6.4. Simulation Results

To illustrate some of the conditions found in the previous section, two examples have been implemented in Matlab™. This section presents the simulations results for different conditions in the system:

- *Scenario 1*: the vehicle moves in circles and the beacon does not move. This corresponds to Proposition 7. Notice that in this case, there are a continuous of points that are indistinguishable between them. The initial position and orientation of the vehicle are ${}^{\mathcal{I}}\mathbf{p}(0) = [10, 5]^\top$ m and $\psi(0) = \pi/4$, respectively. The manipulator's length is set to $l_m = 2$ m and the initial angle to $\chi(0) = \pi/3$, which implies that ${}^{\mathcal{I}}\mathbf{b}(0) = [1.00, 1.73]^\top$ m. The linear and angular velocity of the vehicle are given by ${}^{\mathcal{B}}\mathbf{v} = [2.1, 0.3]^\top$ m/s and $r = 0.2$ rad/s, respectively. The beacon does not move, that is, $\omega_m = 0$ rad/s. The initial ocean current velocity is

${}^{\mathcal{I}}\mathbf{v}_c(0) = [0.2, 0.35]^\top$ m/s. Recall that the set of indistinguishable initial conditions is given by the equation (2.71). Then, by choosing a particular value of β, a pair of indistinguishable initial conditions are given by ${}^{\mathcal{I}}\bar{\mathbf{b}}(0) = [-1.73, 1.00]^\top$ m and ${}^{\mathcal{I}}\bar{\mathbf{p}}(0) = [7.26, 4.26]^\top$ m. Notice that equation (2.71) implies that ${}^{\mathcal{I}}\bar{\mathbf{v}}_c(0) = {}^{\mathcal{I}}\mathbf{v}_c(0)$.

The simulation results are shown in Figure 10. Figure 10(a) shows two different initial conditions that are indistinguishable. Although the initial conditions are different, the output trajectory is the same (see Figure 10(b)). Furthermore, once the beacon's position is known, the dashed black circle disappear and the system is observable (as it was proofed in Corollary 4).

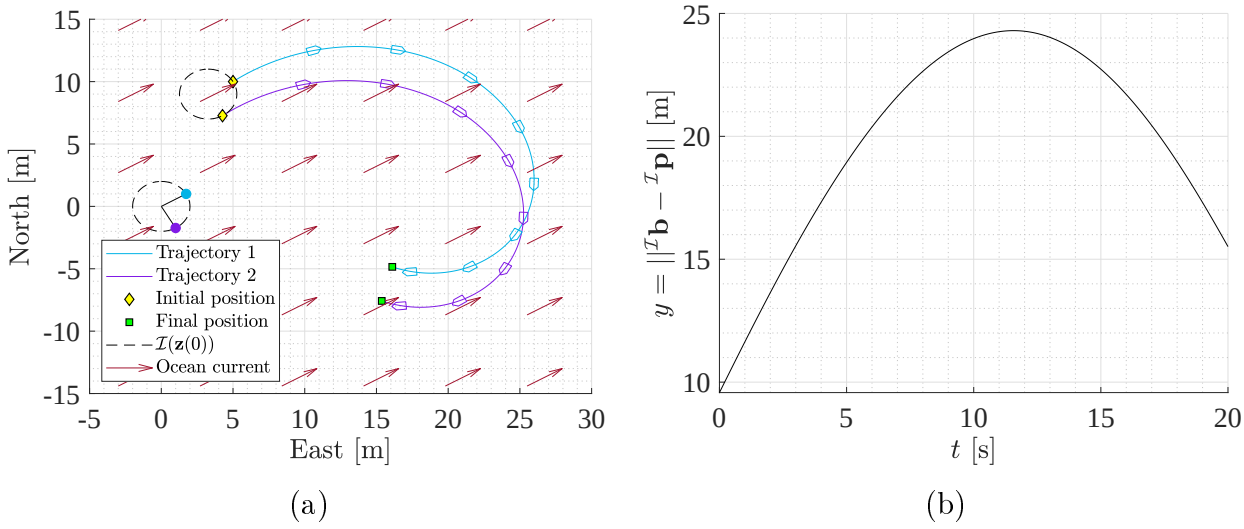

Figure 10: Simulation results for two different initial conditions in VCBN scenario and taking into account ocean currents. Every initial condition in the black dashed line will be indistinguishable.

- *Scenario 2*: the vehicle moves in straight lines and the beacon does not move at the beginning with the same inputs and different initial conditions. At $t = 10$ s, the beacon starts moving with angular velocity $\omega_m = 0.3$ rad/s, while the vehicle does not change its trajectory. The key idea behind this example is to illustrate how by moving the beacon the two indistinguishable trajectories go in different directions, allowing one to distinguish between both initial conditions.

  The simulation results are shown in Figure 11. Figure 11(a) shows two different initial conditions of the vehicle that are indistinguishable since the beacon is not moving. Once the beacon starts moving at $t = 10$ s, both trajectories become distinguishable between them (see Figure 11(b)).

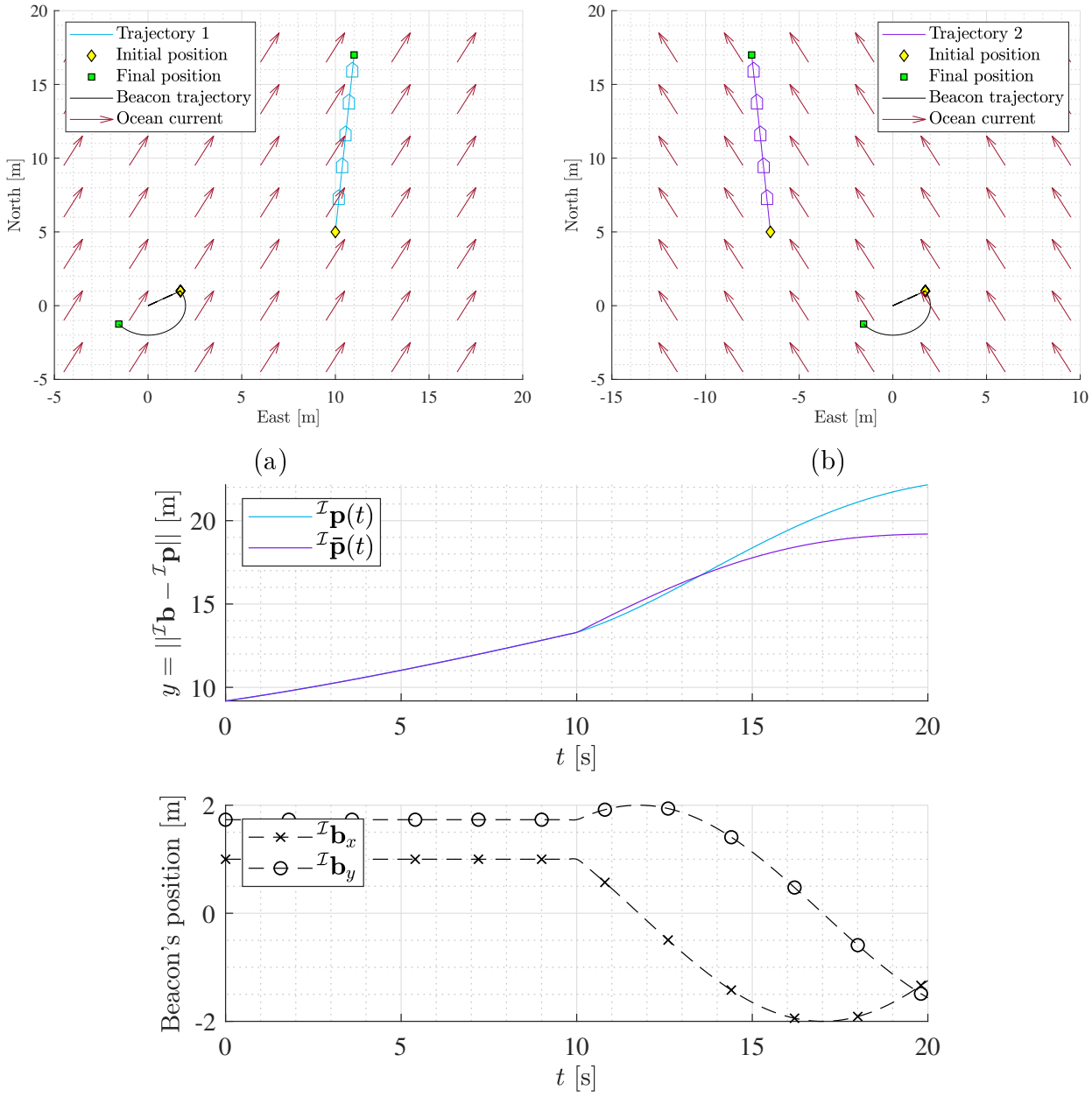

Figure 11: Simulation results for a combination of trajectories and taking into account ocean currents. The beacon's initial position is known, therefore there just two isolated indistinguishable initial conditions. Once the beacon starts moving both trajectories can be distinguished and, hence, the two initial conditions.

2.7. CONCLUDING REMARKS

We addressed the observability conditions for the localization problem of the vehicle and the beacon. The vehicle is equipped with inertial sensors, a Doppler velocity log and an acoustic ranging device to obtain the relative measure to a mobile beacon installed under the hull of a support vessel. We addressed the problem with and without taking into account the ocean current as a new state variable of the system. When the position of the beacon is known, we proved that by moving the beacon under certain conditions, it was possible to ensure the observability of the system all the times.

3. OBSERVER DESIGN

3.1. INTRODUCTION

This chapter presents different methodologies to solve the problem of state observer design. The objective of an state observer is to estimate the unknown state of the system through output measurements and the knowledge of the inputs applied to the system. First, we use the Extended Kalman Filter (EKF) to estimate the vehicle's and beacon's position, as well as, the ocean current velocity. Then, we use a variation of the Kalman Filter known as Exogenous Kalman Filter (XKF), which provides better performance since it is globally convergent and deals with the noise in its original reference frame. This Chapter only presents the state observer design for the system taking into account the unknown ocean currents. For more information regarding the observer design when currents are not taken into account, refer to Appendix B.

3.2. EXTENDED KALMAN FILTER CONSIDERING OCEAN CURRENTS

In this section we propose an observer for the nonlinear system (2.64) introduced in Chapter 2, where we now consider that the system is corrupted with a process $\boldsymbol{\zeta}(t) \in \mathbb{R}^5$ and measurement $\kappa(t) \in \mathbb{R}$ zero mean Gaussian noise

$$\left.\begin{aligned} \dot{\mathbf{x}}(t) &= \boldsymbol{f}(\mathbf{x}(t), \mathbf{u}(t)) + \boldsymbol{\zeta}(t), \\ y(t) &= g(\mathbf{x}(t)) + \kappa(t), \end{aligned}\right\} \tag{3.1}$$

where the state variable $\mathbf{x} := [\mathbf{x}_1^\top, \mathbf{x}_2^\top, x_3]^\top := [{}^{\mathcal{B}}\mathbf{d}, {}^{\mathcal{B}}\mathbf{v}_c, \chi]^\top \in \mathbb{R}^4 \times [0, 2\pi)$, the input vector $\mathbf{u} := [{}^{\mathcal{B}}\mathbf{v}^\top, \omega_m, r]^\top \in \mathbb{R}^4$, the output measurement $y \in \mathbb{R}$,

$$\boldsymbol{f}(\mathbf{x}(t), \mathbf{u}(t)) = \begin{bmatrix} -S(r)\mathbf{x}_1(t) - {}^{\mathcal{B}}\mathbf{v}(t) + l_m\omega_m(t)\mathcal{R}_{\psi(t)}^\top \mathbf{w}^\perp(x_3(t)) - \mathbf{x}_2(t) \\ -S(r)\mathbf{x}_2(t) \\ \omega_m(t) \end{bmatrix},$$

and

$$g(\mathbf{x}(t)) = ||\mathbf{x}_1(t)||.$$

Notice that the system is nonlinear and, therefore, a state observer that accounts of this nonlinearities is required. Additionally, the output measurement was taken as the actual range and not the square range. This is important since it is assumed that the sensors are affected with zero mean Gaussian noise. If the output measurement were taken as the square range, then the output will be $y(t) = \mathbf{x}_1^\top(t)\mathbf{x}_1(t) + ||\mathbf{x}_1(t)||\kappa(t) + \kappa(t)^2 = \mathbf{x}_1^\top(t)\mathbf{x}_1(t) + \lambda(t)$, where $\lambda(t) = ||\mathbf{x}_1(t)||\kappa(t) + \kappa(t)^2$ is neither zero mean nor Gaussian noise. For further details on this, refer to Chapter 2.3.1 of [90].

Then, the objective of the observer is to estimate $\mathbf{x}(t)$ given the time histories of the input $\mathbf{u}(t)$ and the output $y(t)$.

The Extended Kalman Filter (EKF) is the nonlinear version of the Kalman Filter (KF), which is an algorithm that uses a time series of the input and the output corrupted with additive independent white noise, a produces an statistically optimal estimation of the state.

The main objective of the EKF is to extend the results of the KF for nonlinear systems. Basically, the EKF uses a linearized model of the system around the previous estimation of the state. This method has been widely used in different applications such as: attitude estimation [91–95], navigation [96–99], model identification [100–103], biological or chemical process [104–106], among others [107–115].

To apply the EKF on (3.1), first the system should be discretized. We assume that the control input $\mathbf{u}$ is constant over the sampling interval h (zero-order hold). Then, the continuous model (3.1) is discretized using 1st-order approximation Euler method as follows

$$\left.\begin{aligned} \mathbf{x}_{k+1} &= \boldsymbol{f}(\mathbf{x}_k, \mathbf{u}_k) + h\boldsymbol{\zeta}_k, \\ y_k &= g(\mathbf{x}_k) + \kappa_k, \end{aligned}\right\} \tag{3.2}$$

where $\mathbf{x}_k = [\mathbf{x}_{1_k}, \mathbf{x}_{2_k}, x_{3_k}]^\top = [{}^{\mathcal{B}}\mathbf{d}_k^\top, {}^{\mathcal{B}}\mathbf{v}_{c_k}^\top, \chi_k]^\top$ is the state vector at time k, $\mathbf{u}_k = [{}^{\mathcal{B}}\mathbf{v}_k^\top, \omega_{m_k}, r_k]^\top$ is the input vector at time k, y_k is the measurement sampled at time k, $\boldsymbol{f}(\cdot)$ is

$$\boldsymbol{f}(\mathbf{x}_k, \mathbf{u}_k) = \begin{bmatrix} \mathbf{x}_{1_k} + h\left(-S(r_k)\mathbf{x}_{1_k} - {}^{\mathcal{B}}\mathbf{v}_k + l_m\omega_{m_k}\mathcal{R}_{\psi_k}^\top \mathbf{w}^\perp(x_{3_k}) - \mathbf{x}_{2_k}\right) \\ \mathbf{x}_{2_k} + h\left(-S(r_k)\mathbf{x}_{2_k}\right) \\ x_{3_k} + h\omega_{m_k} \end{bmatrix},$$

and $g(\cdot)$ is

$$g(\mathbf{x}_k) = ||\mathbf{x}_{1_k}||.$$

The EKF is executed in two steps: the predictor, which calculates a approximation of the state and covariance; and the corrector, which improves the initial approximation when a new measurement is available. The predictor equations for the EKF are

$$\left.\begin{aligned} \hat{\mathbf{x}}_{k+1}^- &= \boldsymbol{f}(\hat{\mathbf{x}}_k, \mathbf{u}_k), \\ \hat{P}_{k+1}^- &= F_k P_k F_k^\top + Q_k, \end{aligned}\right\} \tag{3.3}$$

and the correction equation are given by

$$\left.\begin{aligned} \tilde{y}_{k+1} &= y_k - g(\hat{\mathbf{x}}_k), \\ S_{k+1} &= H_k P_{k+1}^- H_k^\top + R_k, \\ K_{k+1} &= P_{k+1}^- H_k^\top S_{k+1}^{-1}, \\ \hat{\mathbf{x}}_{k+1} &= \hat{\mathbf{x}}_{k+1}^- + K_{k+1}\tilde{y}_{k+1}, \\ \hat{P}_{k+1} &= \left(I - K_{k+1}H_k\right)\hat{P}_{k+1}^-, \end{aligned}\right\} \tag{3.4}$$

where $\hat{\mathbf{x}}_{k+1}^-$ is the *a priori* state estimation, $\hat{P}_{k+1}^-$ is the predicted covariance estimate, K_{k+1} is the Kalman gain, $\hat{\mathbf{x}}_{k+1}$ is the *a posteriori* state estimation, and $\hat{P}_{k+1}$ is the corrected covariance estimate. Symbols Q_k and R_k are the process and measurement noise covariance matrices at time k, respectively. Furthermore, F_k and H_k are the process and measurement Jacobian matrices at time k, respectively, given by

$$F_k = \begin{bmatrix} I_2 - hS(r_k) & -hI_2 & -hl_m\omega_{m_k}\mathcal{R}_{\psi_k}^\top \mathbf{w}(x_{3_k}) \\ \mathbf{0} & I_2 - hS(r_k) & \mathbf{0} \\ \mathbf{0} & \mathbf{0} & 1 \end{bmatrix}$$

and

$$H_k = \begin{bmatrix} \frac{\mathbf{x}_{1_k}}{||\mathbf{x}_{1_k}||} & \mathbf{0} & 0 \end{bmatrix}.$$

To test the observer, we run a Monte-Carlo simulation with 100 scenarios, in which we choose randomly the beacon's and vehicle's initial position and orientation, as well the ocean current velocity. We restrict the operation of the vehicle to an area larger than the beacon's position ($||^{\mathcal{I}}\mathbf{p}|| > ||^{\mathcal{I}}\mathbf{b}|| + \epsilon$); the foregoing in order to avoid collisions or entanglement between the vehicle and beacon. The inputs of the system are chosen such that Proposition 6 holds, that is, the angular velocity of the vehicle is set to $r = 0.25\,\text{rad/s}$, the velocity of the vehicle ${}^{\mathcal{B}}\mathbf{v} = [1.5, 0]^{\top}\,\text{m/s}$, and the angular velocity of the beacon $\omega_m = 1\,\text{rad/s}$. The manipulator's length is set to $l_m = 2\,\text{m}$ and the simulation time to $t = 200\,\text{s}$. The range measurement is modeled with an additive white Gaussian noise with a standard deviation of 0.3 m [81] and acquired every $T_s = 0.1\,\text{s}$ being T_s the discretization sampling time .

Table 1: Simulation parameters (model with ocean currents)

Parameter	**Variable**	**Value**
Vehicle's angular velocity	r	$0.25\,\text{rad/s}$
Vehicle's linear velocity	${}^{\mathcal{B}}\mathbf{v}$	$[1.5, 0]^{\top}\,\text{m/s}$
Beacon's angular velocity	ω_m	$1\,\text{rad/s}$
Manipulator's length	l_m	$2\,\text{m}$
Simulation time	t	$200\,\text{s}$
Standard deviation noise range sensor	-	$0.3\,\text{m}$

Regarding the state observer, we assume that the initial condition is initialized with a random Gaussian distribution with mean equal to the real value and standard deviation of $\pm 30\,\%$ from the real value. The Kalman filter parameters were chosen as $Q_k = 1 \times 10^{-4}\text{diag}([1, 1, 1, 1, 0.001])$ for the process noise covariance matrix, the output noise variance as $R_k = 0.3^2$, and the initial estimation error covariance $P_0 = I_n$. The performance of the steady state is represented by mean absolute error (MAE). The steady state MAE is obtained from the last 20 s of the simulation. The average steady state MAE for vehicle's position is 2.4 m with a standard deviation of $\pm 3.7\,\text{m}$; for beacon's position is 0.17 m with standard deviation of $\pm 0.32\,\text{m}$; and for ocean current velocity is 0.29 m/s with standard deviation of $\pm 0.14\,\text{m/s}$. Figure 12 shows a histogram of the steady state MAE from all 100 simulation.

Taking into account that the simulation has an associated margin of error, then, the average MAE is not just described as a particular value but instead as a confidence

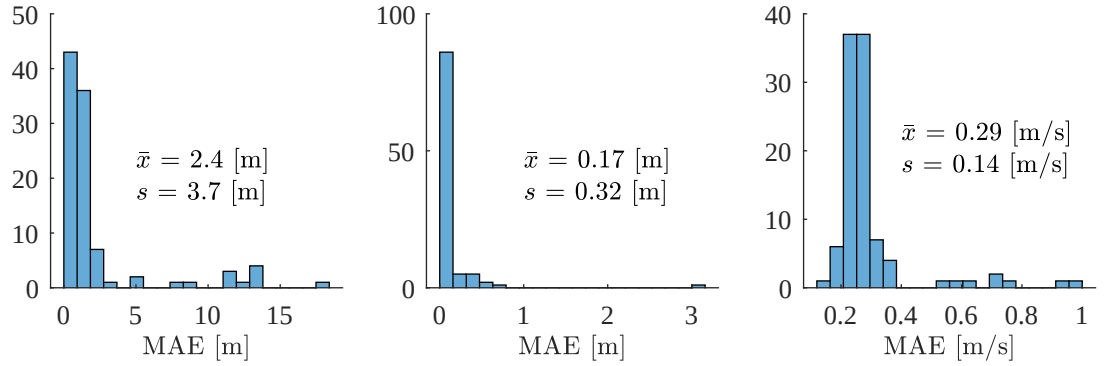

(a) Vehicle's position (b) Beacon's position (c) Ocean current velocity

Figure 12: Histogram of the steady state MAE for EKF simulation taking into account ocean currents. There worst case scenario gave an steady state MAE of 17 m in the vehicle's position.

interval where the level of uncertainty is established as 95 %. Then, for 95 % of simulations the steady state MAE for the vehicle's position is contained in the interval $(1.7632, 2.9776)$ m, for the beacon's position $(0.1176, 0.2234)$ m, and for the ocean current velocity $(0.2708, 0.3180)$ m/s.

Additionally, to understand which was the worst case scenario, not only due to the steady state error, we evaluate the performance by applying the integral of the square of the error (ISE). The ISE is obtained from the whole simulation time (200 s). This metric give us a quantitative behavior of the transient response for all the simulations. Figure 13 shows an histogram of ISE from all 100 simulations.

In the worst case scenario, the vehicle's initial position was set to ${}^{\mathcal{I}}\mathbf{p}_0 = [15.31, 28.29]^\top$ m and the beacon ${}^{\mathcal{I}}\mathbf{b}_0 = [0.73, 1.85]^\top$ m. The state observer was initialized with ${}^{\mathcal{I}}\hat{\mathbf{p}}_0 = [25.58, 35.97]^\top$ m and the beacon ${}^{\mathcal{I}}\hat{\mathbf{b}}_0 = [1.22, 1.57]^\top$ m. Figure 14 shows the vehicle's trajectory and its estimation. Notice, that at the beginning there is a large error between the real position and its estimation. Additionally, the norms of the estimation errors are shown in Figure 15. In the worst case scenario, the EKF takes the complete simulation time to converge to the real value.

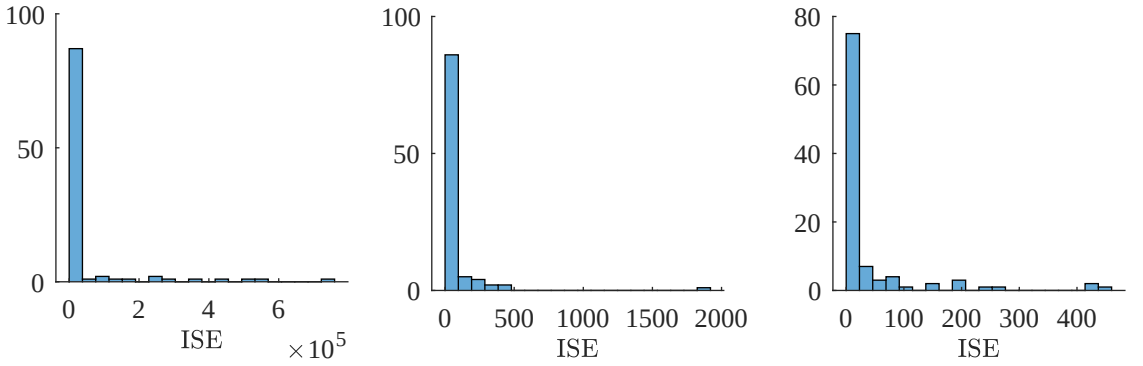

(a) Vehicle's position (b) Beacon's position (c) Ocean current velocity

Figure 13: Histogram of ISE for EKF simulation taking into account ocean currents. The worst case scenario corresponds the same having the worst steady state MAE.

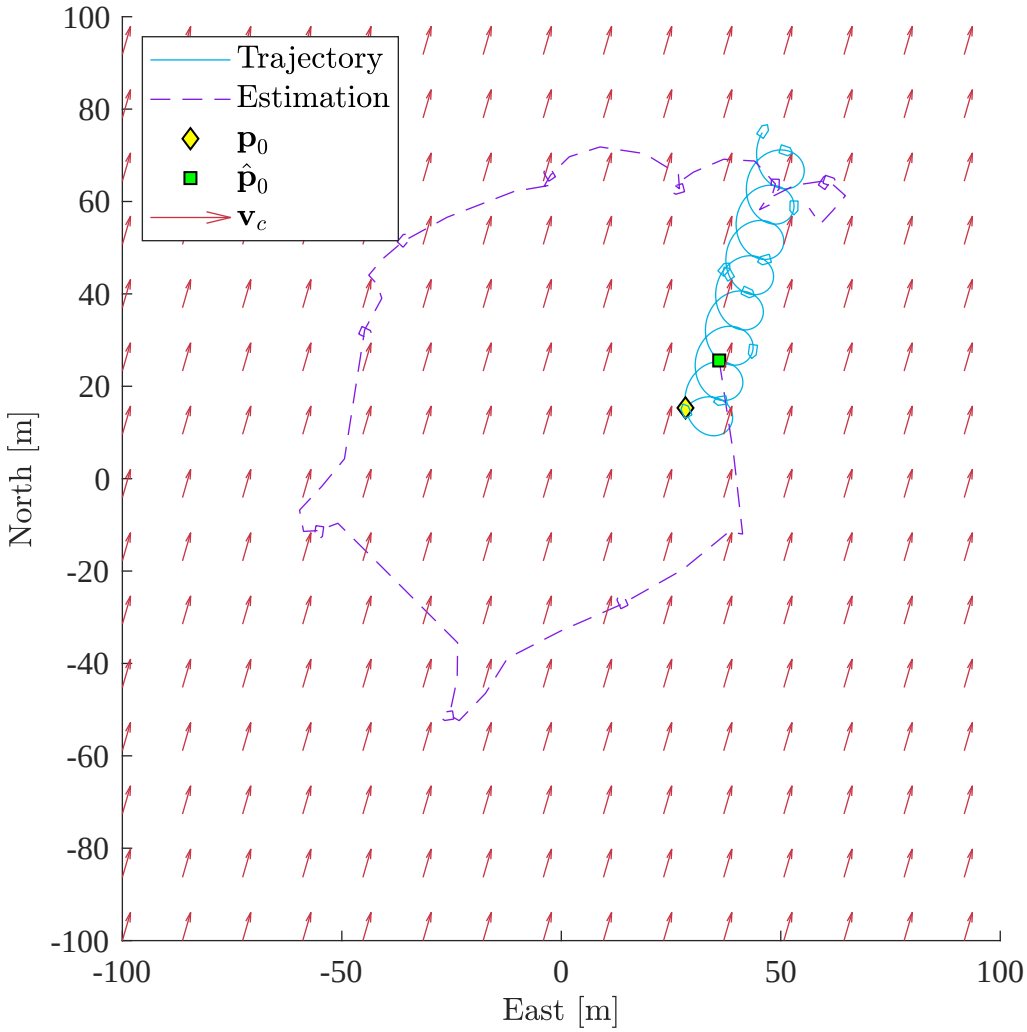

Figure 14: Vehicle's trajectory and its estimation for the EKF. Notice that the filter takes time to converge, but at the end of the simulation is close to the real value.

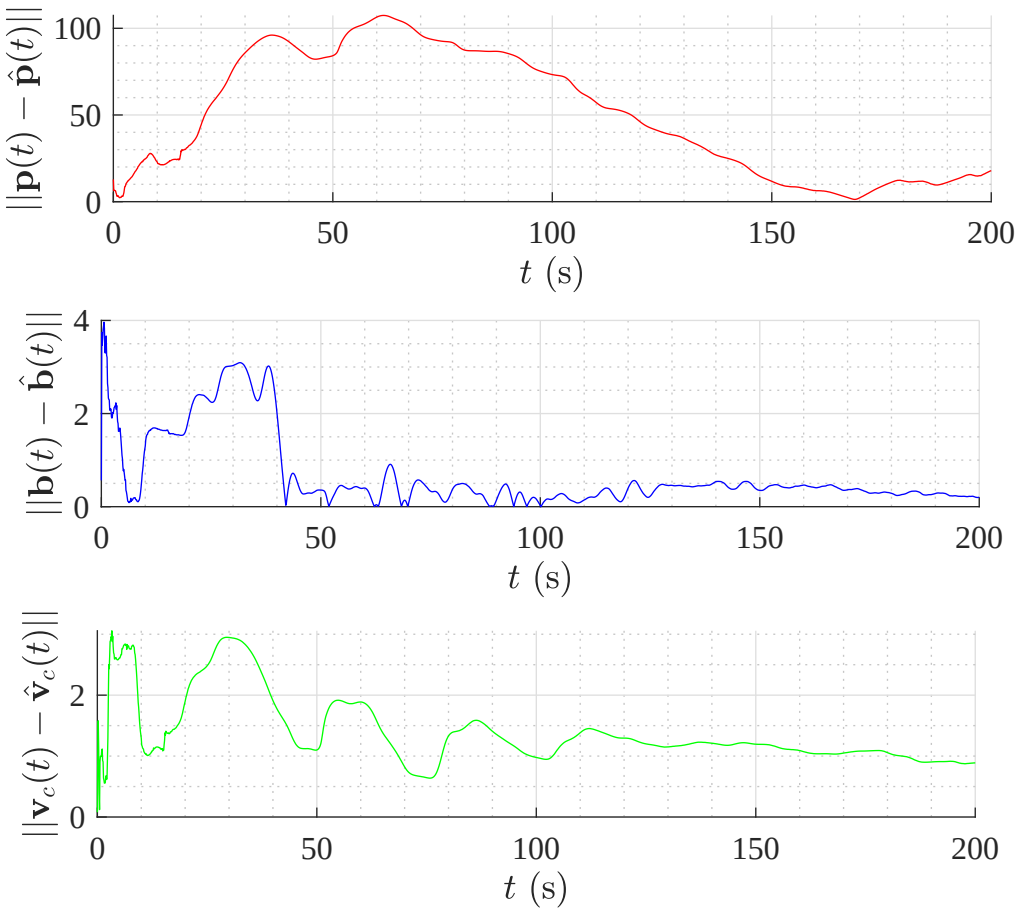

Figure 15: Norm of the estimation errors for the EKF. Notice that the first 200 s there is a large estimation error in the vehicle position.

Recall that the last scenario lies outside the confidence interval. Then, another interesting scenario to show is one that lies between the confidence interval. The vehicle's initial position was set to ${}^{\mathcal{I}}\mathbf{p}_0 = [19.57, 6.45]^\top$ m and the beacon ${}^{\mathcal{I}}\mathbf{b}_0 = [1.06, 1.69]^\top$ m. The state observer was initialized with ${}^{\mathcal{I}}\hat{\mathbf{p}}_0 = [11.23, 3.26]^\top$ m and the beacon ${}^{\mathcal{I}}\hat{\mathbf{b}}_0 = [0.97, 1.74]^\top$ m. Figure 16 shows the vehicle's trajectory and its estimation. Notice, that at the beginning there is a large error between the real position and its estimation. Additionally, the norms of the estimation errors are shown in Figure 17. It is important to note that the behavior of the filter is affected by how far the initial estimation is from the real state of the system.

Additionally, since the output of the system is the range between the beacon and the

vehicle, the further away is far from the other, the filter tends to deteriorate. The above seems to be because the position of the vehicle is larger in magnitude than the position of the beacon, causing it to have a greater weight in the correction phase. Therefore, the accuracy in the estimation decrease. Finally, the initial estimation covariance matrix is fixed for all simulation scenarios. The above can cause that in those scenarios, where the initial estimation value is very close to the real value, the filter exhibits a more aggressive transient response.

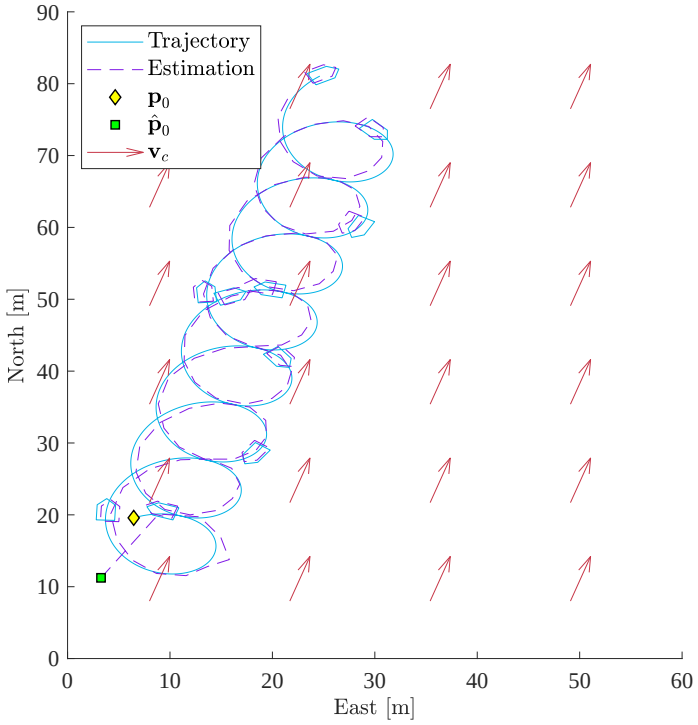

Figure 16: Vehicle's trajectory and its estimation for a simulation that lies within the CI using the EKF.

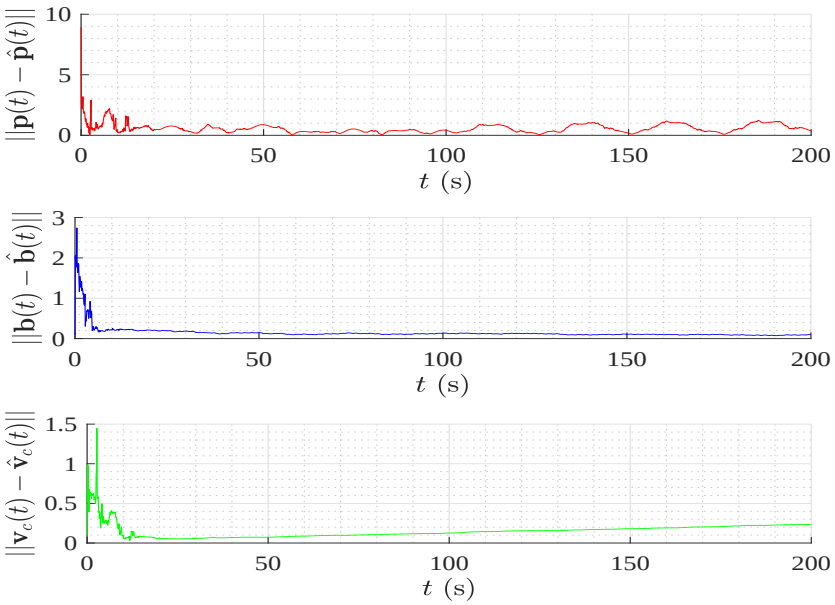

Figure 17: Norm of the estimation errors for a simulation that within the CI using the EKF.

3.3. EXOGENOUS KALMAN FILTER TAKING INTO ACCOUNT OCEAN CURRENTS

Estimation for nonlinear systems is a challenging problem. There are a lot of methods in literature that solve the problem. In the previous section, the nonlinear version of the Kalman Filter (EKF) was used. The EKF is based on the linearization of the system around the current estimation and produces an optimal estimation of the state with respect to noise. Although convergence were achieved in the simulation scenario, in general there are no global stability properties guaranteed for the EKF.

Nonlinear observers have good global stability properties and desired performance. Nevertheless, they can be noise sensitive. To solve both problems, Johansen and Fossen [116] proposed a new version of the Kalman Filter, known as Exogenous Kalman Filter (XKF). The key idea is: rather than linearizing the system around the current estimation (EKF), the XKF proposes to linearize the system around the estimation of a nonlinear observer. Since both system are in cascade, the Kalman Filter inherits the

global stability properties of the nonlinear observer and at the same time is suboptimal with respect to noise.

Inspired by those ideas, we propose the following methodology for the system (3.1): first, a linear augmented-state observer is designed, which guarantees global stability properties; then, an inverse state transformation is applied to recover the original state. This estimation is highly affected by noise since the output used in the process is the square range. To improve this, the estimation of this observer is used in the linearization step of an EKF. Since the linear observer is in cascade with the EKF, then the complete observer inherits the global stability properties. Figure 18 shows the observer scheme.

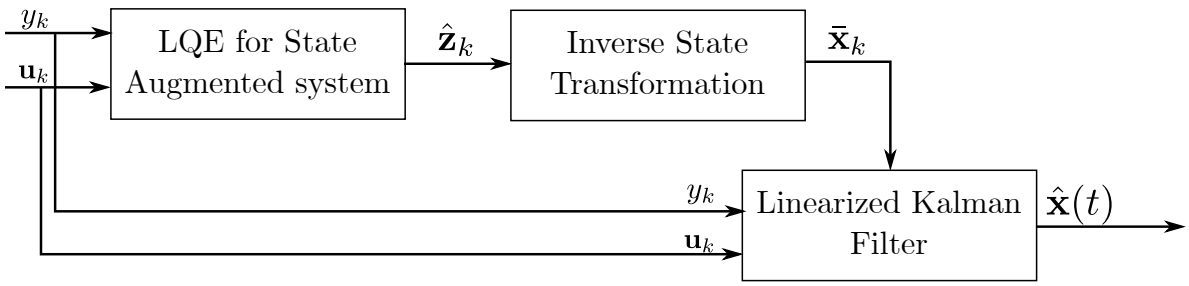

Figure 18: Observer design methodoloy based on XKF

3.3.1. Linear Quadratic Estimator for the state augmented system

The first stage in the procedure is to find an observer for the augmented-state system (2.66). Recall that (2.66) and (3.1) are equivalent in the sense that there is one-to-one correspondence in the state trajectories of both systems. The linear system (2.66) is obtained by applying a state space augmentation to (3.1). Now consider that the system (2.66) is corrupted with zero mean Gaussian disturbance $\boldsymbol{v} \in \mathbb{R}^{15}$ and noise $w \in \mathbb{R}$

$$\left.\begin{aligned} \dot{\mathbf{z}}(t) &= A(\mathbf{u})\mathbf{z}(t) + B\mathbf{u} + \boldsymbol{v} \\ \bar{y}(t) &= C\mathbf{z}(t) + w \end{aligned}\right\} \tag{3.5}$$

where

$$A(\mathbf{u}) = \begin{bmatrix} -S(r) & -I_2 & l_m\omega_m I_2 & \mathbf{0} & \mathbf{0} & \mathbf{0} & \mathbf{0} & \mathbf{0} & \mathbf{0} & \mathbf{0} & \mathbf{0} \\ \mathbf{0} & -S(r) & \mathbf{0} & \mathbf{0} & \mathbf{0} & \mathbf{0} & \mathbf{0} & \mathbf{0} & \mathbf{0} & \mathbf{0} & \mathbf{0} \\ \mathbf{0} & \mathbf{0} & -S(r) & -\omega_m I_2 & \mathbf{0} & \mathbf{0} & \mathbf{0} & \mathbf{0} & \mathbf{0} & \mathbf{0} & \mathbf{0} \\ \mathbf{0} & \mathbf{0} & \omega_m I_2 & -S(r) & \mathbf{0} & \mathbf{0} & \mathbf{0} & \mathbf{0} & \mathbf{0} & \mathbf{0} & \mathbf{0} \\ -2^{\mathcal{B}}\mathbf{v}^\top & \mathbf{0} & \mathbf{0} & \mathbf{0} & 0 & -2 & 2l_m\omega_m & 0 & 0 & 0 & 0 \\ \mathbf{0} & -^{\mathcal{B}}\mathbf{v}^\top & \mathbf{0} & \mathbf{0} & 0 & 0 & 0 & 0 & -1 & l_m\omega_m & 0 \\ \mathbf{0} & \mathbf{0} & -^{\mathcal{B}}\mathbf{v}^\top & \mathbf{0} & 0 & 0 & 0 & -\omega_m & 0 & -1 & 0 \\ \mathbf{0} & \mathbf{0} & \mathbf{0} & -^{\mathcal{B}}\mathbf{v}^\top & 0 & 0 & \omega_m & 0 & 0 & 0 & -1 \\ \mathbf{0} & \mathbf{0} & \mathbf{0} & \mathbf{0} & 0 & 0 & 0 & 0 & 0 & 0 & 0 \\ \mathbf{0} & \mathbf{0} & \mathbf{0} & \mathbf{0} & 0 & 0 & 0 & 0 & 0 & 0 & -\omega_m \\ \mathbf{0} & \mathbf{0} & \mathbf{0} & \mathbf{0} & 0 & 0 & 0 & 0 & 0 & \omega_m & 0 \end{bmatrix},$$

$$B = \begin{bmatrix} -I_2 & \mathbf{0} & \mathbf{0} \\ \mathbf{0} & \mathbf{0} & \mathbf{0} \\ \mathbf{0} & \mathbf{0} & \mathbf{0} \\ \mathbf{0} & \mathbf{0} & \mathbf{0} \\ \mathbf{0} & 0 & 0 \\ \mathbf{0} & 0 & 0 \\ \mathbf{0} & l_m & 0 \\ \mathbf{0} & 0 & 0 \\ \mathbf{0} & 0 & 0 \\ \mathbf{0} & 0 & 0 \\ \mathbf{0} & 0 & 0 \end{bmatrix},$$

$$C = \begin{bmatrix} \mathbf{0} & \mathbf{0} & \mathbf{0} & \mathbf{0} & 1 & 0 & 0 & 0 & 0 & 0 & 0 \end{bmatrix},$$

Remark 3. *Although the disturbances $\boldsymbol{\zeta}(t)$ and $\kappa(t)$ in (3.1) are stochastic variables with known covariance matrices, the stochastic properties of $\boldsymbol{v}$ and w in (3.5) are not the same. The above is because a nonlinear transformation is carried out on the system (3.1) which makes it difficult to relate the stochastic properties of the new disturbances. Additionally, the transformation can lead to correlations between the state and the disturbances.*

Now the problem is to find the estimate $\hat{\mathbf{z}}(t)$ for the system (3.5) given the time histories of $\{\mathbf{u}(\tau) : 0 \leq \tau \leq t\}$ and $\{\bar{y}(\tau) : 0 \leq \tau \leq t\}$. One way to solve the problem is by using

Kalman-Bucy filter, also known as Linear Quadratic Estimator (LQE). The filter was designed to minimize the mean square error $\mathbb{E}\{(\mathbf{z}(t)-\hat{\mathbf{z}}(t))(\mathbf{z}(t)-\hat{\mathbf{z}}(t))^\top\}$.

Proposition 10 (Kalman-Bucy, 1961 [117]). *An optimal estimator for the system (3.5) has the form of a linear observer given by*

$$\dot{\hat{\mathbf{z}}}(t) = A(\mathbf{u})\hat{\mathbf{z}}(t) + B\mathbf{u} + L(\bar{y} - C\hat{\mathbf{z}}(t)), \tag{3.6}$$

where $L = \bar{P}C^\top \bar{R}^{-1}$ *and* $P = \mathbb{E}\{(\mathbf{z}(t)-\hat{\mathbf{z}}(t))(\mathbf{z}(t)-\hat{\mathbf{z}}(t))^\top\}$ *satisfies the following algebraic Riccati equation*

$$A(\mathbf{u})\bar{P} + \bar{P}A(\mathbf{u})^\top - \bar{P}C^\top \bar{R}^{-1}C\bar{P} + \bar{Q} = 0. \tag{3.7}$$

Sketch of the proof. Lets define the state estimation error as $\mathbf{e}(t) = \mathbf{z}(t) - \hat{\mathbf{z}}(t)$. Then $\dot{\mathbf{e}}(t) = (A(\mathbf{u}) - LC)\,\mathbf{e}(t) + \boldsymbol{\gamma}$, where $\boldsymbol{\gamma} = \boldsymbol{v} - Lw$. Notice that in absence of measurement noise and disturbances in the process, $\mathbf{e}(t) \to 0$ as $t \to \infty$ since $(A(\mathbf{u}) - LC)$ is a stability matrix. In the presence of bounded noise measurement and disturbance, the system is BIBO stable from the inputs $\boldsymbol{v}$ and w to the output $\mathbf{e}$.

Additionally, notice that the covariance matrix $\bar{R}_\gamma$ is given by $\bar{R}_\gamma = \mathbb{E}\{(\boldsymbol{v} - Lw)(\boldsymbol{v} - Lw)^\top\} = \bar{Q} + L\bar{R}L^\top$. Now, the idea is to find an L such that $\bar{P}$ is as small as possible. The covariance matrix $\bar{P}$ of the error satisfies $\bar{P} = \mathbb{E}\{\mathbf{e}(t)\mathbf{e}^\top(t)\}$, and its derivative

$$\begin{aligned}
\dot{\bar{P}} &= (A(\mathbf{u}) - LC)\bar{P} + \bar{P}(A(\mathbf{u}) - LC)^\top + \bar{Q} + L\bar{R}L \\
&= A(\mathbf{u})\bar{P} + \bar{P}A(\mathbf{u})^\top + \bar{Q} - LC\bar{P} + \bar{P}C^\top L^\top + L\bar{R}L \\
&= A(\mathbf{u})\bar{P} + \bar{P}A(\mathbf{u})^\top + \bar{Q} + (L\bar{R} - \bar{P}C^\top)\bar{R}^{-1}(L\bar{R} - \bar{P}C^\top)^\top - \bar{P}C^\top \bar{R}C\bar{P}
\end{aligned}$$

Since $\bar{P}$ satisfied (3.7), then $\dot{\bar{P}} = (L\bar{R} - \bar{P}C^\top)\bar{R}^{-1}(L\bar{R} - \bar{P}C^\top)^\top$, which implies that $\dot{P} = 0$ when $L = \bar{P}C^\top \bar{R}^{-1}$. □

Notice that the observer presented in (3.6) assumes that the output $\bar{y}(t)$ is continuous in time, but in reality is not. A straightforward approach is to hold the output between each sample and assume it as continuous time (zero order hold). Other approach would be using Euler's method to discretize the observer (3.6), as

$$\dot{\hat{\mathbf{z}}}_{k+1} = \hat{\mathbf{z}}_k + h\left(A(\mathbf{u}_k)\hat{\mathbf{z}}_k + B\mathbf{u}_k + L(\bar{y}_k - C\hat{\mathbf{z}}_k)\right). \tag{3.8}$$

Remark 4. *Notice that* $\bar{y}_k \neq y_k$. *The output of the state augmented observer (3.8) is related to the original measurement as* $\bar{y}_k = y_k^2$.

3.3.2. *Inverse state transformation*

Notice that in order to develop the linear observer, a state augmentation was performed. The state estimation $\mathbf{z}_k$ is related with the original system through the following inverse state transformation

$$\bar{\mathbf{x}}_k = \begin{bmatrix} \bar{\mathbf{x}}_{1_k} \\ \bar{\mathbf{x}}_{2_k} \\ \bar{\mathbf{x}}_{3_k} \end{bmatrix} = \begin{bmatrix} \hat{\mathbf{z}}_{1_k} \\ \hat{\mathbf{z}}_{2_k} \\ \operatorname{atan2}\left(\mathcal{R}_\psi \hat{\mathbf{z}}_{4_k} \mathbf{e}_2, \mathcal{R}_\psi \hat{\mathbf{z}}_{4_k} \mathbf{e}_1\right) \end{bmatrix}, \tag{3.9}$$

where $\mathbf{e}_i \in \mathbb{R}^2$, $i \in \{1, 2\}$ the i^{th} column of the 2×2 identity matrix, and the function $\operatorname{atan2} : \mathbb{R}^2 \to [0, 2\pi)$ is defined as

$$\operatorname{atan2} = \begin{cases} \arctan(y/x) & \text{if } x > 0 \\ \arctan(y/x) + \pi & \text{if } x < 0 \text{ and } y \geq 0 \\ \arctan(y/x) - \pi & \text{if } x < 0 \text{ and } y < 0 \\ \pi/2 & \text{if } x = 0 \text{ and } y > 0 \\ \pi/2 & \text{if } x = 0 \text{ and } y < 0 \\ \text{undefined} & \text{if } x = 0 \text{ and } y = 0 \end{cases}$$

Remark 5. *It is possible from $\bar{\mathbf{x}}_k$ to recover the vehicle and beacon positions, that is, ${}^{\mathcal{I}}\mathbf{p}(t)$ and ${}^{\mathcal{I}}\mathbf{b}(t)$. Nevertheless, we will see through simulation that this estimation is affected by the noise and it has better performance once it passed through the second stage of the LKF.*

3.3.3. *Linearized Kalman Filter*

Now, we have $\bar{\mathbf{x}}_k$ as an estimate of $\mathbf{x}_k$, which is a bounded signal given by the filter (3.8) and the inverse transformation (3.9). We use this signal as a linearization point for the linear Kalman filter. A first-order Taylor series expansion of (3.2) about the trajectory $\bar{\mathbf{x}}_k$ yields the linearized model

$$\left.\begin{aligned} \mathbf{x}_{k+1} &= \boldsymbol{f}(\bar{\mathbf{x}}_k, \mathbf{u}_k) + F_k(\mathbf{x}_k - \bar{\mathbf{x}}_k) + \epsilon_{x_k} + h\boldsymbol{\zeta}_k, \\ y_k &= g(\bar{\mathbf{x}}_k) + H_k(\mathbf{x}_k - \bar{\mathbf{x}}_k) + \epsilon_{y_k} + \kappa_k, \end{aligned}\right\}, \tag{3.10}$$

where ϵ_{x_k} and ϵ_{y_k} are the high order terms in the linearization processes, F_k and H_k are the Jacobian matrices around the state trajectory $\bar{\mathbf{x}}_k$ given by

$$F_k := \frac{\partial \boldsymbol{f}(\bar{\mathbf{x}}_k, \mathbf{u}_k)}{\partial \mathbf{x}} = \begin{bmatrix} I_2 - hS(r_k) & -hI_2 & -hl_m\omega_{m_k}\mathcal{R}_{\psi_k}^\top \mathbf{w}\left(\bar{x}_{3_k}\right) \\ \mathbf{0} & I_2 - hS(r_k) & \mathbf{0} \\ \mathbf{0} & \mathbf{0} & 1 \end{bmatrix},$$

$$H_k := \frac{\partial g(\bar{\mathbf{x}}_k, \mathbf{u}_k)}{\partial \mathbf{x}} = \begin{bmatrix} \frac{\bar{\mathbf{x}}_{1_k}}{\|\bar{\mathbf{x}}_{1_k}\|} & \mathbf{0} & 0 \end{bmatrix}.$$

Remark 6. *Since $\bar{\mathbf{x}}_k$ is bounded and converges to $\mathbf{x}_k$, then it is possible to design an observer for the system (3.10) without taking into account the high-order terms [116].*

Then, the Linearized Kalman Filter (LKF) formulation for the system (3.10) in the predictor-corrector form is given by

$$\left.\begin{aligned} \hat{\mathbf{x}}_{k+1}^{-} &= \boldsymbol{f}(\bar{\mathbf{x}}_k, \mathbf{u}_k) + F_k(\hat{\mathbf{x}}_k - \bar{\mathbf{x}}_k), \\ \hat{P}_{k+1}^{-} &= F_k \hat{P}_k F_k^{\top} + Q_k, \end{aligned}\right\} \tag{3.11}$$

and the correction equation are given by

$$\left.\begin{aligned} \tilde{y}_k &= y_k - g(\bar{\mathbf{x}}_k) - H_k(\hat{\mathbf{x}}_{k+1}^{-} - \bar{\mathbf{x}}_k), \\ S_{k+1} &= H_k \hat{P}_{k+1}^{-} H_k^{\top} + R_k, \\ K_{k+1} &= \hat{P}_{k+1}^{-} H_k^{\top} S_{k+1}^{-1}, \\ \hat{\mathbf{x}}_{k+1} &= \hat{\mathbf{x}}_{k+1}^{-} + K_{k+1}\tilde{y}_k, \\ \hat{P}_{k+1} &= (I - K_{k+1}H_k)\,\hat{P}_{k+1}^{-}. \end{aligned}\right\} \tag{3.12}$$

Notice that, since $\boldsymbol{\zeta}_k$ and κ_k in the original nonlinear system (3.2) are assumed additive, then, the properties of the disturbances of the linearized system (3.10) are the same. A block diagram showing all stages is presented in Figure 19.

The following assumptions guarantee that the Linear Kalman Filter inherits the stability properties of the LQE.

Assumption 5. *The process noise covariance matrix, the measurement noise covariance matrix, and the initial estimation error covariance matrix are positive definite and symmetric.*

Assumption 6. *The LTV system represented by the matrices F_k and H_k is uniformly completely observable.*

3.3.4. Simulation results

To test the observer, we run a Monte-Carlo simulation with 100 scenarios, in which we choose randomly the beacon's and vehicle's initial position and orientation, and the ocean current velocity. The conditions are the same as the EKF, where we restrict

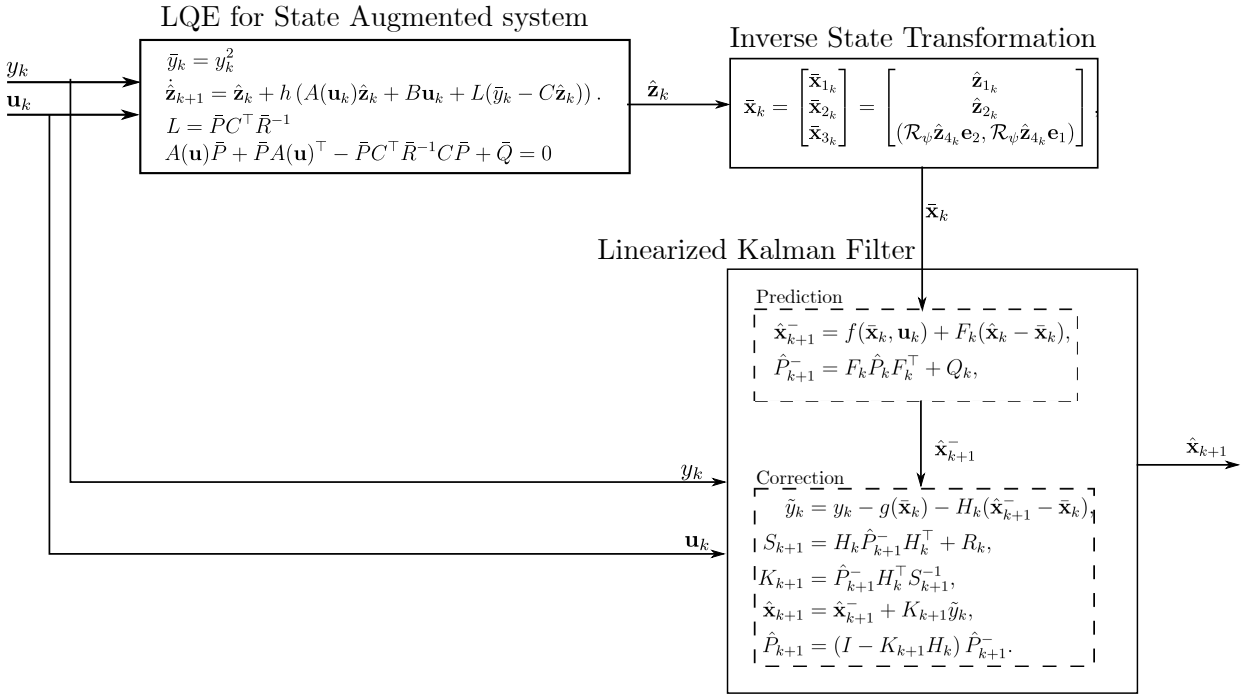

Figure 19: Observer interconnections diagram

the operation of the vehicle to an area larger than the beacon's position ($||^{\mathcal{I}}\mathbf{p}|| > ||^{\mathcal{I}}\mathbf{b}|| + \epsilon$), the foregoing in order to avoid collisions or entanglement between the vehicle and beacon. The inputs of the system are chosen such that Proposition 6 holds, that is, the angular velocity of the vehicle is set to $r = 0.05\,\text{rad/s}$, the velocity of the vehicle ${}^{\mathcal{B}}\mathbf{v} = [1.5, 0]^\top \text{m/s}$, and the angular velocity of the beacon $\omega_m = 0.3\,\text{rad/s}$. The manipulator's length is set to $l_m = 2\,\text{m}$ and the simulation time to $t = 200\,\text{s}$. The range measurement is modeled with an additive white Gaussian noise with a standard deviation of $0.3\,\text{m}$ [81] and acquired every $T_s = 0.1\,\text{s}$ being T_s the discretization sampling time.

Regarding the state observer, we assume that the initial condition is initialized with a random Gaussian distribution with mean equal to the real value and standard deviation of $\pm 30\,\%$ from the real value. The LQE parameters are chosen as $\bar{Q} = 0.001\ \text{diag}([1, 1, 1, 1, 0.001\ \text{ones}(1, 11)])$ for the process noise covariance matrix, and the output noise variance as $\bar{R} = 0.1$. The LKF parameters are chosen as $Q_k = 0.001\text{diag}([1, 1, 1, 1, 0.001])$, $R_k = 0.3^2$, and the initial estimation error covariance $P_0 = I_n$. All 100 simulations converge and the performance of the steady state is represented by the mean absolute error (MAE). The steady-state MAE is obtained from

the last 20 s of the simulation. The average steady state MAE for vehicle's position is 1.1 m with a standard deviation of ±0.3 m; for beacon's position is 0.27 m with standard deviation of ±0.12 m; and for ocean current velocity is 0.064 m/s with standard deviation of ±0.017 m/s. Figure 20 shows an histogram of the steady state MAE from all 100 simulation.

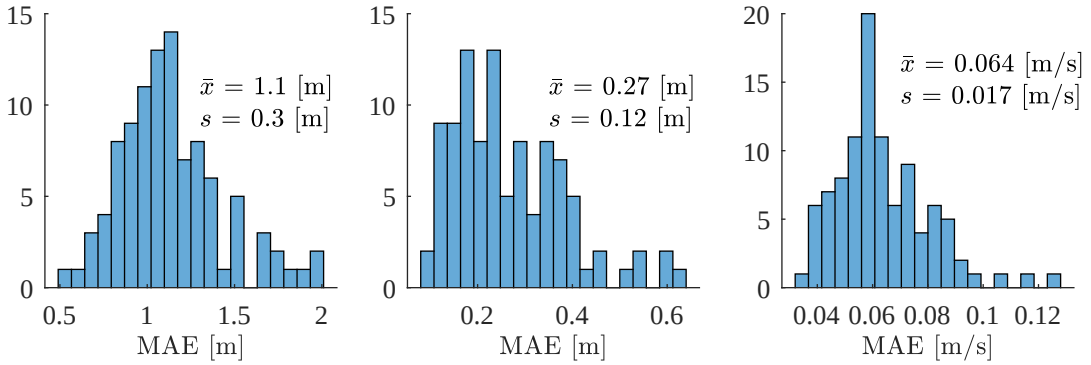

(a) Vehicle's position (b) Beacon's position (c) Ocean current velocity

Figure 20: Histogram of the steady state MAE for XKF simulation taking into account ocean currents. There worst case scenario gave an steady state MAE of 2 m in the vehicle's position.

Taking into account that the simulation has an associated margin of error, then the average MAE is not described as a particular value but instead as a confidence interval where the level of uncertainty is established as 95 %. Then, for 95 % of simulations the steady-state MAE for the vehicle's position is contained in the interval $(1.0866, 1.1850)$ m, for the beacon's position $0.2463, 0.2862)$ m, and for the ocean current velocity $(0.0609, 0.066)$ m/s.

Additionally, to understand which was the worst case scenario not only due to the steady-state error, we evaluate the performance by applying the integral of the square of the error (ISE). The ISE is obtained from the whole simulation time (200 s). This metric gives us a quantitative behavior of the transient response for all 100 simulations. Figure 21 shows an histogram of ISE from all 100 simulation.

From this point, it is interesting to understand how is the state estimation in the worst case scenario and one from the CI. In the worst case scenario, the vehicle's initial position was set to ${}^{\mathcal{I}}\mathbf{p}_0 = [6.29, 41.23]^\top$ m and the beacon ${}^{\mathcal{I}}\mathbf{b}_0 = [1.10, 1.66]^\top$ m. The state observer was initialized with ${}^{\mathcal{I}}\hat{\mathbf{p}}_0 = [6.10, 40.35]^\top$ m and the beacon ${}^{\mathcal{I}}\hat{\mathbf{b}}_0 =$

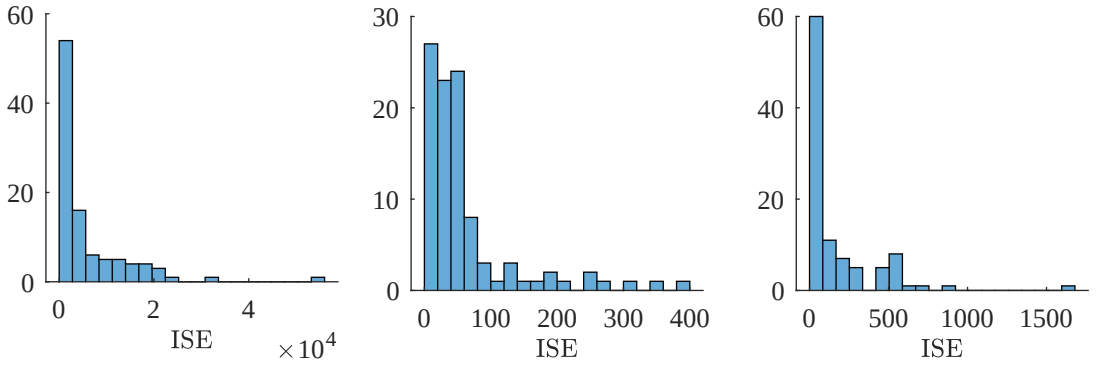

(a) Vehicle's position (b) Beacon's position (c) Ocean current velocity

Figure 21: Histogram of ISE for XKF simulation taking into account ocean currents. The worst case scenario corresponds the same having the worst steady state MAE.

$[1.23, 1.57]^\top$ m. Figure 22 shows the vehicle's trajectory and its estimation. Notice, that at the beginning there is a large error between the real position and its estimation. Additionally, the norm of the estimation errors are shown in Figure 23. Notice, that at the begin it presented large errors in the estimation, but at the end it converges.

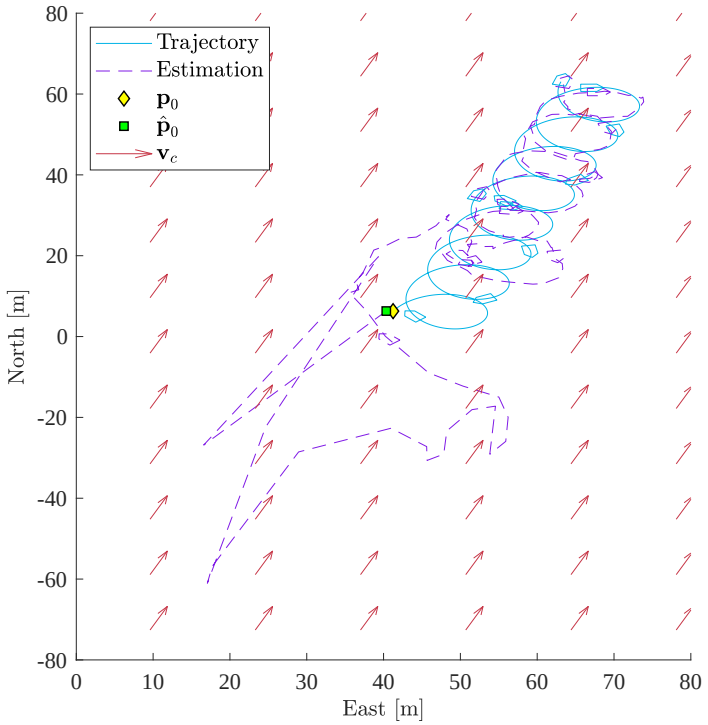

Figure 22: Vehicle's trajectory and its estimation. Notice that the filter takes time to converge, but at the end of the simulation is close to the real value.

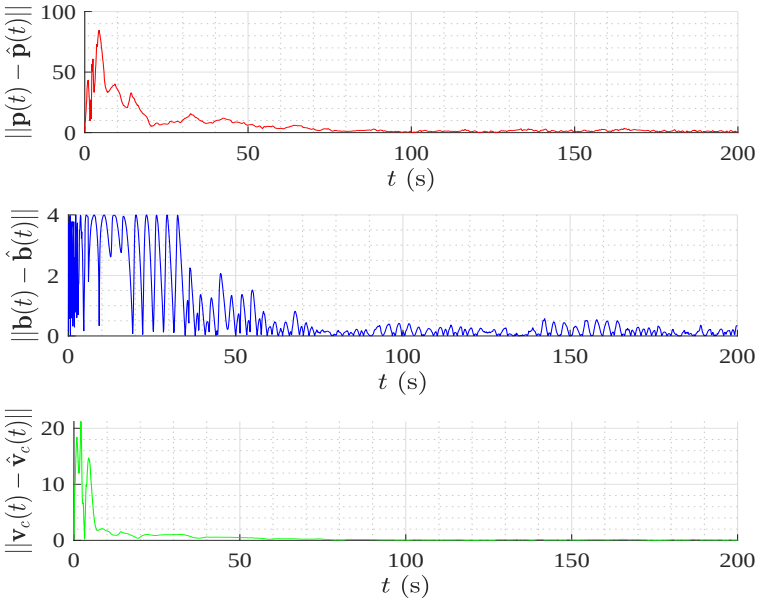

Figure 23: Norm of the estimation errors for the XKF. Notice that the first 200 s there is a large estimation error in the vehicle position.

The last scenario lies outside the confidence interval. Then, another interesting scenario to show is one that lies between the confidence interval. The vehicle's initial position was set to ${}^{\mathcal{I}}\mathbf{p}_0 = [-0.17, 14.22]^\top$ m and the beacon ${}^{\mathcal{I}}\mathbf{b}_0 = [1.10, 1.669]^\top$ m. The state observer was initialized with ${}^{\mathcal{I}}\hat{\mathbf{p}}_0 = [-0.02, 13.79]^\top$ m and the beacon ${}^{\mathcal{I}}\hat{\mathbf{b}}_0 = [1.12, 1.65]^\top$ m. Figure 24 shows the vehicle's trajectory and its estimation. Notice, that the algorithm achieves convergence even in the worst case scenario. Additionally, the norms of the estimation errors are shown in Figure 25.

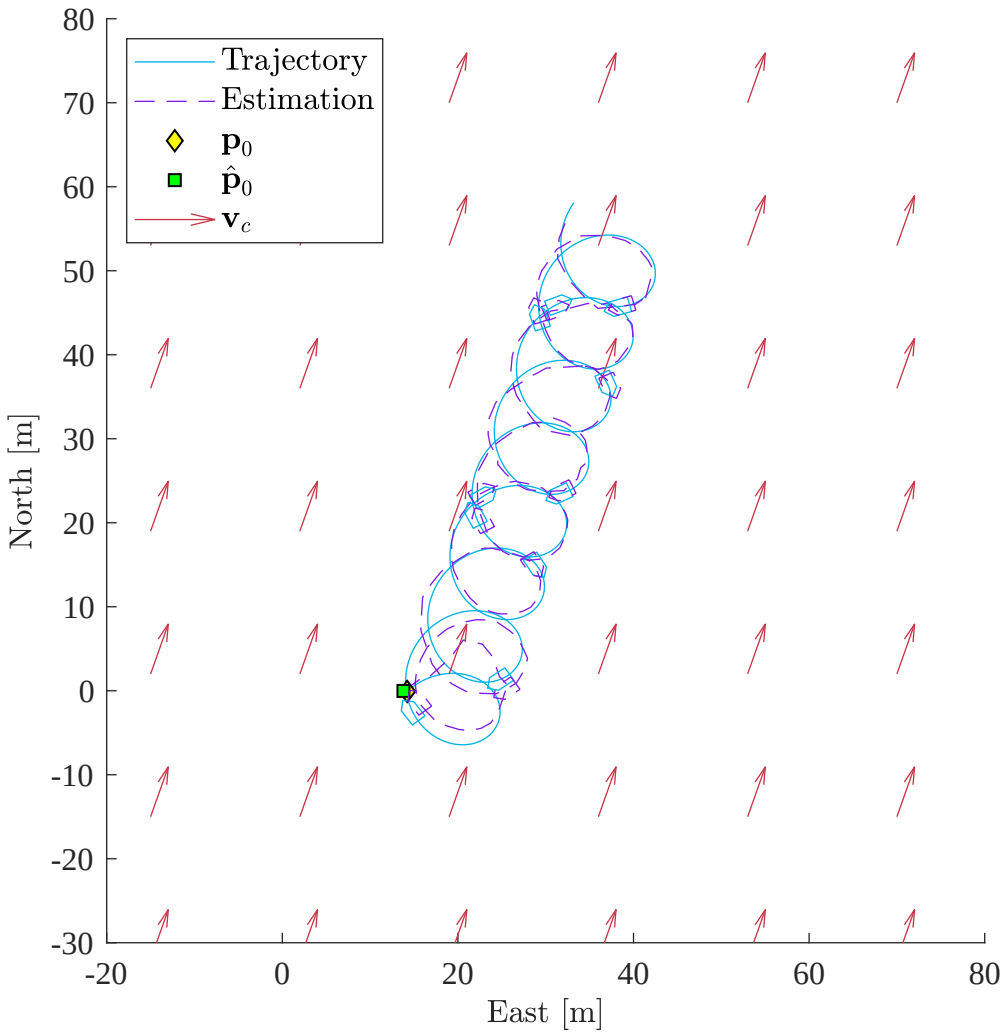

Figure 24: Vehicle's trajectory and its estimation for a simulation that lies within the CI using the XKF.

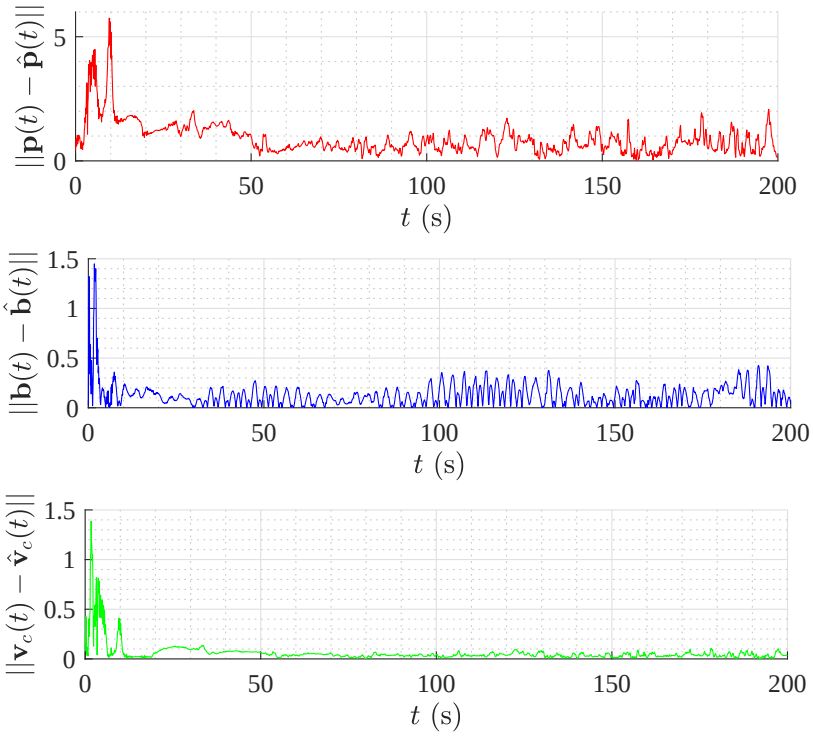

Figure 25: Norm of the estimation errors for a simulation that within the CI using the XKF.

Although both observers were tested with different simulations, it is important to make a qualitative comparison of the performance of both. In the case of XKF, the average MAE has better performance in the vehicle's position and ocean current estimation, which means a better performance in steady state. This can be also seen, if we compare the worst case scenario in both simulations. Finally, comparing the ISE distribution both presented similar shape. It is important to recall, that one of the main advantages of XKF over EKF, is the globally asymptotically stability property. Nevertheless, the observer XKF structure imposes limits in the type of trajectories to perform by the vehicle.

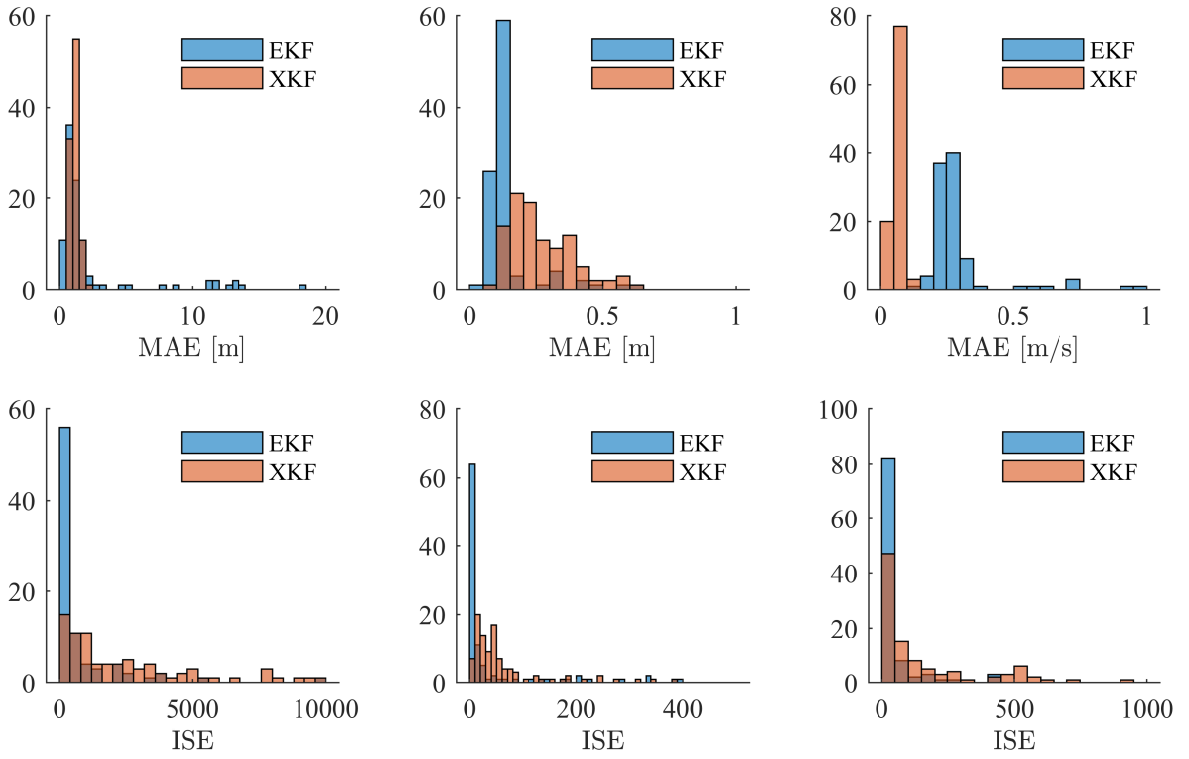

(a) Vehicle's position (b) Beacon's position (c) Ocean current velocity

Figure 26: Histogram comparison of ISE and MAE for both observers

3.4. CONCLUDING REMARKS

We addressed the estimation problem from two different implementations: the Extended Kalman Filter and the Exogenous Kalman Filter. For the EKF, we used the model represented in the $\{\mathcal{B}\}$-frame and assumed a Gaussian noise; this filter is based in the linearization of the the system around the current estimation. On the other hand, the Exogenous Kalman Filter is based on the linearization of the system around the estimation of a second filter with globally convergence properties. Under some assumptions, the cascade filter inherits the convergence properties and it has good response against noise. Finally, both filters were tested in simulation, with and without taking into account ocean currents.

4. OPTIMAL TRAJECTORIES

4.1. INTRODUCTION

Until now, all the analyses carried out in the previous sections about the system observability had been made from a yes or no point of view; this means that we answer the question whether the system is observable or not. This chapter addresses the problem of optimal trajectories for the cooperative underwater navigation system from an observability point of view. First, we derive a cost function based on the Fisher Information Matrix and the trajectories of the vehicle and the beacon. Finally, we find out optimal trajectories for the beacon based on the trajectories of the vehicle.

4.2. PROCESS AND MEASUREMENT MODEL

Consider the system described by the equation (2.61). This time, lets assume that the vehicle's velocity is given by ${}^{\mathcal{B}}\mathbf{v} := [v(t), 0]^{\top} \in \mathbb{R}^2$ and that the vehicle's rotation depends on $\dot{\psi}(t) = r(t)$. The above implies that the process and measurement model are given by

$$\left.\begin{aligned} {}^{\mathcal{I}}\dot{\mathbf{p}}(t) &= v(t)\mathbf{w}\left(\psi(t)\right) + {}^{\mathcal{I}}\mathbf{v}_c(t) \\ \dot{\psi}(t) &= r(t) \\ {}^{\mathcal{I}}\dot{\mathbf{v}}_c(t) &= 0 \\ {}^{\mathcal{I}}\dot{\mathbf{b}}(t) &= l_m\omega_m(t)\mathbf{w}^{\perp}\left(\chi(t)\right) \\ \dot{\chi}(t) &= \omega_m(t) \\ d(t) &= ||{}^{\mathcal{I}}\mathbf{b}(t) - {}^{\mathcal{I}}\mathbf{p}(t)|| \end{aligned}\right\}, \tag{4.1}$$

where $t \in [0, t_f)$ and $t_f > 0$, ${}^{\mathcal{I}}\mathbf{p} \in \mathbb{R}^2$ is the vehicle's position, $v : [0, t_f) \to \mathbb{R}$ is the vehicle's speed, $\psi : [0, t_f) \to [0, 2\pi)$ is the course angle of the vehicle, ${}^{\mathcal{I}}\mathbf{v}_c \in \mathbb{R}^2$ is the

velocity of the current, $r : [0, t_f) \to \mathbb{R}$ is the course rate of the vehicle, ${}^{\mathcal{I}}\mathbf{b} \in \mathbb{R}^2$ is the beacon's position, l_m is the length of the beacon's manipulator, $\omega_m : [0, t_f) \to \mathbb{R}$ is the angular rate of the beacon, $\chi : [0, t_f) \to [0, 2\pi)$ is the angular position of the beacon, and $d \in \mathbb{R}$ is the distance or range between the vehicle and beacon. In what follows, we assume that the beacon's positions is known, and is going to be used to increased the accuracy on the estimation. The solution of the system (4.1) at time t with initial condition $(\mathbf{p}_0, \psi_0, \mathbf{v}_{c_0}, \chi_0)$ is given by

$$\left.\begin{aligned} {}^{\mathcal{I}}\mathbf{p}(t) &= \mathbf{p}_0 + \int_0^t v(\tau)\mathbf{w}\left(\psi(\tau)\right) d\tau + t\,{}^{\mathcal{I}}\mathbf{v}_{c_0} \\ \psi(t) &= \psi_0 + \int_0^t r(\tau) d\tau \\ {}^{\mathcal{I}}\mathbf{v}_c(t) &= \mathbf{v}_{c_0} \\ \chi(t) &= \chi_0 + \int_0^t \omega_m(\tau) d\tau \\ {}^{\mathcal{I}}\mathbf{b}(t) &= l_m \mathbf{w}\left(\chi(t)\right) \\ d(t) &= ||{}^{\mathcal{I}}\mathbf{b}(t) - {}^{\mathcal{I}}\mathbf{p}(t)|| \end{aligned}\right\}, \tag{4.2}$$

In order to avoid collision or entanglement, we assume that the distance between the vehicle and beacon have a safety guard given by

$$||{}^{\mathcal{I}}\mathbf{b}(t) - {}^{\mathcal{I}}\mathbf{p}(t)|| \geq \mathcal{R}$$

for all $t > 0$ and $\mathcal{R} > 0$.

4.3. FISHER INFORMATION MATRIX

Now, we focused on finding the best trajectories for the system to increase the accuracy on the state estimation. One way to quantify this is by using the Fisher Information Matrix (FIM). The FIM give us a quantitative measure of how much information a random variable $\mathcal{X}$ carries about an unknown parameter $\boldsymbol{\theta}$. The problem for the Fisher Information Matrix can be written as follow: consider the problem of estimating an unknown parameter $\boldsymbol{\theta} \in \mathbb{R}^n$ from a set of measured data given by $\boldsymbol{y} \in \mathbb{R}^m$. Let $g(\boldsymbol{y}) : \mathbb{R}^n \to \mathbb{R}^m$ be an unbiased estimation of $\boldsymbol{\theta}$. Then, the error covariance of an

unbiased estimator is bounded by

$$\mathbb{E}\left\{[g(\boldsymbol{y})-\boldsymbol{\theta}][g(\boldsymbol{y})-\boldsymbol{\theta}]^{\top}\right\} \geq FIM(\boldsymbol{\theta})^{-1}, \tag{4.3}$$

where

$$FIM(\boldsymbol{\theta}) = \mathbb{E}\left\{\left(\nabla_{\boldsymbol{\theta}} \ln f(\boldsymbol{y},\boldsymbol{\theta})\right)\left(\nabla_{\boldsymbol{\theta}} \ln f(\boldsymbol{y},\boldsymbol{\theta})\right)^{\top}\right\}, \tag{4.4}$$

and $f(\boldsymbol{y},\boldsymbol{\theta})$ is the probability density function. The result given by the equation (4.3) is called the Cramer-Rao bound. This result establishes a lower bound on the variance of an unbiased estimator. For our purpose, the objective is to minimize as much as possible the bound which ultimately translates in a better performance in the estimation. The unknown parameter for the problem at hand is $\boldsymbol{\theta} := [\mathbf{p}_0^{\top}, \mathbf{v}_{c_0}^{\top}]^{\top}$ and the measured data model is given by

$$\boldsymbol{y} = \boldsymbol{z} + \boldsymbol{\eta}, \tag{4.5}$$

where $\boldsymbol{y} := [y_0, y_1, ..., y_{m-1}]^{\top}$ is a vector containing m range measurements, $\boldsymbol{z} := [d_0, d_1, ..., d_{m-1}]^{\top}$ is the real or actual range measurement given by (4.2), and $\boldsymbol{\eta} := [\eta_1, \eta_2, ..., \eta_{m-1}]^{\top}$ is a vector containing the measurement noise with $\eta_k \sim \mathcal{N}(0, \sigma^2)$. Note that the FIM explicitly depends on the range between the vehicle and beacon, which in turns implies that is going to depend on the inputs of the system.

With this in mind, we first derive the FIM for the problem under consideration. Then, we solve the problem without taking into account any constraint (unconstrained optimization problem). Finally, we solve different numerical scenarios where we put constraints over the motion of the beacon and vehicle. Also, we solve the problem when the vehicle is doing its own mission, and the beacon is helping to improve the observability of the system.

4.4. UNCONSTRAINED TRAJECTORY OPTIMIZATION

So far, just by moving the beacon with constant angular velocity, the system will become observable (recall from Chapter 2, that those are the cases where just the initial position of the vehicle and the initial ocean current are unknown). Now, it is our interest to find out the best sequence of angular velocity for the beacon which can increase the accuracy on the estimation.

Consider the system described by the equations (4.1). Let $m \in \mathbb{N}$ and consider a time sequence of length m, such as $0 = t_0 < t_1 < ... < t_{m-1} = t_f$, where t_k are sampling instants at which the range measure is acquired. For simplicity of the analysis, in what follows, we assume that the speed, course rate of the vehicle, and the angular velocity of the beacon are bounded piecewise constant functions of time, that is

$$v(t) = \bar{v}_k \in [\bar{v}_{\min}, \bar{v}_{\max}], t \in [t_k, t_{k+1}),$$

$$r(t) = \bar{r}_k \in [\bar{r}_{\min}, \bar{r}_{\max}], t \in [t_k, t_{k+1}),$$

and

$$\omega_m(t) = \bar{\omega}_{m_k} \in [\bar{\omega}_{m_{\min}}, \bar{\omega}_{m_{\max}}], t \in [t_k, t_{k+1}).$$

Based on this assumption, for all $t \in [t_k, t_{k+1})$, the model (4.2) can be written as

$$\left.\begin{aligned} {}^{\mathcal{I}}\mathbf{p}(t) &= \begin{cases} {}^{\mathcal{I}}\mathbf{p}_k + \dfrac{\bar{v}_k}{\bar{r}_k}[-\mathbf{w}^{\perp}(\psi(t)) + \mathbf{w}(\psi_k)] + (t - t_k){}^{\mathcal{I}}\mathbf{v}_{c_0}, & \text{if } \bar{r}_k \neq 0 \\ {}^{\mathcal{I}}\mathbf{p}_k + (t - t_k)(\bar{v}_k\mathbf{w}(\psi_k) + {}^{\mathcal{I}}\mathbf{v}_{c_0}), & \text{otherwise,} \end{cases} \\ \psi(t) &= \psi_k + (t - t_k)\bar{r}_k \\ {}^{\mathcal{I}}\mathbf{v}_c(t) &= \mathbf{v}_{c_0} \\ \chi(t) &= \chi_k + (t - t_k)\bar{\omega}_{m_k} \\ {}^{\mathcal{I}}\mathbf{b}(t) &= l_m\mathbf{w}(\chi(t)) \end{aligned}\right\} \tag{4.6}$$

Then, the model at time t_{k+1} and with constant sample time $\Delta t = t_{k-1} - t_k$, is given by

$$\left.\begin{aligned} {}^{\mathcal{I}}\mathbf{p}_{k+1} &= \begin{cases} {}^{\mathcal{I}}\mathbf{p}_k + \dfrac{\bar{v}_k}{\bar{r}_k}[-\mathbf{w}^{\perp}(\psi_{k+1}) + \mathbf{w}(\psi_k)] + \Delta t{}^{\mathcal{I}}\mathbf{v}_{c_0}, & \text{if } \bar{r}_k \neq 0 \\ {}^{\mathcal{I}}\mathbf{p}_k + \Delta t(\bar{v}_k\mathbf{w}(\psi_k) + {}^{\mathcal{I}}\mathbf{v}_{c_0}), & \text{otherwise,} \end{cases} \\ \psi_{k+1} &= \psi_k + \Delta t\ \bar{r}_k \\ {}^{\mathcal{I}}\mathbf{v}_{c_{k+1}} &= \mathbf{v}_{c_0} \\ \chi_{k+1} &= \chi_k + \Delta t\ \bar{\omega}_{m_k} \\ {}^{\mathcal{I}}\mathbf{b}_{k+1} &= l_m\mathbf{w}(\chi_{k+1}) \end{aligned}\right\} \tag{4.7}$$

Now that the model of the system has been described, it is possible to derive the particular FIM for the problem at hand. Recall that the FIM is given by (4.4) and the

measured data vector by (4.5). Since the model of the measured data has a normal distribution, then, the probability density function for the measurement vector $\boldsymbol{y}$ with respect to the unknown parameter $\boldsymbol{\theta} := [\mathbf{p}_0^\top, \mathbf{v}_{c_0}^\top]^\top$ is given by

$$f(\boldsymbol{y}, \boldsymbol{\theta}) = (2\pi)^{-m/2}|R|^{-1} \exp\left(-\frac{1}{2}(\boldsymbol{y} - \boldsymbol{z})^\top R^{-1}(\boldsymbol{y} - \boldsymbol{z})\right),$$

where $R = \sigma^2 I_m$ is the covariance matrix. Now, in order to obtain the FIM for our problem, we need the gradient of the logarithm, that is,

$$\nabla_{\boldsymbol{\theta}} \ln f(\boldsymbol{y}, \boldsymbol{\theta}) = (\nabla_{\boldsymbol{\theta}} \boldsymbol{z})^\top R^{-1}(\boldsymbol{y} - \boldsymbol{z})$$

Recall that the range vector $\boldsymbol{d}$ which is formed by stacking the range measurements, implicitly depends on the initial conditions of the system. Straightforward computation shows that the FIM for our problem is given by

$$FIM_{\mathbf{u}}(\boldsymbol{\theta}) = \sigma^{-2}(\nabla_{\boldsymbol{\theta}} \boldsymbol{z})^\top (\nabla_{\boldsymbol{\theta}} \boldsymbol{z}), \tag{4.8}$$

where

$$\nabla_\theta \boldsymbol{z} = \begin{bmatrix} -\frac{\mathbf{d}_0^\top}{d_0} & -t_0\frac{\mathbf{d}_0^\top}{d_0} \\ \vdots & \vdots \\ -\frac{\mathbf{d}_{m-1}^\top}{d_{m-1}} & -t_{m-1}\frac{\mathbf{d}_{m-1}^\top}{d_{m-1}} \end{bmatrix}_{m\times 4}$$

In the above, remember that $\mathbf{d}_k$ denotes the relative position vector at time t_k from the beacon with respect to the vehicle, that is, $\mathbf{d}_k = \mathbf{b}_k - \mathbf{p}_k$ and the norm is given by $d_k = ||\mathbf{d}_k||$. Additionally, the range vector depends on the inputs of the system, which in turn the FIM is going to depend on the inputs. For the sake of simplicity, the following compact notation will be used

$$\mathcal{D} := \begin{bmatrix} \frac{\mathbf{d}_0^\top}{d_0} \\ \vdots \\ \frac{\mathbf{d}_{m-1}^\top}{d_{m-1}} \end{bmatrix} \in \mathbb{R}^{m\times 2}$$

$$\mathcal{T} := \text{diag}(t_0, t_1, ..., t_{m-1}) \in \mathbb{R}^{m\times m}.$$

Then, the Fisher information matrix is given by

$$\begin{aligned} FIM_{\mathbf{u}}(\boldsymbol{\theta}) &= \sigma^{-2} \begin{bmatrix} -\mathcal{D}^\top \\ -\mathcal{D}^\top\mathcal{T} \end{bmatrix} \begin{bmatrix} -\mathcal{D} & -\mathcal{T}\mathcal{D} \end{bmatrix} \\ &= \sigma^{-2} \begin{bmatrix} \mathcal{D}^\top\mathcal{D} & \mathcal{D}^\top\mathcal{T}\mathcal{D} \\ \mathcal{D}^\top\mathcal{T}\mathcal{D} & \mathcal{D}^\top\mathcal{T}^2\mathcal{D} \end{bmatrix} \end{aligned} \tag{4.9}$$

Remark 7. *The Fisher information for our problem has the same structure that the one tackled in [77]. Nevertheless it is important to point out that the constraint in the motion for the beacon is different. Recall that the motion of the beacon is restricted to a small area given by the manipulator. At first glance it can be a disadvantage compared to using another vehicle as a beacon since the manipulator will impose a smaller range operation of the system. However, the dynamics of the manipulator is much faster than another underwater vehicle, which allows the system to execute more excited maneuvers.*

In order to solve an optimization problem, we define the following cost function based on the FIM like

$$J(\mathbf{u}) = \ln \det FIM_{\mathbf{u}}(\boldsymbol{\theta}), \tag{4.10}$$

which we seek to maximize.

Now, with a cost function that relates the amount of information that the range measurement carries about the initial condition of the system, it is possible to state an optimization problem. First, we solve the unconstrained optimization problem. To that end, we recall the results of Popescu et al. [118].

Proposition 11 (*Theorem 1.2 from* [118])**.** *Let* $\mathcal{Q} \in \mathbb{R}^{mn \times mn}$

$$\mathcal{Q} := \begin{bmatrix} Q_{11} & \dots. & Q_{1m} \\ \vdots & \ddots & \vdots \\ Q_{m1} & \dots & Q_{mm} \end{bmatrix},$$

where $Q_{ij} \in \mathbb{R}^{n \times n}$ *with* $i, j = 0, 1, \dots, m$*;* $Q_{ij} \succ 0$*;* $Q_{ij} = Q_{ij}^{\top}$*; and* $a_{ij} = \operatorname{tr}(Q_{ij})$*. Then the determinant of* $\mathcal{Q}$ *is maximized when each block is a scaled identity matrix of the form* $Q_{ij} = n^{-1} a_{ij} I_n$ *and the maximum value of the* $\det \mathcal{Q}$ *is given by* $(n^{-m} \det \mathcal{E})^n$*, where the elements of the square matrix* $\mathcal{E}$ *are* $\{a_{ij}\}$*.*

With this tool, we can find out what is the maximum cost function for the FIM given by (4.10). Let $Q_{11} := \mathcal{D}^{\top}\mathcal{D}$, $Q_{12} = Q_{21} := \mathcal{D}^{\top}\mathcal{T}\mathcal{D}$, and $Q_{22} := \mathcal{D}^{\top}\mathcal{T}\mathcal{D}$. Then, the matrix $\mathcal{Q}$ is given by

$$\mathcal{Q} = \begin{bmatrix} Q_{11} & Q_{12} \\ Q_{21} & Q_{22} \end{bmatrix}.$$

Notice that $Q_{ij} \succ 0$ and $Q_{ij} = Q_{ij}^{\top} \in \mathbb{R}^{2 \times 2}$ for $i, j = 1, 2$. Now, the

$$a_{11} = \operatorname{tr}(Q_{11}) = m,$$

$$a_{12} = a_{21} = \mathrm{tr}(Q_{12}) = \mathrm{tr}(Q_{21}) = \sum_{k=0}^{m-1} t_k,$$

and

$$a_{22} = \mathrm{tr}(Q_{22}) = \sum_{k=0}^{m-1} t_k^2.$$

Then, the cost function J for the optimal value $\mathbf{u}^*$ is given by

$$\begin{aligned} J(\mathbf{u}^*) &= \ln\det FIM_{\mathbf{u}^*}(\boldsymbol{\theta}) \\ &= \ln\det\left(\sigma^{-2}\left(\mathcal{Q}\right)\right) \\ &= \ln\left(\sigma^{-8}(2^{-2}\det\mathcal{E})^2\right) \end{aligned} \tag{4.11}$$

In the special case when the measurements are taken with uniform sampling, that is $t_k = kT$, then

$$\begin{aligned} \det\mathcal{E} &= \det\left(\begin{bmatrix} m & T\sum_{k=0}^{m-1} k \\ T\sum_{k=0}^{m-1} k & T^2\sum_{k=0}^{m-1} k^2 \end{bmatrix}\right), \\ &= \det\left(\begin{bmatrix} m & T\frac{m(m-1)}{2} \\ T\frac{m(m-1)}{2} & T^2\frac{m(m-1)(2m-1)}{6} \end{bmatrix}\right), \\ &= \frac{1}{12}T^2m^2(m^2-1). \end{aligned}$$

Finally, it is possible to find out the optimal cost function for the unconstrained optimization problem

$$J(\mathbf{u}^*) = \ln\left(\frac{T^4m^4(m^2-1)^2}{2304\sigma^8}\right) \tag{4.12}$$

Remark 8. *Notice that the optimal value for the cost function is directly proportional to the number of range measurements taken into account in the optimization problem. Additionally, if the variance of the sensor is to large, the accuracy of the system is going to decrease.*

Remark 9. *Although the optimization did not take into account any of the constraints for the vehicle and beacon, this value gives us an overview of the maximum value that we can achieve in our optimization problem with constraints.*

4.5. CONSTRAINED TRAJECTORY OPTIMIZATION

In the previous section, we tried to solve the problem without taking into account any restriction for the inputs in the vehicle and the beacon. Basically, equation (4.12) gives us an intuition of the maximum value that we can achieve if the vehicle and beacon can perform any trajectory. Now, with the constraint on the type of movement for the vehicle and beacon given by (4.7) and bounds for the inputs, we try to solve the problem using numerical optimization methods. Four different optimization problems are proposed:

- **Problem 1**: both inputs from vehicle and beacon are optimization variables. That is $\mathbf{u} := [\bar{v}_k,\ \bar{r}_k,\ \bar{\omega}_{m_k}]^\top$
- **Problem 2**: the vehicle will be executing a particular mission, while the input of the beacon is the optimization variable. That is $\mathbf{u} := [\bar{\omega}_{m_k}]$.
- **Problem 3**: the vehicle will be executing a particular mission, and we want to find the optimal constant angular velocity for the beacon.
- **Problem 4**: in the last we proposed a multi-objective optimization taking into account an energy cost function.

To solve all these problems, we resort to numerical methods to maximize the determinant of the FIM using the *Genetic Algorithm* toolbox from Matlab [119]. This toolbox aims to make accessible GAs to the scientific community. GAs are stochastic global search and optimization methods that mimic the nature of the evolution and are suitable for solving nonlinear optimization problems.

4.5.1. Problem 1 - Vehicle and Beacon help to improve observability

For the first problem at hand, the inputs from the vehicle and the beacon are going to be used as optimization variables. The above means that, both the vehicle and the beacon will help to maximize the FIM, which in turns means to improve the accuracy on the estimation. Additionally, we will impose upper and lower bounds for the vehicle's speed and course rate, as well as, bounds for the angular velocity of the beacon. The optimization problem will be

$$
\begin{aligned}
\max_{\mathbf{u}} \quad & \ln\det FIM_{\mathbf{u}}(\boldsymbol{\theta}) \\
\text{s.t.} \quad & {}^{\mathcal{I}}\mathbf{p}_{k+1} = \begin{cases} {}^{\mathcal{I}}\mathbf{p}_k + \dfrac{\bar{v}_k}{\bar{r}_k}[-\mathbf{w}^{\perp}(\psi_{k+1}) + \mathbf{w}(\psi_k)] + T\,{}^{\mathcal{I}}\mathbf{v}_{c_0}, & \text{if } \bar{r}_k \neq 0 \\ {}^{\mathcal{I}}\mathbf{p}_k + T(\bar{v}_k\mathbf{w}(\psi_k) + {}^{\mathcal{I}}\mathbf{v}_{c_0}), & \text{otherwise,} \end{cases} \\
& \psi_{k+1} = \psi_k + T\ \bar{r}_k \\
& {}^{\mathcal{I}}\mathbf{v}_{c_{k+1}} = \mathbf{v}_{c_0} \\
& \chi_{k+1} = \chi_k + T\ \bar{\omega}_{m_k} \\
& {}^{\mathcal{I}}\mathbf{b}_{k+1} = l_m\mathbf{w}(\chi_{k+1}) \\
& 0 < \bar{v}_k < \bar{v}_{ub} \\
& -\bar{r}_{ub} < \bar{r}_k < \bar{r}_{ub} \\
& -\bar{\omega}_{m_{ub}} < \bar{\omega}_{m_k} < \bar{\omega}_{m_{ub}}
\end{aligned}
\tag{4.13}
$$

where $\mathbf{u} := [\bar{v}_k,\ \bar{r}_k,\ \bar{\omega}_{m_k}]^{\top}$, $\boldsymbol{\theta} := [\mathbf{p}_0^{\top}, \mathbf{v}_{c_0}^{\top}]^{\top}$, $k \in \{1, 2, ..., m\}$ and $FIM_{\mathbf{u}}(\boldsymbol{\theta})$ is given by equation (4.9). For the first problem, the idea is to find out the best sequence of actions for the vehicle and beacon that maximizes the FIM. We solve the problem with four different conditions and bounds (see Table 2).

Table 2: Simulation scenarios for Problem 1

Scenarios	$\bar{v}_{ub}$ [m/s]	$\bar{r}_{ub}$ [rad/s]	$\bar{\omega}_{m_{ub}}$ [rad/s]	m	T [s]	σ [m]	$\mathbf{p}_0^{\top}$ [m]	$\mathbf{v}_{c_0}^{\top}$ [m/s]	$J_u(\mathbf{u}^*)$	$J_c(\mathbf{u}^*)$
Scenario 1 (S1)	1.5	$\pi/9$	π	12	1	0.1	$[3, 4.5]^{\top}$	$[0.3, 0.1]^{\top}$	30.54	29.56
Scenario 2 (S2)	1.5	$\pi/6$	π	16	4	0.5	$[-5, 5]^{\top}$	$[0.1, 0.3]^{\top}$	25.52	25.52
Scenario 3 (S3)	1.0	$\pi/9$	π	12	1	0.1	$[3, 4.5]^{\top}$	$[0.3, 0.1]^{\top}$	30.54	29.28
Scenario 4 (S4)	1.0	$\pi/6$	$\pi/2$	16	4	0.5	$[-5, 5]^{\top}$	$[0.1, 0.3]^{\top}$	25.52	25.52

For all scenarios the beacon positions were set up to $\mathbf{b}_0^{\top} = [1.4142, 1.4142]^{\top}$ and the initial orientation of the vehicle was $\psi_0 = \pi/3$. In Table 2, J_u and J_c stand by unconstrained and constraint optimal solution, respectively. Figure 27, 28 and 29 show the solution of the problem for the four different scenarios. Notice that for all four solutions, the constrained problem reach the maximum cost function or is close to the unconstrained solution. When we compare S2 and S4, despite the vehicle's velocity and the beacon's rotation have a more restricted bound, the solution reaches its maximum.

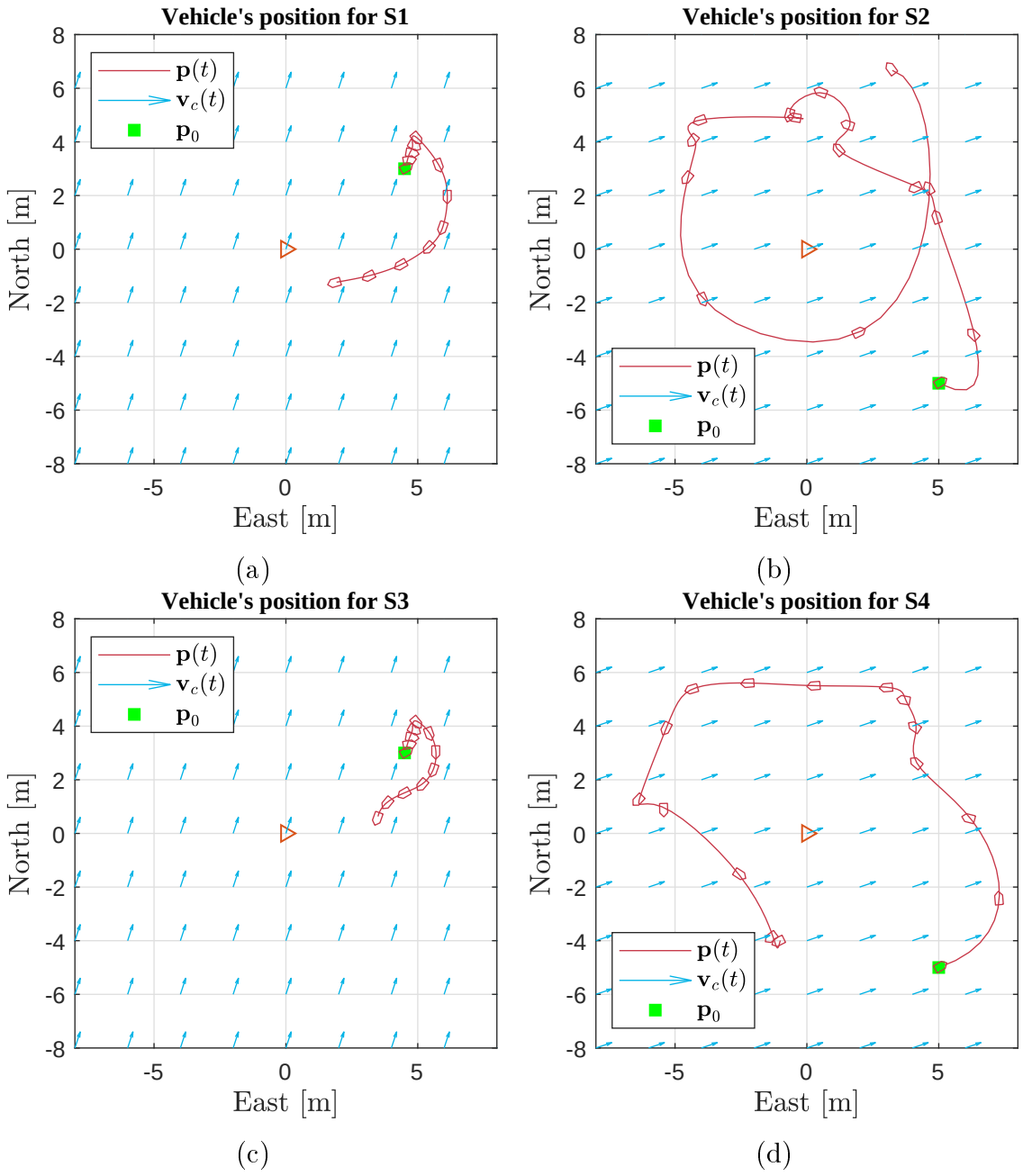

Figure 27: Vehicle's trajectory optimal solution for problem one and all four scenarios. Even though, the beacon trajectory is not reflected in the figures, beacon is rotating around the origin. Additionally, beacon and vehicle are at different depth in order to avoid collisions or entanglement.

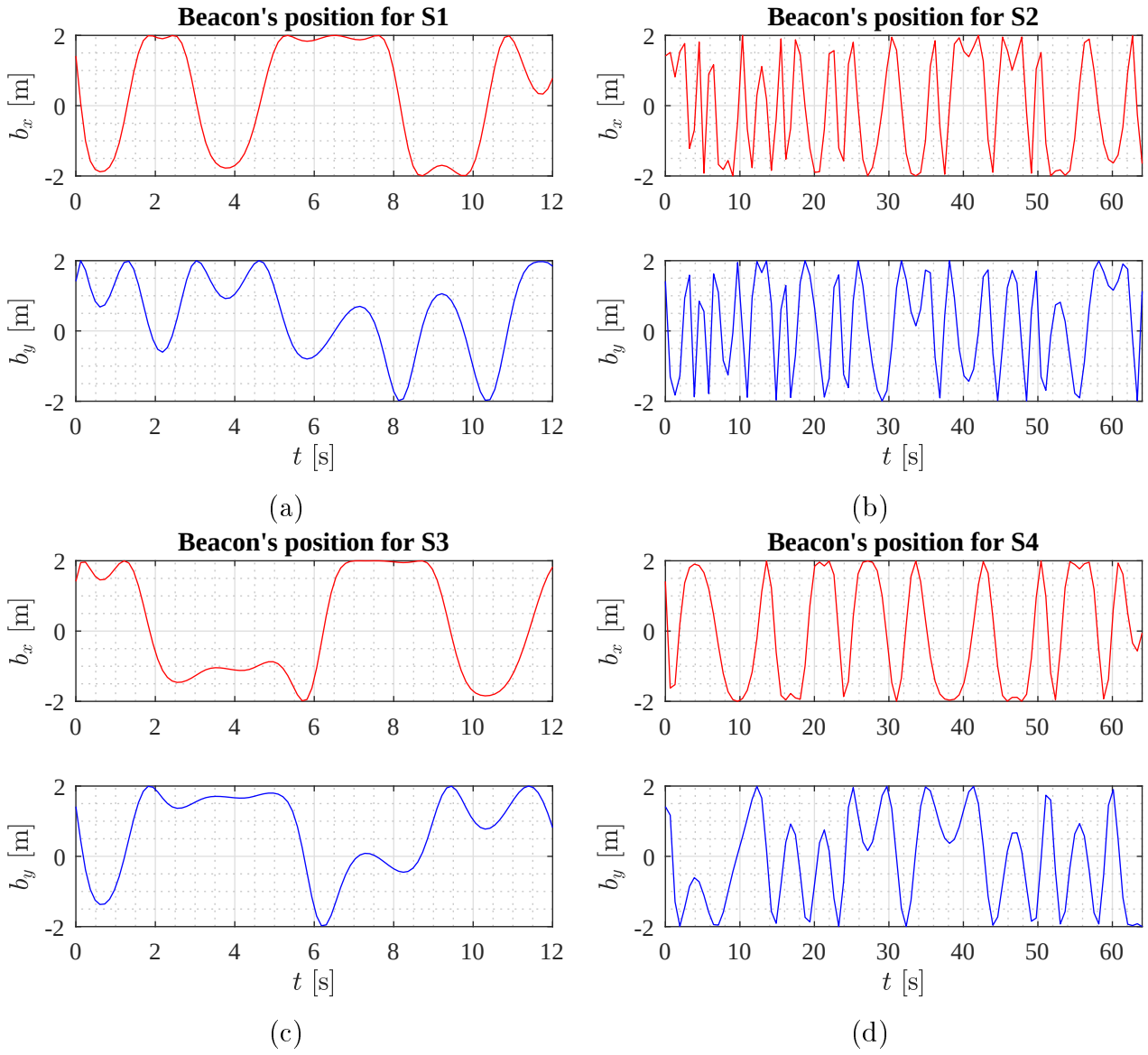

Figure 28: Beacon's trajectory optimal solution for problem one and all four scenarios. Simulation time is different between scenarios; since m and T are different between them.

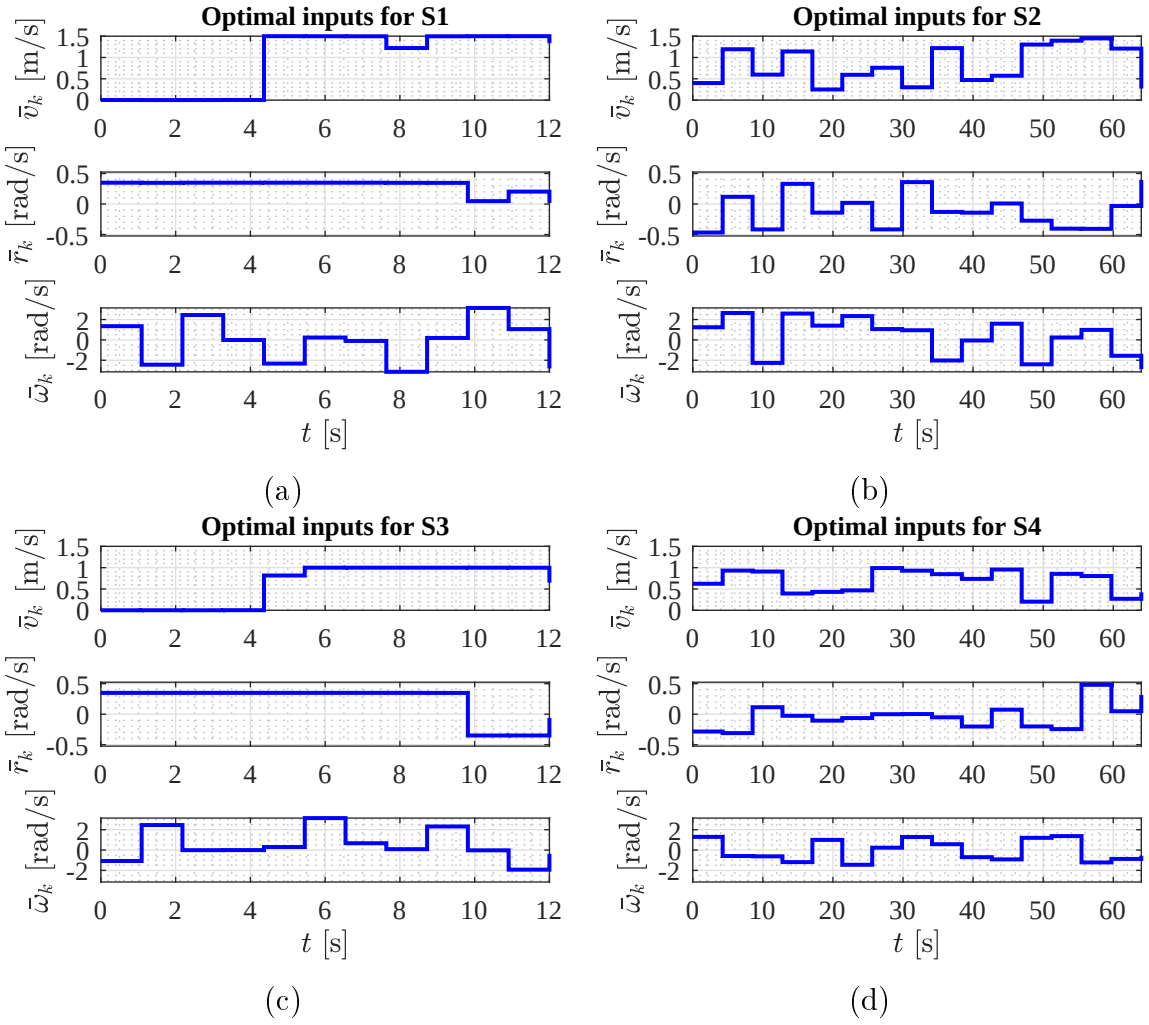

Figure 29: Optimal solution for problem one and all four scenarios. Notice that in some solutions is necessary to continuously changing the rotation of the vehicle.

4.5.2. Problem 2 - Beacon helps to improve observability

For the second problem at hand, the inputs from the vehicle are given for a particular mission, which means that the vehicle is not going to help to maximize the FIM. Therefore, just the rotation of the beacon is used in the optimization process. Additionally, we impose upper and lower bounds for the beacon's rotation. The optimization problem is given by (4.13), where this time $\mathbf{u} := [\bar{\omega}_{m_k}]$. The unknown parameter $\boldsymbol{\theta}$ and k remain the same and the upper bound for the rotation speed of the beacon is given by

$\bar{\omega}_{m_{ub}} = \pi/6$. For this particular problem, we solve two different scenarios. First, the vehicle is going in straight line, that is, $v(t) = 1.5$ m/s and $r = 0$ rad/s. The initial position of the beacon is given by $\mathbf{b}_0 = [1.4142, 1.4142]^\top$ [m] and the initial position and orientation of the vehicle are $\mathbf{p}_0 = [3, 3]^\top$ [m] and $\psi_0 = 0$ rad, respectively. The ocean current is $\mathbf{v}_{c_0} = [0, 0.3]^\top$ [m/s]. The sample time T and the number of samples m were set up to 1 s and 10, respectively. For these conditions, the unconstrained problem reaches its maximum at $J_u = 29.079$, while the solution of the problem at hand is $J_c = 24.254$. Although, only the beacon's rotation was involved in the optimization process, the optimal value is very close to the unconstrained solution. Figure 30(a), 31(a), and 32(a) show the vehicle's trajectory, beacon's trajectory and optimal input for the beacon, respectively.

For the second scenario, the inputs for the vehicle are zero. The above, implies that the vehicle is just moving by the current. The rest of parameters were set up as the previous scenario. The optimal cost function is $J_c = 26.171$. Notice that in the last scenario it reaches a better solution than in the case that the vehicle is moving in straight line. This is in part due to the proximity of the vehicle to the beacon, which in turn implies that the angles between consecutive range measurement are more different than in the first scenario. Figure 30(b), 31(b), and 32(b) show the solution for the second scenario.

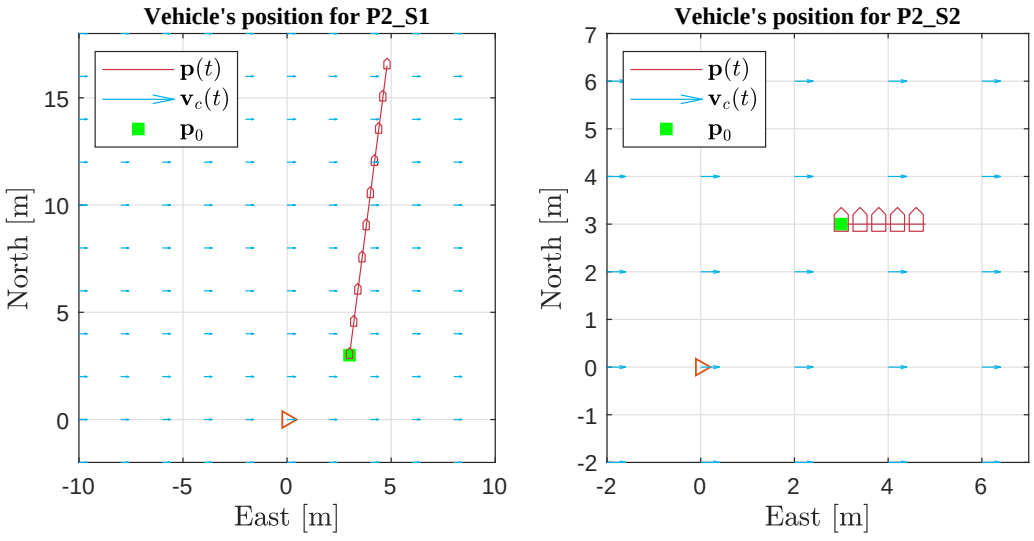

(a) (b)

Figure 30: Vehicle's trajectory for the second problem. The vehicle's trajectory is not generated as result of the optimization problem.

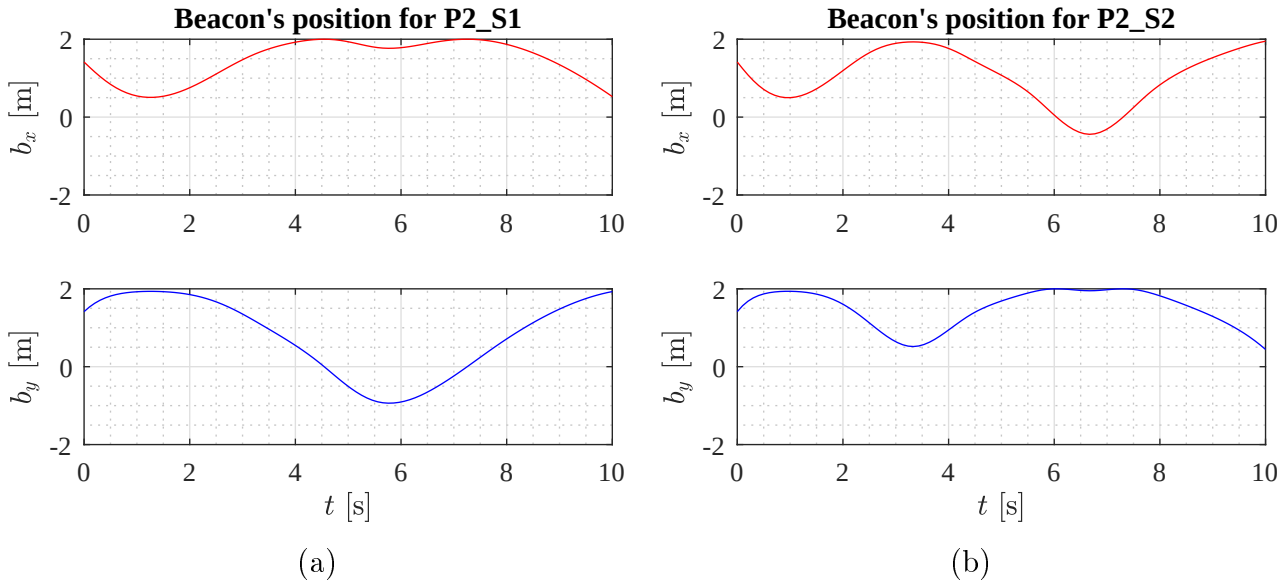

Figure 31: Beacon's trajectory optimal solution for the second problem.

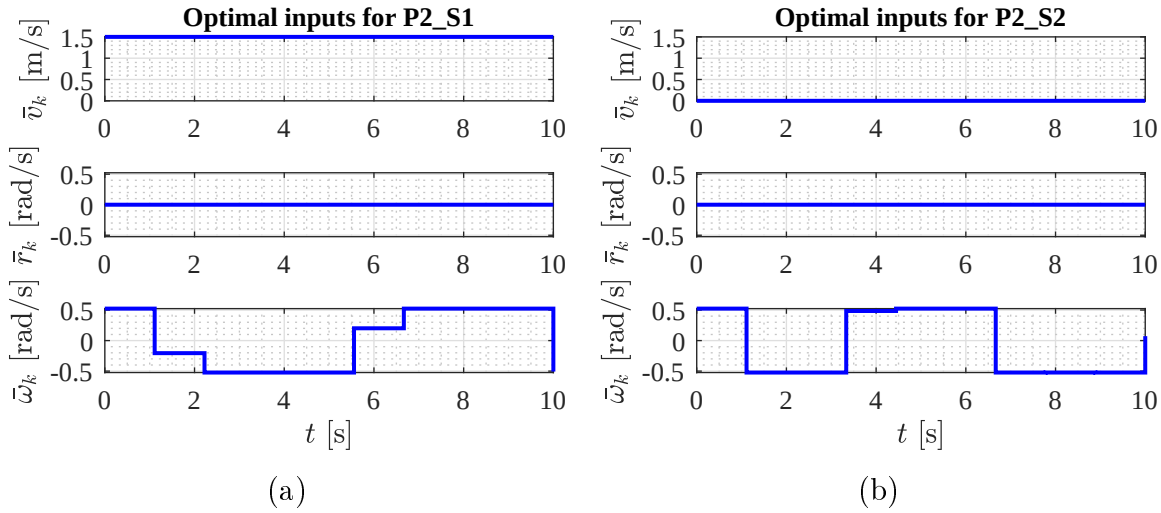

Figure 32: Optimal solution for the second problem. Recall that just $\bar{\omega}_k$ was used in the optimization process.

Figure 32(b) shows that the effort to get the best optimal cost function is higher in comparison with (a). Basically, the rotation velocity goes from one extreme to the other.

4.5.3. Problem 3 - Best constant rotation for the beacon

For the third problem, the objective is to find the best optimal constant rotation of the beacon which maximizes the FIM. Therefore, just the rotation of the beacon is used in the optimization process and it is constant all the time. The above implies that $\mathbf{u} := \bar{\omega}_{m_k}$, with $\bar{\omega}_{m_k}$ being constant for all $k \in \{1, 2, ..., m\}$. The unknown parameter $\boldsymbol{\theta}$ remains the same. The same two different scenarios from the previous problem were solved with these conditions. The vehicle's trajectories are the same as shown in Figure 30. The results of the beacon's position and the inputs are shown in Figure 33 and 34. The optimal cost function for the first scenario is $J_c = 21.936$ and for the second $J_c = 24.876$. It is important to highlight at this point, that although it was shown in previous chapters that the system was observable when the beacon was rotating, it had not been concluded which would be the best rotational speed for it. Additionally, the observability could be improved if a sequence of actions for rotational speed was performed. Finally, since the optimization problem was transformed to the point of having only one input variable, we can plot the cost function for different values of beacon's angular velocity and speed for the vehicle (see Figure 35). Notice, that even for different vehicle's speed, the optimal input for the beacon remains approximately the same.

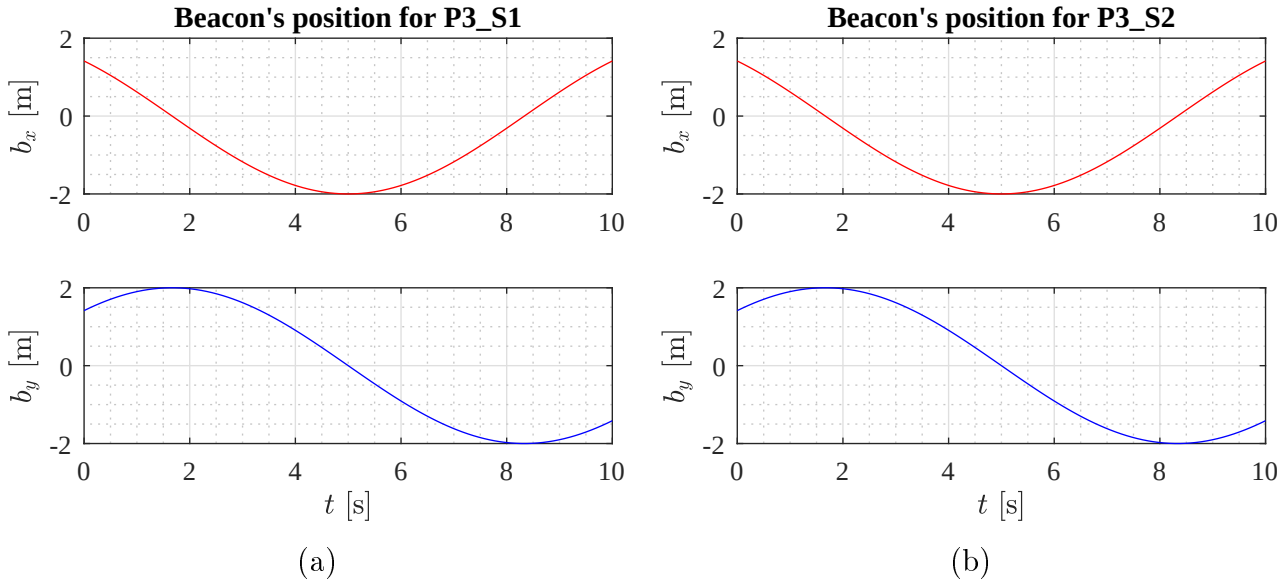

Figure 33: Beacon's trajectory optimal solution for the third problem.

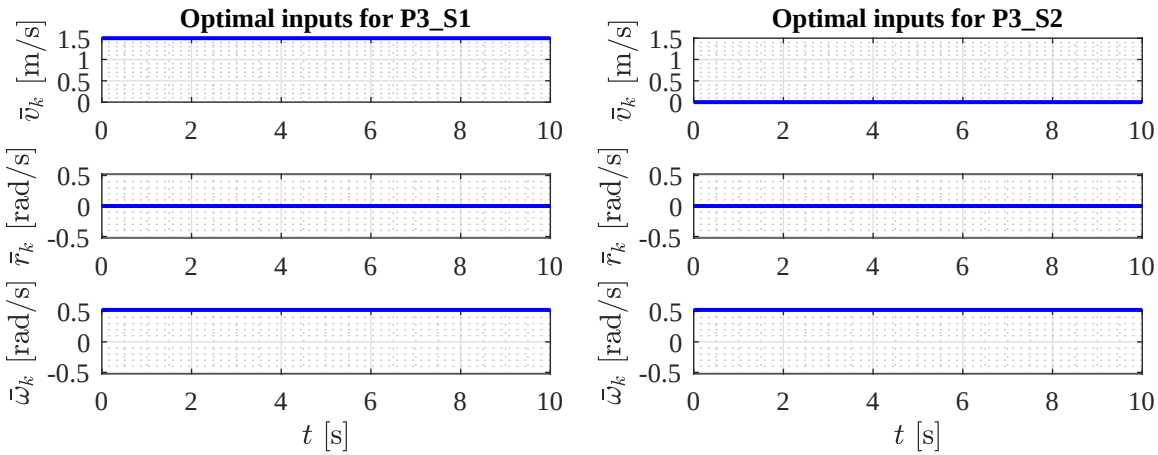

Figure 34: Optimal solution for the third problem. Recall that $\bar{\omega}_k$ was used in the optimization process and remains constant for the different sample times.

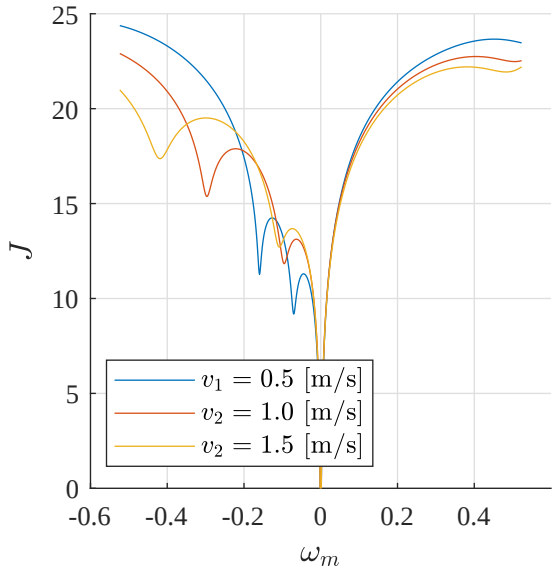

Figure 35: Cost Function plot for constant beacon's angular velocity and different vehicle's speed.

4.5.4. Problem 4 - Energy Cost Function

Up to this time, the optimization problem has been based in one goal: maximizing the Fisher Information Matrix in order to improve the accuracy on the estimation. We have found that different inputs achieve good performance in relation with the maximum optimal cost from the solution of the unconstrained optimization. This performance was achieved in most of the cases by accelerating the beacon from one direction the the other (see Figure 31). Now, we are interested in the inclusion of a second cost function that relates the energy required for the beacon's movement. The above implies, that we want to maximize the FIM while at the same time than minimizing the energy consumption of the beacon. Then, we have a multi-objective optimization problem that involves two cost functions: the FIM and the energy consumption.

The energy consumption of the beacon can be related mostly to the rotational kinetic energy, which is given by $K_e = \frac{1}{2} I \omega_m^2(t)$, where I is the moment of inertia and ω_m is the beacon's angular velocity. Since the moment of inertia is a constant and is not within the optimization variables, the energy cost function can be written as

$$J_2 = \int_0^{t_f} \omega_m^2(\tau) d\tau, \tag{4.14}$$

and for a piecewise constant input, then

$$J_2 = T \sum_{k=0}^{m-1} \bar{\omega}_{m_k}^2. \tag{4.15}$$

Now, the multiple optimization formulation is given by

$$\begin{aligned} \min_{\mathbf{u}} \quad & (J_1, J_2) \\ \text{s.t.} \quad & -\bar{\omega}_{m_{ub}} < \bar{\omega}_{m_k} < \bar{\omega}_{m_{ub}} \end{aligned} \tag{4.16}$$

where $J_1 = -\ln \det FIM_{\mathbf{u}}(\boldsymbol{\theta})$ and J_2 is given by (4.15). To solve this problem, we resort to numerical algorithms, particularly with the *Global Optimization Toolbox* from Matlab. For this problem, we tested just the scenario where the vehicle moves in straight lines like Figure 30(a). Same parameters as the second problem were set up for this case. Since we are solving a multi-objective optimization problem, Figure 36 shows the Pareto Front and some of the solution for the beacon's input. Notice that if we want to improve the FIM, then we need to spend more energy, which means that there is a

compromise between both of them. Additionally, even if we continuously increase the energy of the system, we are not going to improve the navigation system.

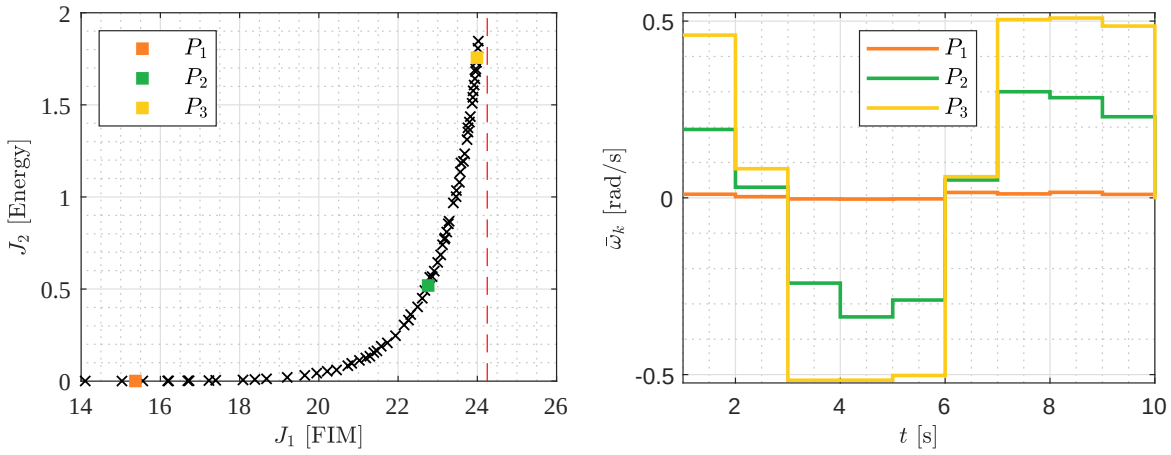

(a) (b)

Figure 36: Pareto front for the multi-objective optimization problem. Notice that even if we increased more the energy, the observability is not going to improve further.

4.6. CONCLUDING REMARKS

We addressed the observability problem from a different perspective, instead of the classical yes or no point of view. We formulated an optimization problem for finding the best sequence of action for the system that improves the observability. To achieve this, a cost function using the Fisher Information Matrix was derived. Next, the problem was solved from an unconstrained and constrained perspective. For the first, an analytical solution was found, which give us the best FIM that the system can achieve without taking into account any constraint in the motion of the vehicle or beacon. For the constrained problem, we solved four different scenarios, where the motion of the vehicle and beacon were involved, as well as the energy consumption.

5. CONCLUSIONS AND FUTURE WORK

In this final chapter, some conclusions and future directions are given, based on the work done in this thesis.

5.1. CONCLUSIONS

This thesis proposed a new methodology for underwater navigation of autonomous system based on single-range measurements. This new methodology is based on a cooperative system that uses a beacon with circular motion installed on board the support platform. In the first part of the thesis, the observability problem of the system was addressed in order to understand which type of trajectories the beacon should execute to ensure the localization of both (vehicle and beacon). We addressed the problem with and without taking into account the ocean current as a new state variable of the system. We have shown that under certain parameterization of the system inputs (constant inputs), it is possible to find a trajectory for the beacon that guarantees observability at all times.

In the second part of this thesis, we addressed the observer design problem for the proposed system. First, we used the classical approach of the Extended Kalman Filter. We used a representation of the system with respect to the body frame and the linearization of the system around the current estimation. We have shown through numerical simulations that for both scenarios (with and without taking into account ocean currents), the observer converges. Then, we implemented the Exogenous Kalman Filter for the system. The XKF was developed in three stages: first a linear state augmented observer was designed to ensure global stability; then, an inverse transformation applied to recover the state of the original system; and finally, a linearized Kalman filter around the last was performed. We tested the proposed observer through numerical

simulations.

The final part of the thesis addressed the observability problem from an optimization point of view. By using the Fisher Information Matrix and the proposed mechanism, we found an optimal sequence of actions for the beacon that increase the accuracy on the estimation of the vehicle's position and ocean current. Then, we included in the optimization problem, a second cost function which relates the energy consumption used by the beacon. We have proven that, there is a point where increasing the energy of the beacon is not going to improve the FIM.

5.2. FUTURE WORK

This work can be continued in different directions both experimentally and theoretically.

From the experimental point of view, the first step to follow is the construction, testing and validation of the mechanism. It would be valuable to analyze the effects of having the beacon near the hull of the vessel, such as generation of outliers. Also, analyzing the effects on the length of the mechanism in terms of the accuracy of the observer, which estimates the position of the vehicle; when the observability of the system in Chapter 2 was analyzed, it is only concluded that the arm length must be different from zero for certain conditions. Additionally, Chapter 4 does not such length within the optimization parameters either.

From the theoretical point of view, the first step is to perform the analysis in three dimensions of the observability of the system, without taking into account the pressure sensor. This means assessing whether the mechanism together with the movement strategy can guarantee the observability of the system in three dimensions. Additionally, to test the observer at the same time with the optimal strategy for the beacon. The above means comparing the accuracy of an observer to the strategy generated by the optimization solution, and the accuracy of this before a constant movement of the beacon.

From the observer chapter, it is interesting to evaluate the possibility of using another non-linear observer that guarantees the overall stability of the system without having

to resort to an augmentation in the state system.

APPENDIX

A. FURTHER OBSERVABILITY ANALYSIS

In this appendix, we provide some part of the observability analysis that was not taken into account in the Observability analysis chapter, as well as, some mathematical procedures used there.

A.1. STATE AUGMENTATION WITHOUT TAKING INTO ACCOUNT OCEAN CURRENTS

In Section 2.5., a state augmentation was applied to the system

$$\left.\begin{aligned} \dot{\mathbf{x}}_1 &= -S(r)\mathbf{x}_1 - {}^{\mathcal{B}}\mathbf{v} + l_m\omega_m\mathcal{R}_\psi^\top\mathbf{w}^\perp(x_2), \\ \dot{x}_2 &= \omega_m, \\ d_{xy}^2 &= \mathbf{x}_1^\top\mathbf{x}_1, \end{aligned}\right\} \tag{A.1}$$

in order to transform the system into a linear one. The state augmentation performed was $\mathbf{z} := [\mathbf{z}_1, \mathbf{z}_2, \mathbf{z}_3, z_4, z_5, z_6] := [\mathbf{x}_1, \mathcal{R}_\psi^\top\mathbf{w}^\perp(x_2), \mathcal{R}_{\pi/2}^\top\mathbf{z}_2,\ \mathbf{z}_1^\top\mathbf{z}_1,\ \mathbf{z}_1^\top\mathbf{z}_2,\ \ \mathbf{z}_1^\top\mathbf{z}_3]$. To find the new state representation of the system (A.1), the derivatives of each term are given by

$$\dot{\mathbf{z}}_1 = -S(r)\mathbf{z}_1 - {}^{\mathcal{B}}\mathbf{v} + l_m\omega_m\mathbf{z}_2, \tag{A.2}$$

$$\begin{aligned} \dot{\mathbf{z}}_2 &= \dot{\mathcal{R}}_\psi^\top\mathbf{w}^\perp(x_2) - \omega_m\mathcal{R}_\psi^\top\mathbf{w}(x_2), \\ &= -S(r)\mathcal{R}_\psi^\top\mathbf{w}^\perp(x_2) - \omega_m\mathbf{z}_3, \\ &= -S(r)\mathbf{z}_2 - \omega_m\mathbf{z}_3, \end{aligned} \tag{A.3}$$

$$\begin{aligned} \dot{\mathbf{z}}_3 &= \mathcal{R}_{\pi/2}^\top\dot{\mathbf{z}}_2, \\ &= \mathcal{R}_{\pi/2}^\top(-S(r)\mathbf{z}_2 - \omega_m\mathbf{z}_3), \\ &= (\omega_m - r)\mathbf{z}_2, \end{aligned} \tag{A.4}$$

$$
\begin{aligned}
\dot{z}_4 &= 2\mathbf{z}_1^\top \dot{\mathbf{z}}_1, \\
&= 2\mathbf{z}_1^\top \left(-S(r)\mathbf{z}_1 - {}^{\mathcal{B}}\mathbf{v} + l_m\omega_m\mathbf{z}_2\right), \\
&= -2{}^{\mathcal{B}}\mathbf{v}^\top\mathbf{z}_1 + 2l_m\omega_m\mathbf{z}_1^\top\mathbf{z}_2, \\
&= -2{}^{\mathcal{B}}\mathbf{v}^\top\mathbf{z}_1 + 2l_m\omega_m z_5,
\end{aligned} \tag{A.5}
$$

$$
\begin{aligned}
\dot{z}_5 &= \dot{\mathbf{z}}_1^\top\mathbf{z}_2 + \mathbf{z}_1^\top\dot{\mathbf{z}}_2, \\
&= \left(-S(r)\mathbf{z}_1 - {}^{\mathcal{B}}\mathbf{v} + l_m\omega_m\mathbf{z}_2\right)^\top\mathbf{z}_2 + \mathbf{z}_1^\top\left(-S(r)\mathbf{z}_2 - \omega_m\mathbf{z}_3\right), \\
&= -{}^{\mathcal{B}}\mathbf{v}^\top\mathbf{z}_2 + l_m\omega_m - \omega_m\mathbf{z}_1^\top\mathbf{z}_3, \\
&= -{}^{\mathcal{B}}\mathbf{v}^\top\mathbf{z}_2 + l_m\omega_m - \omega_m z_6,
\end{aligned} \tag{A.6}
$$

$$
\begin{aligned}
\dot{z}_6 &= \dot{\mathbf{z}}_1^\top\mathbf{z}_3 + \mathbf{z}_1^\top\dot{\mathbf{z}}_3, \\
&= \left(-S(r)\mathbf{z}_1 - {}^{\mathcal{B}}\mathbf{v} + l_m\omega_m\mathbf{z}_2\right)^\top\mathbf{z}_3 + \mathbf{z}_1^\top\left(\omega_m - r\right)\mathbf{z}_2, \\
&= \mathbf{z}_1^\top S(r)\mathbf{z}_3 - {}^{\mathcal{B}}\mathbf{v}^\top\mathbf{z}_3 + \left(\omega_m - r\right)z_5, \\
&= \mathbf{z}_1^\top S(r)\mathcal{R}_{\pi/2}^\top\mathbf{z}_2 - {}^{\mathcal{B}}\mathbf{v}^\top\mathbf{z}_3 + \left(\omega_m - r\right)z_5, \\
&= rz_5 - {}^{\mathcal{B}}\mathbf{v}^\top\mathbf{z}_3 + \left(\omega_m - r\right)z_5, \\
&= -{}^{\mathcal{B}}\mathbf{v}^\top\mathbf{z}_3 + \omega_m z_5.
\end{aligned} \tag{A.7}
$$

Additionally, the output is given by $y = d_{xy}^2 = \mathbf{z}_1^\top\mathbf{z}_1 = z_4$. Now, it is possible to rewrite the system (A.8) in matrix form as

$$
\left.\begin{aligned}
\dot{\mathbf{z}} &= A(\mathbf{u})\mathbf{z} + B\mathbf{u} \\
y &= C\mathbf{z}
\end{aligned}\right\} \tag{A.8}
$$

where

$$
A(\mathbf{u}) = \begin{bmatrix}
-S(r) & l_m\omega_m I_2 & \mathbf{0} & \mathbf{0} & \mathbf{0} & \mathbf{0} \\
\mathbf{0} & -S(r) & -\omega_m I_2 & \mathbf{0} & \mathbf{0} & \mathbf{0} \\
\mathbf{0} & (\omega_m - r)I_2 & \mathbf{0} & \mathbf{0} & \mathbf{0} & \mathbf{0} \\
-2{}^{\mathcal{B}}\mathbf{v}^\top & \mathbf{0} & \mathbf{0} & 0 & 2l_m\omega_m & 0 \\
\mathbf{0} & -{}^{\mathcal{B}}\mathbf{v}^\top & \mathbf{0} & 0 & 0 & -\omega_m \\
\mathbf{0} & \mathbf{0} & -{}^{\mathcal{B}}\mathbf{v}^\top & 0 & \omega_m & 0
\end{bmatrix},
$$

$$
B = \begin{bmatrix}
-I_2 & \mathbf{0} & \mathbf{0} \\
\mathbf{0} & \mathbf{0} & \mathbf{0} \\
\mathbf{0} & \mathbf{0} & \mathbf{0} \\
\mathbf{0} & 0 & 0 \\
\mathbf{0} & l_m & 0 \\
\mathbf{0} & 0 & 0
\end{bmatrix},
$$

$$C = \begin{bmatrix} \mathbf{0} & \mathbf{0} & \mathbf{0} & 1 & 0 & 0 \end{bmatrix}.$$

A.2. OBSERVABILITY ANALYSIS WHEN THE VEHICLE AND THE BEACON DOES NOT MOVE (WITHOUT OCEAN CURRENT)

In the last part of the subsection 2.5., the observability analysis of the system was carried out taking into account different kind inputs for the vehicle and beacon. Particularly, in this appendix the observability analysis is done by assuming that the vehicle and the beacon do not move. This conditions can be fulfilled by assuming that $\omega_m = 0$ and $||^{\mathcal{B}}\mathbf{v}|| = 0$. It is easy to proof that the system is not observable using the original coordinate system (2.18). The output of the system is given $y(t) = ||\mathbf{p}_0 - \mathbf{b}_0||$. Recall that for observability purpose it is the same to analyze the range square measurement.

Let $\mathcal{I}(\mathbf{x}_0)$ denotes the set of initial conditions that are indistinguishable from the given initial condition $\mathbf{x}_0 = (\mathbf{p}_0, \mathbf{b}_0)$. Now, consider an initial condition $\bar{\mathbf{x}}_0 = (\bar{\mathbf{p}}_0, \bar{\mathbf{b}}_0)$ be such that $\bar{\mathbf{x}}_0 \in \mathcal{I}(\mathbf{x}_0)$. Then, $||\bar{\mathbf{p}}_0 - \bar{\mathbf{b}}_0||^2 = ||\mathbf{p}_0 - \mathbf{b}_0||^2$ for every $t \geq 0$. Notice that there are less equations than variables, therefore the system is not observable. It is possible to parametrize the set of indistinguishable initial condition by computing $\bar{\mathbf{b}}_0 = r_m \mathbf{u}_\alpha$ with $\alpha \in [0, 2\pi)$ and $\bar{\mathbf{p}}_0 = r_m \mathbf{u}_\alpha + ||\mathbf{p}_0 - \mathbf{b}_0|| \mathbf{u}_\beta$ with $\beta \in [0, 2\pi)$.

Corollary 5. *Knowing the initial condition of the beacon does not change the observability of the system.*

To know the initial condition of the beacon, implies that $\bar{\mathbf{b}}(0) = \mathbf{b}(0)$. Then, it implies that the vehicle's initial condition is given by $\bar{\mathbf{p}}_0 = \mathbf{b}_0 + ||\mathbf{p}_0 - \mathbf{b}_0|| \mathbf{u}_\beta$ with $\beta \in [0, 2\pi)$. Figure 37 shows a geometric interpretation of the indistinguishable set for both scenarios.

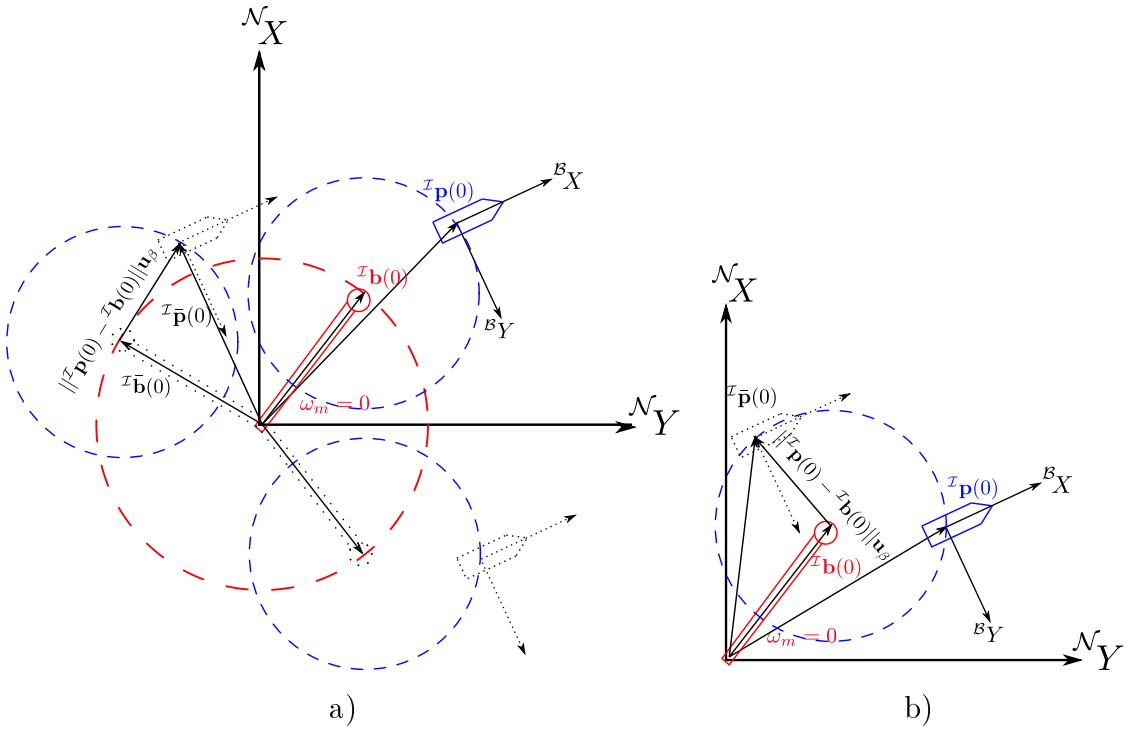

Figure 37: Geometric interpretation of indistinguishable initial conditions in the case that neither the vehicle nor the beacon are moving. Notice that, once the beacon's initial conditions is known, the set of indistinguishable initial conditions shrinks to a circle centered in the beacon.

A.3. COMPLEMENTS TO THE PROOF OF PROPOSITION 5

The proof of this section relies in solving the set of nonlinear equation given by

$$||\boldsymbol{\alpha}_a + \mathbf{z}_1(0)||^2 = ||\mathbf{z}_1(0)||^2, \tag{A.9}$$

$$||\boldsymbol{\alpha}_b + \mathbf{z}_2(0)||^2 = 1, \tag{A.10}$$

$$\boldsymbol{\alpha}_a^\top \boldsymbol{\alpha}_b + \boldsymbol{\alpha}_a^\top \mathbf{z}_2(0) + \boldsymbol{\alpha}_b^\top \mathbf{z}_1(0) = 0. \tag{A.11}$$

Recall that there are four variables and just three equations to solve the system, therefore, the solution will have one free parameter. To solve the system, first we apply the following operation (A.9) + (A.10) + 2(A.11), that is

$$\begin{aligned}
||\boldsymbol{\alpha}_a + \mathbf{z}_1(0)||^2 - ||\mathbf{z}_1(0)||^2 + ||\boldsymbol{\alpha}_b + \mathbf{z}_2(0)||^2 - 1 + 2\boldsymbol{\alpha}_a^\top \boldsymbol{\alpha}_b + 2\boldsymbol{\alpha}_a^\top \mathbf{z}_2(0) + 2\boldsymbol{\alpha}_b^\top \mathbf{z}_1(0) = 0,\\
||\boldsymbol{\alpha}_a||^2 + 2\boldsymbol{\alpha}_a^\top \mathbf{z}_1(0) + ||\boldsymbol{\alpha}_b||^2 + 2\boldsymbol{\alpha}_b^\top \mathbf{z}_2(0) + 2\boldsymbol{\alpha}_a^\top \boldsymbol{\alpha}_b + 2\boldsymbol{\alpha}_a^\top \mathbf{z}_2(0) + 2\boldsymbol{\alpha}_b^\top \mathbf{z}_1(0) = 0,\\
||\boldsymbol{\alpha}_a + \boldsymbol{\alpha}_b||^2 + 2\boldsymbol{\alpha}_a^\top (\mathbf{z}_1(0) + \mathbf{z}_2(0)) + 2\boldsymbol{\alpha}_b^\top (\mathbf{z}_1(0) + \mathbf{z}_2(0)) = 0,\\
||\boldsymbol{\alpha}_a + \boldsymbol{\alpha}_b||^2 + 2(\boldsymbol{\alpha}_a + \boldsymbol{\alpha}_b)^\top (\mathbf{z}_1(0) + \mathbf{z}_2(0)) = 0.
\end{aligned} \tag{A.12}$$

Let us define $\mathbf{z}_+ := \boldsymbol{\alpha}_a + \boldsymbol{\alpha}_b$, $\mathbf{c}_+ := \mathbf{z}_1(0) + \mathbf{z}_2(0)$ and $\mathbf{s}_\gamma : [0, 2\pi) \to \mathcal{S}^1$ as the map described by $\mathbf{s}_\gamma := [\cos\gamma \ \ \sin\gamma]^\top$, then

$$\begin{aligned}
||\mathbf{z}_+||^2 + 2\mathbf{z}_+^\top \mathbf{c}_+ = 0,\\
||\mathbf{z}_+ + \mathbf{c}_+||^2 = ||\mathbf{c}_+||^2,\\
\mathbf{z}_+ = -\mathbf{c}_+ + ||\mathbf{c}_+||\mathbf{s}_\alpha.
\end{aligned} \tag{A.13}$$

Following a similar procedure, except this time (A.9) + (A.10) − 2(A.11), we obtain

$$\begin{aligned}
||\boldsymbol{\alpha}_a + \mathbf{z}_1(0)||^2 - ||\mathbf{z}_1(0)||^2 + ||\boldsymbol{\alpha}_b + \mathbf{z}_2(0)||^2 - 1 - 2\boldsymbol{\alpha}_a^\top \boldsymbol{\alpha}_b - 2\boldsymbol{\alpha}_a^\top \mathbf{z}_2(0) - 2\boldsymbol{\alpha}_b^\top \mathbf{z}_1(0) = 0,\\
||\boldsymbol{\alpha}_a||^2 + 2\boldsymbol{\alpha}_a^\top \mathbf{z}_1(0) + ||\boldsymbol{\alpha}_b||^2 + 2\boldsymbol{\alpha}_b^\top \mathbf{z}_2(0) - 2\boldsymbol{\alpha}_a^\top \boldsymbol{\alpha}_b - 2\boldsymbol{\alpha}_a^\top \mathbf{z}_2(0) - 2\boldsymbol{\alpha}_b^\top \mathbf{z}_1(0) = 0,\\
||\boldsymbol{\alpha}_a - \boldsymbol{\alpha}_b||^2 + 2\boldsymbol{\alpha}_a^\top (\mathbf{z}_1(0) - \mathbf{z}_2(0)) - 2\boldsymbol{\alpha}_b^\top (\mathbf{z}_1(0) - \mathbf{z}_2(0)) = 0,\\
||\boldsymbol{\alpha}_a + \boldsymbol{\alpha}_b||^2 + 2(\boldsymbol{\alpha}_a - \boldsymbol{\alpha}_b)^\top (\mathbf{z}_1(0) - \mathbf{z}_2(0)) = 0.
\end{aligned} \tag{A.14}$$

Let us define $\mathbf{z}_- := \boldsymbol{\alpha}_a - \boldsymbol{\alpha}_b$ and $\mathbf{c}_- := \mathbf{z}_1(0) - \mathbf{z}_2(0)$, then

$$\begin{aligned}
||\mathbf{z}_-||^2 + 2\mathbf{z}_-^\top \mathbf{c}_- = 0,\\
||\mathbf{z}_- + \mathbf{c}_-||^2 = ||\mathbf{c}_-||^2,\\
\mathbf{z}_- = -\mathbf{c}_- + ||\mathbf{c}_-||\mathbf{s}_\beta.
\end{aligned} \tag{A.15}$$

By doing (A.13) + (A.15) and (A.13) - (A.15), it follows that

$$\boldsymbol{\alpha}_a = -\mathbf{z}_1(0) + \frac{1}{2}||\mathbf{z}_1(0) + \mathbf{z}_2(0)||\mathbf{s}_\alpha + \frac{1}{2}||\mathbf{z}_1(0) - \mathbf{z}_2(0)||\mathbf{s}_\beta, \tag{A.16}$$

$$\boldsymbol{\alpha}_b = -\mathbf{z}_2(0) + \frac{1}{2}||\mathbf{z}_1(0) + \mathbf{z}_2(0)||\mathbf{s}_\alpha - \frac{1}{2}||\mathbf{z}_1(0) - \mathbf{z}_2(0)||\mathbf{s}_\beta. \tag{A.17}$$

We can replace $\boldsymbol{\alpha}_a$ or $\boldsymbol{\alpha}_b$ in (A.9) or (A.10) respectively, what leads to

$$\begin{aligned}
\left\| \frac{1}{2}||\mathbf{c}_+||\mathbf{s}_\alpha + \frac{1}{2}||\mathbf{c}_-||\mathbf{s}_\beta \right\|^2 &= ||\mathbf{z}_1(0)||^2 \\
||\mathbf{c}_+||^2 + 2||\mathbf{c}_+||||\mathbf{c}_-||\mathbf{s}_\alpha^\top \mathbf{s}_\beta + ||\mathbf{c}_-||^2 &= 4||\mathbf{z}_1(0)||^2 \\
\cos(\alpha - \beta) &= \frac{2||\mathbf{z}_1(0)||^2}{||\mathbf{c}_+||||\mathbf{c}_-||} - \frac{1}{2}\frac{||\mathbf{c}_+||}{||\mathbf{c}_-||} - \frac{1}{2}\frac{||\mathbf{c}_-||}{||\mathbf{c}_+|} \\
\cos(\alpha - \beta) &= \frac{4||\mathbf{z}_1(0)||^2 - ||\mathbf{z}_1(0) + \mathbf{z}_2(0)||^2 - ||\mathbf{z}_1(0) - \mathbf{z}_2(0)||^2}{2||\mathbf{z}_1(0) + \mathbf{z}_2(0)||||\mathbf{z}_1(0) - \mathbf{z}_2(0)||} \\
\cos(\alpha - \beta) &= \frac{2||\mathbf{z}_1(0)||^2 - 2||\mathbf{z}_2(0)||^2}{2||\mathbf{z}_1(0) + \mathbf{z}_2(0)||||\mathbf{z}_1(0) - \mathbf{z}_2(0)||} \\
\cos(\alpha - \beta) &= \left(\frac{\mathbf{z}_1(0) + \mathbf{z}_2(0)}{||\mathbf{z}_1(0) + \mathbf{z}_2(0)||} \right)^\top \left(\frac{\mathbf{z}_1(0) - \mathbf{z}_2(0)}{||\mathbf{z}_1(0) - \mathbf{z}_2(0)||} \right) \\
\alpha &= \cos^{-1}\left(\left(\frac{\mathbf{z}_1(0) + \mathbf{z}_2(0)}{||\mathbf{z}_1(0) + \mathbf{z}_2(0)||} \right)^\top \left(\frac{\mathbf{z}_1(0) - \mathbf{z}_2(0)}{||\mathbf{z}_1(0) - \mathbf{z}_2(0)||} \right) \right) + \beta
\end{aligned} \tag{A.18}$$

A.4. STATE AUGMENTATION WITHOUT TAKING INTO ACCOUNT OCEAN CURRENTS

In Section 2.6., a state augmentation was applied to the system

$$\left.\begin{aligned}
{}^{\mathcal{B}}\dot{\mathbf{d}} &= -S(r){}^{\mathcal{B}}\mathbf{d} - {}^{\mathcal{B}}\mathbf{v} + l_m\omega_m\mathcal{R}_\psi^\top \mathbf{w}^\perp(\chi) - {}^{\mathcal{B}}\mathbf{v}_c, \\
{}^{\mathcal{B}}\dot{\mathbf{v}}_c &= -S(r){}^{\mathcal{B}}\mathbf{v}_c, \\
\dot{\chi} &= \omega_m, \\
d_{xy}^2 &= {}^{\mathcal{B}}\mathbf{d}^\top {}^{\mathcal{B}}\mathbf{d},
\end{aligned}\right\} \tag{A.19}$$

in order to transform the system into a linear one. The state augmentation performed was $\mathbf{z} := [\mathbf{z}_1, \mathbf{z}_2, \mathbf{z}_3, \mathbf{z}_4, z_5, z_6, z_7, z_8, z_9, z_{10}, z_{11}] :=$

$[{}^{\mathcal{B}}\mathbf{d}, {}^{\mathcal{B}}\mathbf{v}_c, \mathcal{R}_{\psi}^{\top}\mathbf{w}^{\perp}(\chi), \mathcal{R}_{\pi/2}^{\top}\mathbf{z}_3, \mathbf{z}_1^{\top}\mathbf{z}_1, \mathbf{z}_1^{\top}\mathbf{z}_2, \mathbf{z}_1^{\top}\mathbf{z}_3, \mathbf{z}_1^{\top}\mathbf{z}_4, \mathbf{z}_2^{\top}\mathbf{z}_2, \mathbf{z}_2^{\top}\mathbf{z}_3, \mathbf{z}_2^{\top}\mathbf{z}_4]$. To find the new state representation of the system (A.19), the derivatives of each term are given by

$$\dot{\mathbf{z}}_1 = -S(r)\mathbf{z}_1 - {}^{\mathcal{B}}\mathbf{v} + l_m\omega_m\mathbf{z}_3 - \mathbf{z}_2, \tag{A.20}$$

$$\dot{\mathbf{z}}_2 = -S(r)\mathbf{z}_2, \tag{A.21}$$

$$\begin{aligned}\dot{\mathbf{z}}_3 &= \dot{\mathcal{R}}_{\psi}^{\top}\mathbf{w}^{\perp}(x_2) - \omega_m\mathcal{R}_{\psi}^{\top}\mathbf{w}(x_2), \\ &= -S(r)\mathcal{R}_{\psi}^{\top}\mathbf{w}^{\perp}(x_2) - \omega_m\mathbf{z}_4, \\ &= -S(r)\mathbf{z}_3 - \omega_m\mathbf{z}_4,\end{aligned} \tag{A.22}$$

$$\begin{aligned}\dot{\mathbf{z}}_4 &= \mathcal{R}_{\pi/2}^{\top}\dot{\mathbf{z}}_3, \\ &= \mathcal{R}_{\pi/2}^{\top}\left(-S(r)\mathbf{z}_3 - \omega_m\mathbf{z}_4\right), \\ &= \omega_m\mathbf{z}_3 - S(r)\mathbf{z}_4,\end{aligned} \tag{A.23}$$

$$\begin{aligned}\dot{z}_5 &= 2\mathbf{z}_1^{\top}\dot{\mathbf{z}}_1, \\ &= 2\mathbf{z}_1^{\top}\left(-S(r)\mathbf{z}_1 - {}^{\mathcal{B}}\mathbf{v} + l_m\omega_m\mathbf{z}_3 - \mathbf{z}_2\right), \\ &= -2{}^{\mathcal{B}}\mathbf{v}^{\top}\mathbf{z}_1 + 2l_m\omega_m\mathbf{z}_1^{\top}\mathbf{z}_3 - 2\mathbf{z}_1^{\top}\mathbf{z}_2, \\ &= -2{}^{\mathcal{B}}\mathbf{v}^{\top}\mathbf{z}_1 + 2l_m\omega_m z_7 - 2z_6,\end{aligned} \tag{A.24}$$

$$\begin{aligned}\dot{z}_6 &= \dot{\mathbf{z}}_1^{\top}\mathbf{z}_2 + \mathbf{z}_1^{\top}\dot{\mathbf{z}}_2, \\ &= \left(-S(r)\mathbf{z}_1 - {}^{\mathcal{B}}\mathbf{v} + l_m\omega_m\mathbf{z}_3 - \mathbf{z}_2\right)^{\top}\mathbf{z}_2 + \mathbf{z}_1^{\top}\left(-S(r)\mathbf{z}_2\right), \\ &= -{}^{\mathcal{B}}\mathbf{v}^{\top}\mathbf{z}_2 + l_m\omega_m\mathbf{z}_3^{\top}\mathbf{z}_2 - \mathbf{z}_2^{\top}\mathbf{z}_2, \\ &= -{}^{\mathcal{B}}\mathbf{v}^{\top}\mathbf{z}_2 + l_m\omega_m z_{10} - z_9,\end{aligned} \tag{A.25}$$

$$\begin{aligned}\dot{z}_7 &= \dot{\mathbf{z}}_1^{\top}\mathbf{z}_3 + \mathbf{z}_1^{\top}\dot{\mathbf{z}}_3, \\ &= \left(-S(r)\mathbf{z}_1 - {}^{\mathcal{B}}\mathbf{v} + l_m\omega_m\mathbf{z}_3 - \mathbf{z}_2\right)^{\top}\mathbf{z}_3 + \mathbf{z}_1^{\top}\left(-S(r)\mathbf{z}_3 - \omega_m\mathbf{z}_4\right), \\ &= -{}^{\mathcal{B}}\mathbf{v}^{\top}\mathbf{z}_3 + l_m\omega_m - \mathbf{z}_2^{\top}\mathbf{z}_3 - \omega_m\mathbf{z}_1^{\top}\mathbf{z}_4, \\ &= -{}^{\mathcal{B}}\mathbf{v}^{\top}\mathbf{z}_3 + l_m\omega_m - z_{10} - \omega_m z_8,\end{aligned} \tag{A.26}$$

$$
\begin{aligned}
\dot{z}_8 &= \dot{\mathbf{z}}_1^\top \mathbf{z}_4 + \mathbf{z}_1^\top \dot{\mathbf{z}}_4, \\
&= \left(-S(r)\mathbf{z}_1 - {}^{\mathcal{B}}\mathbf{v} + l_m\omega_m\mathbf{z}_3 - \mathbf{z}_2\right)^\top \mathbf{z}_4 + \mathbf{z}_1^\top \left(-S(r)\mathbf{z}_4 + \omega_m\mathbf{z}_3\right), \\
&= -{}^{\mathcal{B}}\mathbf{v}^\top \mathbf{z}_4 - \mathbf{z}_2^\top \mathbf{z}_4 + \omega_m \mathbf{z}_1^\top \mathbf{z}_3, \\
&= -{}^{\mathcal{B}}\mathbf{v}^\top \mathbf{z}_4 - z_{10} + \omega_m z_7, \qquad \text{(A.27)}
\end{aligned}
$$

$$
\begin{aligned}
\dot{z}_9 &= \dot{\mathbf{z}}_2^\top \mathbf{z}_2 + \mathbf{z}_2^\top \dot{\mathbf{z}}_2, \\
&= \left(-S(r)\mathbf{z}_2\right)^\top \mathbf{z}_2 + \mathbf{z}_2^\top \left(-S(r)\mathbf{z}_2\right), \\
&= 0, \qquad \text{(A.28)}
\end{aligned}
$$

$$
\begin{aligned}
\dot{z}_{10} &= \dot{\mathbf{z}}_2^\top \mathbf{z}_3 + \mathbf{z}_2^\top \dot{\mathbf{z}}_3, \\
&= \left(-S(r)\mathbf{z}_2\right)^\top \mathbf{z}_3 + \mathbf{z}_2^\top \left(-S(r)\mathbf{z}_3 - \omega_m\mathbf{z}_4\right), \\
&= -\omega_m z_{11}, \qquad \text{(A.29)}
\end{aligned}
$$

$$
\begin{aligned}
\dot{z}_{11} &= \dot{\mathbf{z}}_2^\top \mathbf{z}_4 + \mathbf{z}_2^\top \dot{\mathbf{z}}_4, \\
&= \left(-S(r)\mathbf{z}_2\right)^\top \mathbf{z}_4 + \mathbf{z}_2^\top \left(\omega_m\mathbf{z}_3 - S(r)\mathbf{z}_4\right), \\
&= \omega_m z_{10}. \qquad \text{(A.30)}
\end{aligned}
$$

Additionally, the output is given by $y = d_{xy}^2 = {}^{\mathcal{B}}\mathbf{d}^\top {}^{\mathcal{B}}\mathbf{d} = z_5$. Now, it is possible to rewrite the system (A.31) in matrix form as

$$
\left.
\begin{aligned}
\dot{\mathbf{z}} &= A(\mathbf{u})\mathbf{z} + B\mathbf{u} \\
y &= C\mathbf{z}
\end{aligned}
\right\} \qquad \text{(A.31)}
$$

where

$$
A(\mathbf{u}) = \begin{bmatrix}
-S(r) & -I_2 & l_m\omega_m I_2 & \mathbf{0} & \mathbf{0} & \mathbf{0} & \mathbf{0} & \mathbf{0} & \mathbf{0} & \mathbf{0} & \mathbf{0} \\
\mathbf{0} & -S(r) & \mathbf{0} & \mathbf{0} & \mathbf{0} & \mathbf{0} & \mathbf{0} & \mathbf{0} & \mathbf{0} & \mathbf{0} & \mathbf{0} \\
\mathbf{0} & \mathbf{0} & -S(r) & -\omega_m I_2 & \mathbf{0} & \mathbf{0} & \mathbf{0} & \mathbf{0} & \mathbf{0} & \mathbf{0} & \mathbf{0} \\
\mathbf{0} & \mathbf{0} & \omega_m I_2 & -S(r) & \mathbf{0} & \mathbf{0} & \mathbf{0} & \mathbf{0} & \mathbf{0} & \mathbf{0} & \mathbf{0} \\
-2{}^{\mathcal{B}}\mathbf{v}^\top & \mathbf{0} & \mathbf{0} & \mathbf{0} & 0 & -2 & 2l_m\omega_m & 0 & 0 & 0 & 0 \\
\mathbf{0} & -{}^{\mathcal{B}}\mathbf{v}^\top & \mathbf{0} & \mathbf{0} & 0 & 0 & 0 & 0 & -1 & l_m\omega_m & 0 \\
\mathbf{0} & \mathbf{0} & -{}^{\mathcal{B}}\mathbf{v}^\top & \mathbf{0} & 0 & 0 & 0 & -\omega_m & 0 & -1 & 0 \\
\mathbf{0} & \mathbf{0} & \mathbf{0} & -{}^{\mathcal{B}}\mathbf{v}^\top & 0 & 0 & \omega_m & 0 & 0 & 0 & -1 \\
\mathbf{0} & \mathbf{0} & \mathbf{0} & \mathbf{0} & 0 & 0 & 0 & 0 & 0 & 0 & 0 \\
\mathbf{0} & \mathbf{0} & \mathbf{0} & \mathbf{0} & 0 & 0 & 0 & 0 & 0 & 0 & -\omega_m \\
\mathbf{0} & \mathbf{0} & \mathbf{0} & \mathbf{0} & 0 & 0 & 0 & 0 & 0 & \omega_m & 0
\end{bmatrix},
$$

$$B = \begin{bmatrix} -I_2 & \mathbf{0} & \mathbf{0} \\ \mathbf{0} & \mathbf{0} & \mathbf{0} \\ \mathbf{0} & \mathbf{0} & \mathbf{0} \\ \mathbf{0} & \mathbf{0} & \mathbf{0} \\ \mathbf{0} & 0 & 0 \\ \mathbf{0} & 0 & 0 \\ \mathbf{0} & l_m & 0 \\ \mathbf{0} & 0 & 0 \\ \mathbf{0} & 0 & 0 \\ \mathbf{0} & 0 & 0 \\ \mathbf{0} & 0 & 0 \end{bmatrix},$$

and

$$C = \begin{bmatrix} \mathbf{0} & \mathbf{0} & \mathbf{0} & \mathbf{0} & 1 & 0 & 0 & 0 & 0 & 0 & 0 \end{bmatrix}.$$

B. OBSERVER DESIGN WITHOUT TAKING INTO ACCOUNT OCEAN CURRENTS

In this appendix, we provide the observer design procedure for the system without taking currents into account. This appendix is complementary to the results given in the **??** section.

B.1. EXTENDED KALMAN FILTER

Based on the results of Chapter **??**, we propose an EKF observer for the nonlinear system (2.21) introduced in Chapter 2, where we now consider that the system is corrupted with a process $\boldsymbol{\zeta}(t) \in \mathbb{R}^3$ and measurement $\kappa(t) \in \mathbb{R}$ zero mean Gaussian noise

$$\left.\begin{aligned} \dot{\mathbf{x}}(t) &= \boldsymbol{f}(\mathbf{x}(t), \mathbf{u}(t)) + \boldsymbol{\zeta}(t), \\ y(t) &= g(\mathbf{x}(t)) + \kappa(t), \end{aligned}\right\} \tag{B.1}$$

where the state variable $\mathbf{x} := [\mathbf{x}_1^\top, x_2]^\top := [{}^{\mathcal{B}}\mathbf{d}^\top, \chi] \in \mathbb{R}^2 \times [0, 2\pi)$, the input vector $\mathbf{u} := [{}^{\mathcal{B}}\mathbf{v}^\top, \omega_m, r]^\top \in \mathbb{R}^4$, the output measurement $y \in \mathbb{R}$,

$$\boldsymbol{f}(\mathbf{x}(t), \mathbf{u}(t)) = \begin{bmatrix} -S(r)\mathbf{x}_1(t) - {}^{\mathcal{B}}\mathbf{v}(t) + l_m \omega_m(t) \mathcal{R}_{\psi(t)}^\top \mathbf{w}^\perp(x_2(t)) \\ \omega_m(t) \end{bmatrix},$$

and

$$g(\mathbf{x}(t)) = ||\mathbf{x}_1(t)||.$$

Recall that the first step to apply EKF on (B.1), the system should be discretized. We assume that the control input $\mathbf{u}$ is constant over the sampling interval h (zero-order hold). Then, the continuous model (B.1) is discretized using 1st-order approximation Euler method as follows

$$\left.\begin{aligned} \mathbf{x}_{k+1} &= \boldsymbol{f}(\mathbf{x}_k, \mathbf{u}_k) + h\boldsymbol{\zeta}_k, \\ y_k &= g(\mathbf{x}_k) + \kappa_k, \end{aligned}\right\} \tag{B.2}$$

where $\mathbf{x}_k = [\mathbf{x}_{1_k}, x_{2_k}]^\top = [{}^{\mathcal{B}}\mathbf{d}_k^\top, \chi_k]^\top$ is the state vector at time k, $\mathbf{u}_k = [{}^{\mathcal{B}}\mathbf{v}_k^\top, \omega_{m_k}, r_k]^\top$ is the input vector at time k, y_k is the measurement sampled at time k, $\boldsymbol{f}(\cdot)$ is

$$\boldsymbol{f}(\mathbf{x}_k, \mathbf{u}_k) = \begin{bmatrix} \mathbf{x}_{1_k} + h\left(S(r_k)\mathbf{x}_{1_k} - {}^{\mathcal{B}}\mathbf{v}_k + l_m\omega_{m_k}\mathcal{R}_{\psi_k}^\top \mathbf{w}^\perp(x_{2_k})\right) \\ x_{2_k} + h\omega_{m_k} \end{bmatrix},$$

and $g(\cdot)$ is

$$g(\mathbf{x}_k) = ||\mathbf{x}_{1_k}||.$$

The EKF is executed with the same two steps (prediction (3.3) and correction (3.4)), but with the process and measurement Jacobian matrices at time k described by

$$F_k = \begin{bmatrix} I_2 - hS(r_k) & -hl_m\omega_{m_k}\mathcal{R}_{\psi_k}^\top \mathbf{w}(x_{2_k}) \\ \mathbf{0} & 1 \end{bmatrix}$$

and

$$H_k = \begin{bmatrix} \frac{\mathbf{x}_{1_k}}{||\mathbf{x}_{1_k}||} & 0 \end{bmatrix}.$$

To test the observer, we run a Monte-Carlo simulation with 100 scenarios, in which we choose randomly the beacon's and vehicle's initial position and orientation. We restrict the operation of the vehicle to an area larger than the beacon's position ($||{}^{\mathcal{I}}\mathbf{p}|| > ||{}^{\mathcal{I}}\mathbf{b}|| + \epsilon$) and the inputs of the system are chosen such that Proposition 6 holds. The rest of parameters are set with the values of Table 3.

Table 3: Simulation parameters (without ocean currents)

Parameter	**Variable**	**Value**
Vehicle's angular velocity	r	$0.025\,\mathrm{rad/s}$
Vehicle's linear velocity	${}^{\mathcal{B}}\mathbf{v}$	$[0.7, 0]^\top\mathrm{m/s}$
Beacon's angular velocity	ω_m	$0.5\,\mathrm{rad/s}$
Manipulator's length	l_m	$2\,\mathrm{m}$
Simulation time	t	$200\,\mathrm{s}$
Standard deviation noise range sensor	-	$0.3\,\mathrm{m}$

Regarding the state observer, we assume that the initial condition is initialized with a random Gaussian distribution with mean equal to the real value and standard deviation of $\pm 30\,\%$ from the real value. The Kalman filter parameters were chosen as $Q_k = 1 \times 10^{-3}\mathrm{diag}([1, 1, 0.01])$ for the process noise covariance matrix, the output noise

variance as $R_k = 0.3^2$, and the initial estimation error covariance $P_0 = I_n$. The performance of the steady state is represented by mean absolute error (MAE). The steady state MAE is obtained from the last 20 s of simulation. The average steady state MAE for vehicle's position is 0.87 m with a standard deviation of ± 0.75 m; and for beacon's position is 0.041 m with standard deviation of ± 0.037 m. Figure 38 shows an histogram of the steady state MAE from all 100 simulation.

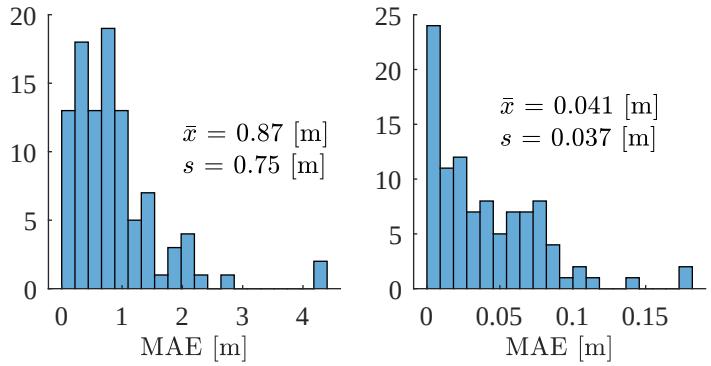

(a) Vehicle's position (b) Beacon's position

Figure 38: Histogram of the steady-state MAE for EKF simulation without ocean currents. There worst case scenario gives an steady-state MAE of 4.3 m in the vehicle's position.

Recall, that the average MAE is not just described as a particular value but instead as a confidence interval where the level of uncertainty is established as 95 %. Then, for 95 % of simulations the steady-state MAE for the vehicle's position is contained in the interval $(0.7490, 0.9987)$ m, and for the beacon's position $(0.0347, 0.0470)$ m.

Additionally, to understand which was the worst case scenario not only due to the steady state error, we evaluate the performance by applying the integral of the square of the error (ISE). The ISE is obtained from the whole simulation time (200 s). This metric gives us a quantitative behavior of the transient for all 100 simulations. Figure 39 shows an histogram of ISE from all 100 simulation.

In the worst case scenario, the vehicle's initial position was set to ${}^{\mathcal{I}}\mathbf{p}_0 = [19.20, 36.16]^\top$ m and the beacon ${}^{\mathcal{I}}\mathbf{b}_0 = [0.96, 1.75]^\top$ m. The state observer was initialized with ${}^{\mathcal{I}}\hat{\mathbf{p}}_0 = [8.50, 36.03]^\top$ m and the beacon ${}^{\mathcal{I}}\hat{\mathbf{b}}_0 = [0.52, 1.92]^\top$ m. Figure 40 shows the vehicle's trajectory and its estimation. Notice, that at the begin is a large error between the real position and its estimation. Additionally, the norm of the estimation errors are shown

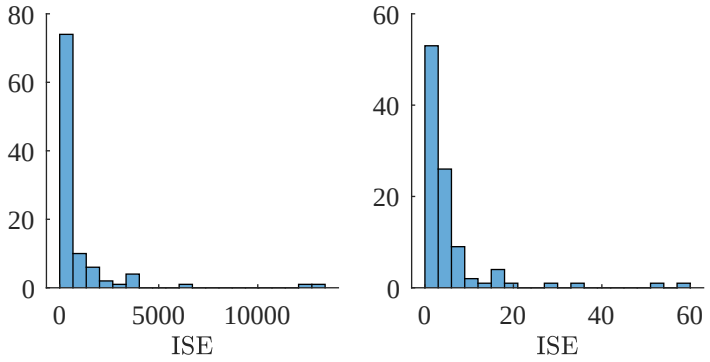

(a) Vehicle's position (b) Beacon's position

Figure 39: Histogram of ISE for EKF simulation without taking into account ocean currents. The worst case scenario corresponds the same having the worst steady state MAE.

in Figure 41. In the worst case scenario, EKF takes the complete simulation time to converge to the real value.

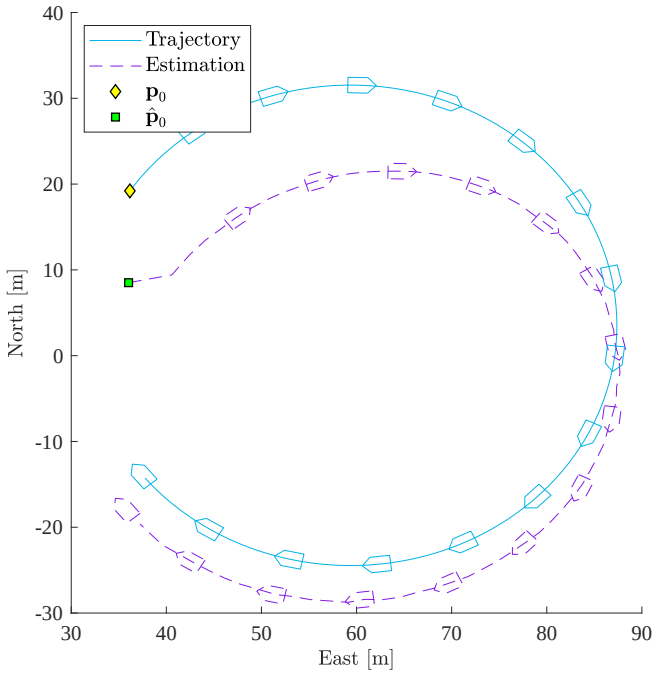

Figure 40: Vehicle's trajectory and its estimation for the EKF. Notice that the filter takes time to converge, but at the end of the simulation is close to the real value. Additionally, we let the simulation run more time and after a while the error converges to zero for all cases.

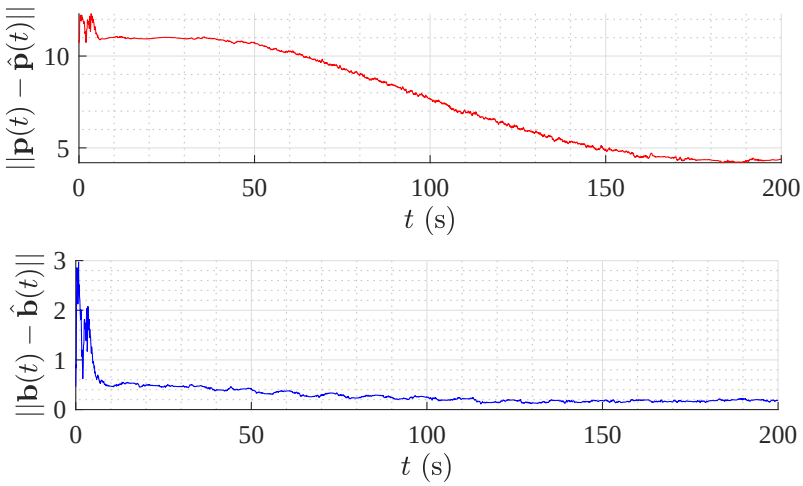

Figure 41: Norm of the estimation errors for the EKF. Notice that the first 200 s there is a large estimation error in the vehicle position.

Another interesting scenario to show is one that lies between the confidence interval. The vehicle's initial position was set to ${}^{\mathcal{I}}\mathbf{p}_0 = [24.41, 15.52]^\top$ m and the beacon ${}^{\mathcal{I}}\mathbf{b}_0 = [1.20, 1.59]^\top$ m. The state observer was initialized with ${}^{\mathcal{I}}\hat{\mathbf{p}}_0 = [22.96, 15.28]^\top$ m and the beacon ${}^{\mathcal{I}}\hat{\mathbf{b}}_0 = [0.94, 1.76]^\top$ m. Figure 42 shows the vehicle's trajectory and its estimation. Notice, that at the beginning there is a large error between the real position and its estimation. Additionally, the norms of the estimation errors are shown in Figure 43.

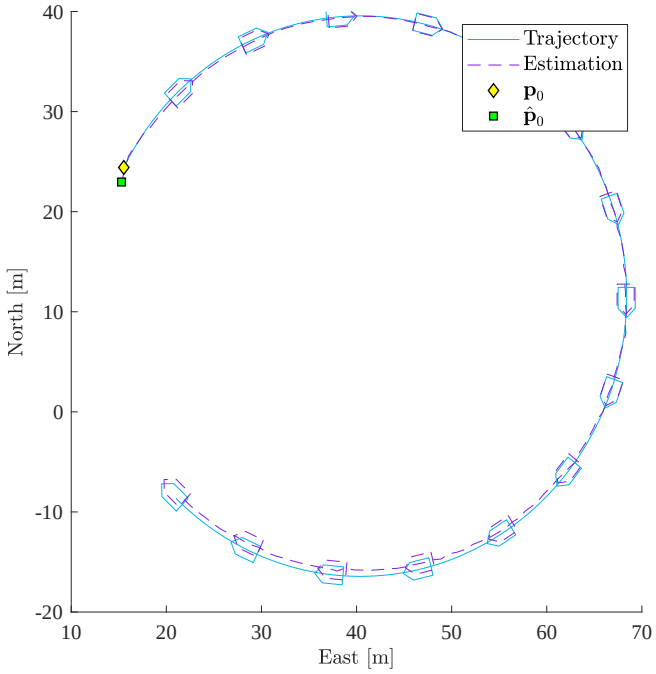

Figure 42: Vehicle's trajectory and its estimation for a simulation that lies within the CI using the EKF.

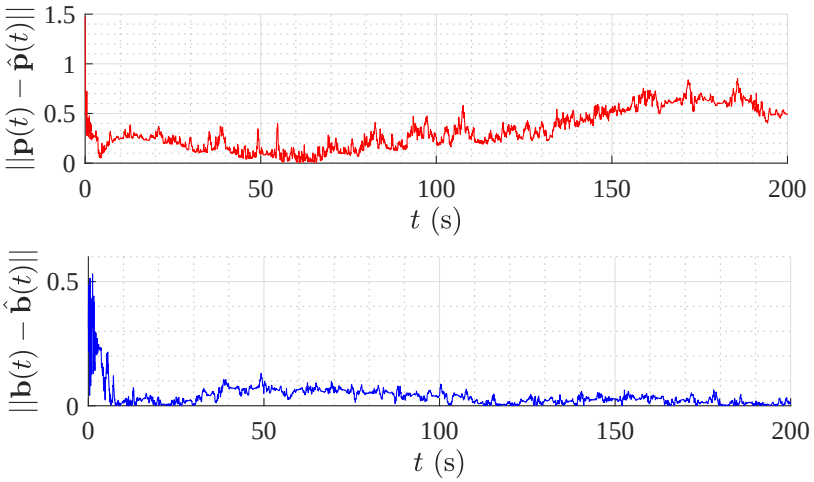

Figure 43: Norm of the estimation errors for a simulation that within the CI using the EKF.

B.2. EXOGENOUS KALMAN FILTER

Based on the results of Chapter **??**, we propose an XKF observer for the nonlinear system (B.1) introduced in Appendix B.1.. We applied the same methodology described in Figure 18 for the system without currents.

- *LQE for the state augmented system*: the first step in the approach is to design an LQE for the augmented-state system represented by Equation (2.23). This observer has the form

$$\dot{\hat{\mathbf{z}}}_{k+1} = \hat{\mathbf{z}}_k + h\left(A(\mathbf{u}_k)\hat{\mathbf{z}}_k + B\mathbf{u}_k + L(\bar{y}_k - C\hat{\mathbf{z}}_k)\right). \tag{B.3}$$

where $\hat{\mathbf{z}}_k \in \mathbb{R}^9$ is the state estimation vector, $L \in \mathbb{R}^9$ satisfies $L = \bar{P}C^\top \bar{R}^{-1}$ and $P = \mathbb{E}\{(\mathbf{z}(t) - \hat{\mathbf{z}}(t))(\mathbf{z}(t) - \hat{\mathbf{z}}(t))^\top\}$ satisfies the algebraic Riccati equation (3.7).

Additionally, the matrices A, B and C are given by

$$A(\mathbf{u}_k) = \begin{bmatrix} -S(r_k) & l_m\omega_{m_k} I_2 & \mathbf{0} & \mathbf{0} & \mathbf{0} & \mathbf{0} \\ \mathbf{0} & -S(r_k) & -\omega_{m_k} I_2 & \mathbf{0} & \mathbf{0} & \mathbf{0} \\ \mathbf{0} & (\omega_{m_k} - r_k) I_2 & \mathbf{0} & \mathbf{0} & \mathbf{0} & \mathbf{0} \\ -2{}^{\mathcal{B}}\mathbf{v}_k^\top & \mathbf{0} & \mathbf{0} & 0 & 2l_m\omega_{m_k} & 0 \\ \mathbf{0} & -{}^{\mathcal{B}}\mathbf{v}_k^\top & \mathbf{0} & 0 & 0 & -\omega_{m_k} \\ \mathbf{0} & \mathbf{0} & -{}^{\mathcal{B}}\mathbf{v}_k^\top & 0 & \omega_{m_k} & 0 \end{bmatrix},$$

$$B = \begin{bmatrix} -I_2 & \mathbf{0} & \mathbf{0} \\ \mathbf{0} & \mathbf{0} & \mathbf{0} \\ \mathbf{0} & \mathbf{0} & \mathbf{0} \\ \mathbf{0} & 0 & 0 \\ \mathbf{0} & l_m & 0 \\ \mathbf{0} & 0 & 0 \end{bmatrix},$$

$$C = \begin{bmatrix} \mathbf{0} & \mathbf{0} & \mathbf{0} & 1 & 0 & 0 \end{bmatrix}.$$

Recall that $\bar{y}_k \neq y_k$. The output of the augmented-state observer (B.3) is related to the original measurement as $\bar{y}_k = y_k^2$.

- *Inverse state transformation*: the state estimation $\mathbf{z}_k \in \mathbb{R}^9$ is related with the original system through the following inverse state transformation

$$\bar{\mathbf{x}}_k = \begin{bmatrix} \bar{\mathbf{x}}_{1_k} \\ \bar{\mathbf{x}}_{2_k} \end{bmatrix} = \begin{bmatrix} \hat{\mathbf{z}}_{1_k} \\ \operatorname{atan2}\left(\mathcal{R}_\psi \hat{\mathbf{z}}_{3_k} \mathbf{e}_2, \mathcal{R}_\psi \hat{\mathbf{z}}_{3_k} \mathbf{e}_1\right) \end{bmatrix}. \tag{B.4}$$

- *Linearized Kalman Filter*: now, $\bar{\mathbf{x}}_k$ is used as linearization point to build the Kalman Filter. A first-order Taylor series expansion of (B.1) about the trajectory $\bar{\mathbf{x}}_k$ gives the linearized model

$$\left.\begin{aligned} \mathbf{x}_{k+1} &= \boldsymbol{f}(\bar{\mathbf{x}}_k, \mathbf{u}_k) + F_k(\mathbf{x}_k - \bar{\mathbf{x}}_k) + \epsilon_{x_k} + h\boldsymbol{\zeta}_k, \\ y_k &= g(\bar{\mathbf{x}}_k) + H_k(\mathbf{x}_k - \bar{\mathbf{x}}_k) + \epsilon_{y_k} + \kappa_k, \end{aligned}\right\}, \tag{B.5}$$

where ϵ_{x_k} and ϵ_{y_k} are the high-order terms in the linearization processes, F_k and H_k are the Jacobian matrices around the state trajectory $\bar{\mathbf{x}}_k$ given by

$$F_k := \frac{\partial \boldsymbol{f}(\bar{\mathbf{x}}_k, \mathbf{u}_k)}{\partial \mathbf{x}} = \begin{bmatrix} I_2 - hS(r_k) & -hl_m\omega_{m_k}\mathcal{R}_{\psi_k}^\top \mathbf{w}\left(\bar{x}_{2_k}\right) \\ \mathbf{0} & 1 \end{bmatrix},$$

$$H_k := \frac{\partial g(\bar{\mathbf{x}}_k, \mathbf{u}_k)}{\partial \mathbf{x}} = \begin{bmatrix} \frac{\bar{\mathbf{x}}_{1_k}}{||\bar{\mathbf{x}}_{1_k}||} & 0 \end{bmatrix}.$$

Then, the Linearized Kalman Filter (LKF) formulation for the system (B.5) in the predictor-corrector form is given by

$$\left.\begin{aligned}\hat{\mathbf{x}}_{k+1}^{-} &= \boldsymbol{f}(\bar{\mathbf{x}}_k, \mathbf{u}_k) + F_k(\hat{\mathbf{x}}_k - \bar{\mathbf{x}}_k),\\ \hat{P}_{k+1}^{-} &= F_k \hat{P}_k F_k^{\top} + Q_k,\end{aligned}\right\} \tag{B.6}$$

and the correction equations are given by

$$\left.\begin{aligned}\tilde{y}_k &= y_k - g(\bar{\mathbf{x}}_k) - H_k(\hat{\mathbf{x}}_{k+1}^{-} - \bar{\mathbf{x}}_k),\\ S_{k+1} &= H_k \hat{P}_{k+1}^{-} H_k^{\top} + R_k,\\ K_{k+1} &= \hat{P}_{k+1}^{-} H_k^{\top} S_{k+1}^{-1},\\ \hat{\mathbf{x}}_{k+1} &= \hat{\mathbf{x}}_{k+1}^{-} + K_{k+1}\tilde{y}_k,\\ \hat{P}_{k+1} &= (I - K_{k+1}H_k)\,\hat{P}_{k+1}^{-}.\end{aligned}\right\} \tag{B.7}$$

To test the observer, we run a Monte-Carlo simulation with 100 scenarios, in which we randomly choose the beacon's and vehicle's initial position and orientation. The conditions are the same as the EKF, where we restrict the operation of the vehicle to an area larger than the beacon's position ($||^{\mathcal{I}}\mathbf{p}|| > ||^{\mathcal{I}}\mathbf{b}|| + \epsilon$), the foregoing in order to avoid collisions or entanglement between the vehicle and beacon. The inputs of the system are chosen such that Proposition 6 holds. The parameters and inputs are set with the values of Table 3.

Regarding the state observer, we assume that the initial condition is initialized with a random Gaussian distribution with mean equal to the real value and standard deviation of $\pm 30\,\%$ from the real value. The LQE parameters are chosen as $\bar{Q} = 0.001\ \text{diag}([1, 1, 0.001\ \text{ones}(1, 7)])$ for the process noise covariance matrix, and the output noise variance as $\bar{R} = 0.1$. The LKF parameters are chosen as $Q_k = 0.001\text{diag}([1, 1, 0.001])$, $R_k = 0.3^2$, and the initial estimation error covariance $P_0 = I_n$. All 100 simulations converge and the performance of the steady state is represented by mean absolute error (MAE). The steady- state MAE is obtained from the last 20 s of the simulation. The average steady-state MAE for vehicle's position is 0.31 m with a standard deviation of ± 0.17 m; and for beacon's position is 0.09 m with standard deviation of ± 0.036 m. Figure 44 shows an histogram of the steady-state MAE from all 100 simulation.

Recall, that the average MAE is better represented as a confidence interval where the level of uncertainty is established as 95 %. Then, for 95 % of simulations the steady-

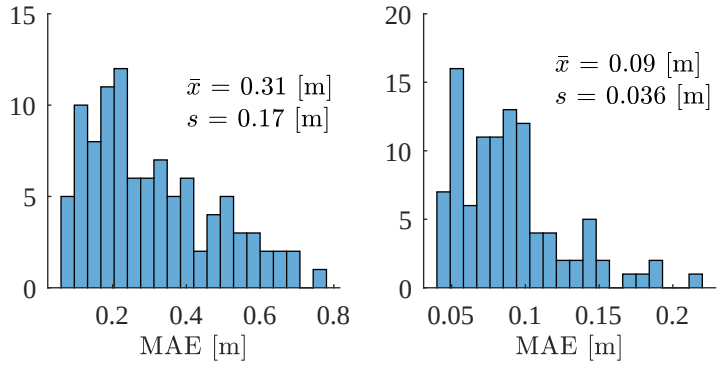

(a) Vehicle's position (b) Beacon's position

Figure 44: Histogram of the steady state MAE for XKF simulation without taking into account ocean currents. There worst case scenario gives an steady state MAE of 0.78 m in the vehicle's position.

state MAE for the vehicle's position is contained in the interval $(0.2788, 0.3351)$ m, and for the beacon's position $(0.0837, 0.0957)$ m.

Finally, to understand which was the worst case scenario not only due to the steady-state error, we evaluate the performance by applying the integral of the square of the error (ISE). The ISE is obtained from the whole simulation time (200 s). Figure 45 shows an histogram of ISE from all 100 simulation.

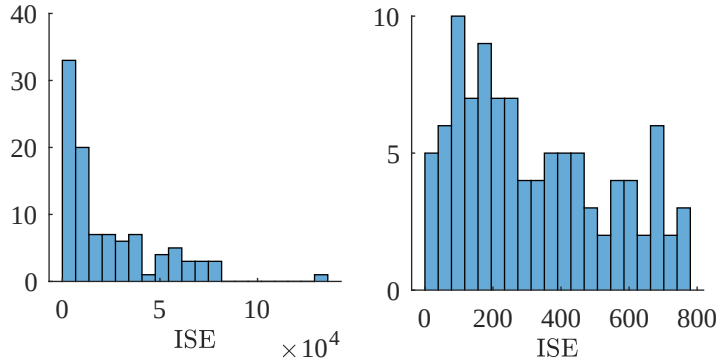

(a) Vehicle's position (b) Beacon's position

Figure 45: Histogram of ISE for XKF simulation without taking into account ocean currents. The worst case scenario corresponds the same having the worst steady-state MAE.

Now, we show the time-history of the state estimation in the worst case scenario and one scenario within the CI. In the worst case scenario, the vehicle's initial position was set to ${}^{\mathcal{I}}\mathbf{p}_0 = [47.03, 40.01]^\top$ m and the beacon ${}^{\mathcal{I}}\mathbf{b}_0 = [0.41, -1.96]^\top$ m. The state observer was initialized with ${}^{\mathcal{I}}\hat{\mathbf{p}}_0 = [47.21, 42.07]^\top$ m and the beacon ${}^{\mathcal{I}}\hat{\mathbf{b}}_0 = [0.13, -1.99]^\top$ m. Figure 46 shows the vehicle's trajectory and its estimation. Additionally, the norms of the estimation errors are shown in Figure 47. There is a large error at the beginning, but it converges at the end of the simulation.

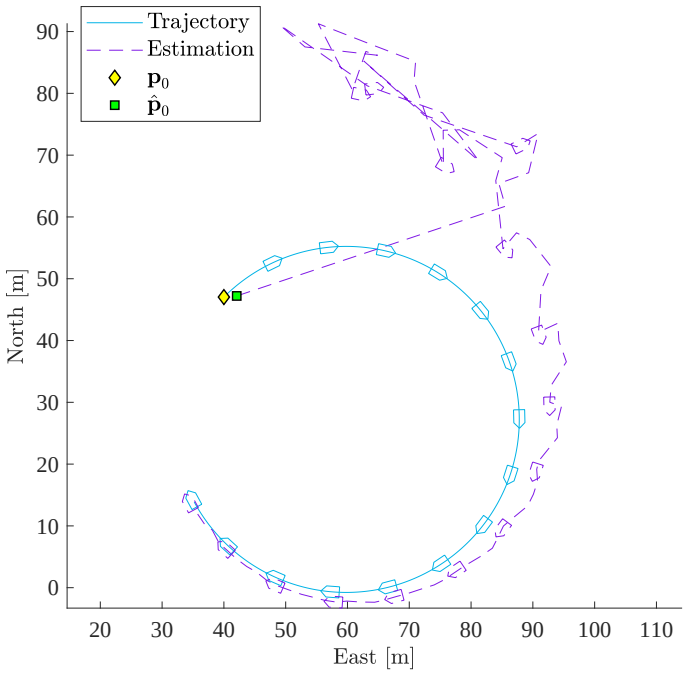

Figure 46: Vehicle's trajectory and its estimation. Notice that the filter diverges at the beginning, nevertheless at converges close to the real value.

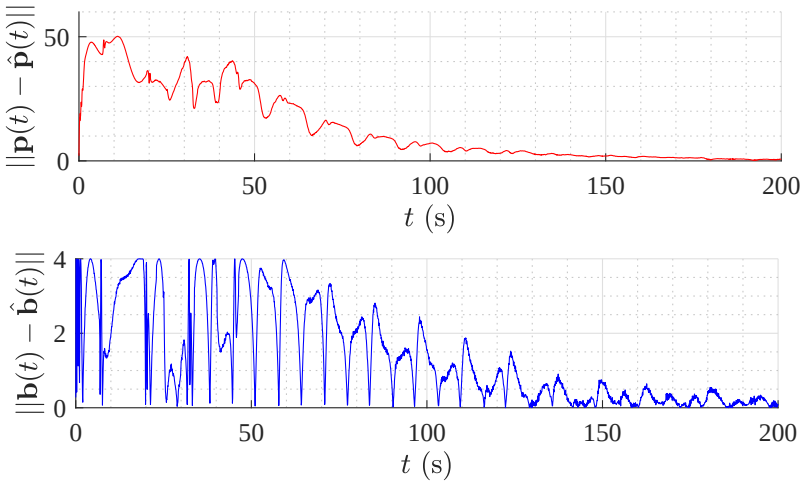

Figure 47: Norm of the estimation errors for the XKF. Notice that at the beginning the estimation error reaches almost 50 m.

The other scenario was the one that lies between the confidence interval. The vehicle's initial position was set to ${}^{\mathcal{I}}\mathbf{p}_0 = [29.27, 22.99]^\top$ m and the beacon ${}^{\mathcal{I}}\mathbf{b}_0 = [-1.38, -1.44]^\top$ m. The state observer was initialized with ${}^{\mathcal{I}}\hat{\mathbf{p}}_0 = [30.02, 22.73]^\top$ m and the beacon ${}^{\mathcal{I}}\hat{\mathbf{b}}_0 = [-1.28, -1.40]^\top$ m. Figure 48 shows the vehicle's trajectory and its estimation. Additionally, the norms of the estimation errors are shown in Figure 49.

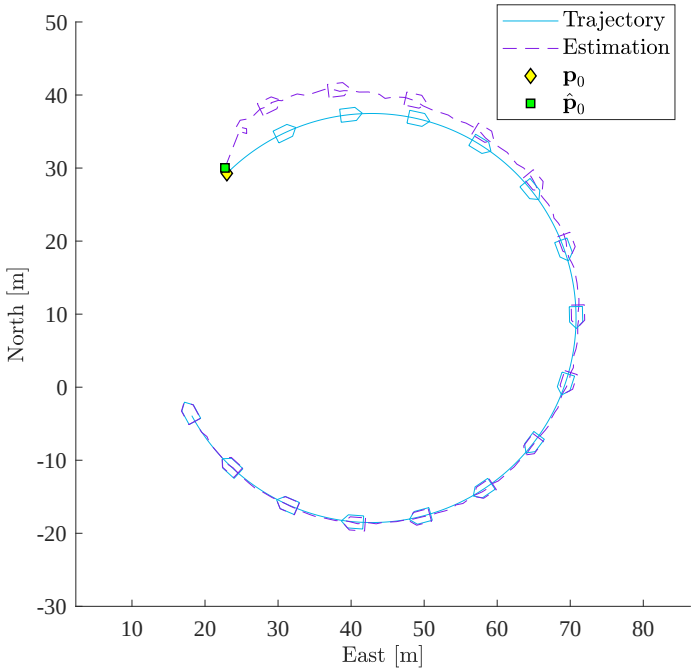

Figure 48: Vehicle's trajectory and its estimation for a simulation that lies within the CI using the XKF.

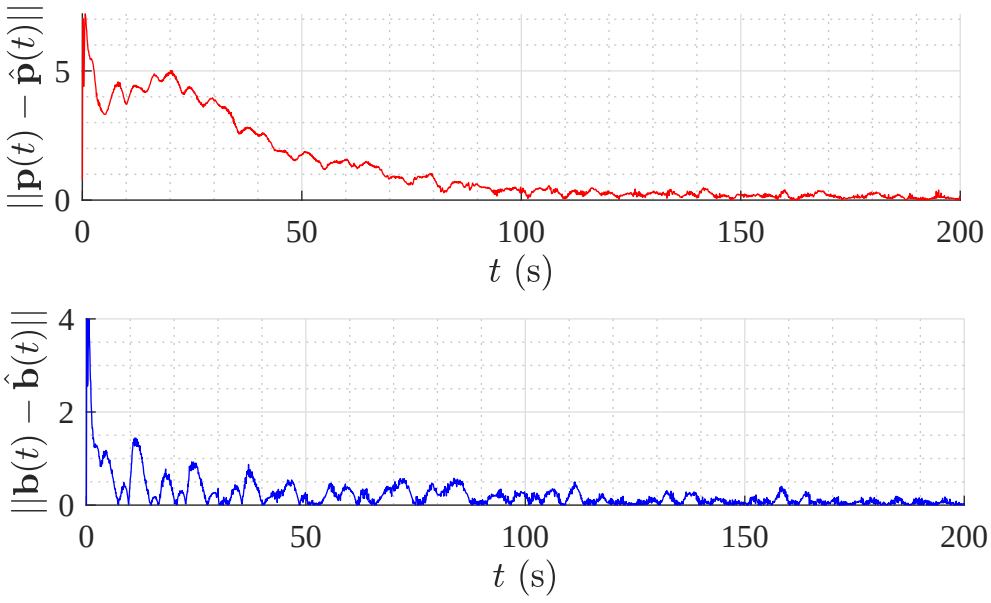

Figure 49: Norm of the estimation errors for a simulation that within the CI using the XKF.

BIBLIOGRAPHY

[1] Davis, P., and Brockhurst, J., 2015. "Subsea pipeline infrastructure monitoring: A framework for technology review and selection". *Ocean Engineering,* ***104***, Aug., pp. 540–548.

[2] Bonin-Font, F., Oliver, G., Wirth, S., Massot, M., Negre, P. L., and Beltran, J.-P., 2015. "Visual sensing for autonomous underwater exploration and intervention tasks". *Ocean Engineering,* ***93***, Jan., pp. 25–44.

[3] Ludvigsen, M., and Sørensen, A. J., 2016. "Towards integrated autonomous underwater operations for ocean mapping and monitoring". *Annual Reviews in Control,* ***42***, pp. 145–157.

[4] Choyekh, M., Kato, N., Yamaguchi, Y., Dewantara, R., Chiba, H., Senga, H., Yoshie, M., Tanaka, T., Kobayashi, E., and Short, T., 2017. *Development and Operation of Underwater Robot for Autonomous Tracking and Monitoring of Subsea Plumes After Oil Spill and Gas Leak from Seabed and Analyses of Measured Data.* Springer Japan, Tokyo, pp. 17–93.

[5] Griffiths, G., 2002. *Technology and Applications of Autonomous Underwater Vehicles*, Vol. 2. Taylor & Francis.

[6] Wadoo, S., and Kachroo, P., 2011. *Autnomous Underwater Vehicles: Modeling, Control Design and Simulation*, 1 ed. CRC Press, Dec.

[7] Christ, R. D., and Wernli, R. L., 2014. *The ROV manual, a user guide for Remotely Operated Vehicles*, 2 ed. Butterworth-Heinemann, Oxford.

[8] Roberts, G., 2008. "Trends in marine control systems". *Annual Reviews in Control,* ***32***(2), Dec., pp. 263 – 269.

[9] Chyba, M., Haberkorn, T., Smith, R. N., and Choi, S. K., 2008. "Design

and implementation of time efficient trajectories for autonomous underwater vehicles". *Ocean Engineering,* ***35***(1), Jan., pp. 63–76.

[10] Rúa, S., 2015. "Simulation of the control system for a remotely operated underwater vehicle". Master's thesis, Universidad Pontificia Bolivariana, sede Medellín.

[11] Rúa, S., and Vásquez, R. E., 2016. "Development of a low-level control system for the ROV Visor3". *International Journal of Navigation and Observation*(8029124), pp. 1–12.

[12] Nađ, Đ., Mišković, N., and Mandić, F., 2015. "Navigation, guidance and control of an overactuated marine surface vehicle". *Annual Reviews in Control,* ***40***, pp. 172–181.

[13] Al-Khatib, H., Antonelli, G., Caffaz, A., Caiti, A., Casalino, G., de Jong, I. B., Duarte, H., Indiveri, G., Jesus, S., Kebkal, K., Pascoal, A., and Polani, D., 2015. "Navigation, guidance and control of underwater vehicles within the widely scalable mobile underwater sonar technology project: an overview★". *IFAC-PapersOnLine,* ***48***(2), pp. 189–193.

[14] Ridao, P., Ribas, D., and Sanz, P. J., 2016. "Special section on navigation, guidance and control of underwater vehicles". *Annual Reviews in Control,* ***42***, pp. 143–144.

[15] Kinsey, J. C., Eustive, R. M., and Whitcomb, L. L., 2006. "A survey of underwater vehicle navigation: Recent advances and new challenges". In IFAC Conference of Manoeuvering and Control of Marine Craft.

[16] Chitre, M., Shahabudeen, S., Freitag, L., and Stojanovic, M., 2008. "Recent advances in underwater acoustic communications & networking". In OCEANS 2008.

[17] Tan, H.-P., Diamant, R., Seah, W. K. G., and Waldmeyer, M., 2011. "A survey of techniques and challenges in underwater localization". *Ocean Engineering,* ***38***(14-15), Oct., pp. 1663–1676.

[18] Fossen, T. I., 1994. *Guidance and Control of Ocean Vehicles.* John Wiley and

Sons.

[19] Fossen, T. I., 2011. *Handbook of marine craft hydrodynamics and motion control.* John Wiley & Sons, West Sussex, United Kingdom.

[20] Jekeli, C., 2001. *Inertial Navigation Systems with Geodetic Applications.* De Gruyter.

[21] Groves, P. D., 2013. *Principles of GNSS, Inertial, and Multisensor Integrated Navigation Systems.* Artech House Publishers.

[22] Chen, Z., and Hung, J. C., 1991. "Navigation schemes for underwater robots using strapdown inertial navigation system". In International Conference on Industrial Electronics, Control and Instrumentation, IECON '91., pp. 1075–1078 vol.2.

[23] Troni, G., McFarland, C. J., Nichols, K. A., and Whitcomb, L. L., 2011. "Experimental evaluation of an inertial navigation system for underwater robotic vehicles". In 2011 IEEE International Conference on Robotics and Automation, pp. 3064–3071.

[24] Nebot, E., and Durrant-Whyte, H., 1997. "Initial calibration and alignment of an inertial navigation". In Proceedings Fourth Annual Conference on Mechatronics and Machine Vision in Practice, pp. 175–180.

[25] Ishibashi, S., 2013. "A compact and high-performance ins for underwater vehicle developed with homegrown technology". In 2013 IEEE International Underwater Technology Symposium (UT), pp. 1–5.

[26] Li, J.-H., Kim, J.-T., Lee, M.-J., Jee, S. C., Kang, H.-J., Kim, M.-G., Hong, S.-M., and Suh, J.-H., 2015. "Initial alignment consideration for underwater robot's strapdown inertial navigation system". In 2015 12th International Conference on Ubiquitous Robots and Ambient Intelligence (URAI), pp. 231–234.

[27] Yuan, D., Ma, X., Liu, Y., and Zhang, C., 2016. "Dynamic initial alignment of the MEMS-based low-cost SINS for AUV based on unscented Kalman filter". In OCEANS 2016 - Shanghai, pp. 1–6.

[28] Leonard, J. J., and Bahr, A., 2016. *Springer Handbook of Ocean Engineering*. Springer International Publishing, ch. Autnomous Underwater Vehicle Navigation, pp. 341–358.

[29] Teixeira, F. C., 2007. "Terrain-aided navigation and geophysical navigation of autonomous underwater vehicles". Ph.D. thesis, Instituto Superior Técnico.

[30] Melo, J., and Matos, A., 2017. "Survey on advances on terrain based navigation for autonomous underwater vehicles". *Ocean Engineering,* ***139***, pp. 250–264.

[31] Larsen, M., 2000. "Synthetic long baseline navigation of underwater vehicles". In OCEANS 2000 MTS/IEEE Conference and Exhibition. Conference Proceedings, IEEE.

[32] Bayat, M., 2015. "Nonlinear robust adaptive state estimation". Ph.D. thesis, Universidade de Lisboa, Instituto Superior Técnico.

[33] Scherbatyuk, A. P., 1995. "The AUV positioning using ranges from one transponder LBL". In OCEANS '95. MTS/IEEE. Challenges of Our Changing Global Environment. Conference Proceedings., Vol. 3, pp. 1620–1623.

[34] Song, T. L., 1999. "Observability of target tracking with range-only measurements". *IEEE Journal of Oceanic Engineering,* ***24***(3), jul, pp. 383–387.

[35] Vaganay, J., Baccou, P., and Jouvencel, B., 2000. "Homing by acoustic ranging to a single beacon". In OCEANS 2000 MTS/IEEE Conference and Exhibition.

[36] Newman, P., and Leonard, J., 2003. "Pure range-only sub-sea SLAM". In 2003 IEEE International Conference on Robotics and Automation, Vol. 2, pp. 1921–1926.

[37] Gadre, A. S., and Stilwell, D. J., 2004. "Toward underwater navigation based on range measurements from a single location". In IEEE International Conference on Robotics and Automation., IEEE.

[38] Gadre, A. S., and Stilwell, D. J., 2005. "A complete solution to underwater navigation in the presence of unknown currents based on range measurements from a single location". In 2005 IEEE/RSJ International Conference on Intelligent

Robots and Systems, IEEE.

[39] Hartsfield, C., 2005. "Single Transponder Range Only Navigation Geometry (STRONG) applied to remus autonomous under water vechiles". Master's thesis, Massachusetts Institute of Technology.

[40] Jouffroy, J., and Ross, A., 2005. "Remarks on the observability of single beacon underwater navigation". In International Symposium on Unmanned Untethered Submersible Technology.

[41] LaPointe, C. E. G., 2006. "Virtual long baseline (VLBL) autonomous underwater vehicle navigation using a single transponder". Master thesis, Massachusetts Institute of Technology, June.

[42] Jouffroy, J., and Reger, J., 2006. "An algebraic perspective to single-transponder underwater navigation". In 2006 IEEE Conference on Computer Aided Control System Design, 2006 IEEE International Conference on Control Applications, 2006 IEEE International Symposium on Intelligent Control.

[43] Casey, T., Guimond, B., and Hu, J., 2007. "Underwater vehicle positioning based on time of arrival measurements from a single beacon". In OCEANS 2007, pp. 1–8.

[44] Lee, P. M., Jun, B. H., and Lim, Y. K., 2008. "Review on underwater navigation system based on range measurements from one reference". In OCEANS 2008 - MTS/IEEE Kobe Techno-Ocean, pp. 1–5.

[45] Dandach, S. H., Fidan, B., Dasgupta, S., and Anderson, B. D., 2009. "A continuous time linear adaptive source localization algorithm, robust to persistent drift". *Systems & Control Letters,* ***58***(1), pp. 7 – 16.

[46] Huang, G. P., Zhou, K. X., Trawny, N., and Roumeliotis, S. I., 2010. "A bank of maximum a posteriori estimators for single-sensor range-only target tracking". In Proceedings of the 2010 American Control Conference, pp. 6974–6980.

[47] Webster, S., Whitcomb, L., and Eustice, R., 2011. *Preliminary results in decentralized estimation for single-beacon acoustic underwater navigation*, Vol. 6. MIT Press Journals, United States, pp. 81–88.

[48] Parlangeli, G., Pedone, P., and Indiveri, G., 2012. "Relative pose observability analysis for 3D nonholonomic vehicles based on range measurements only". *IFAC Proceedings Volumes,* ***45***(27), Sept., pp. 182–187.

[49] Tan, Y. T., Gao, R., and Chitre, M., 2014. "Cooperative path planning for range-only localization using a single moving beacon". *IEEE Journal of Oceanic Engineering,* ***39***(2), April, pp. 371–385.

[50] Huang, G., Zhou, K., Trawny, N., and Roumeliotis, S. I., 2015. "A Bank of Maximum A Posteriori (MAP) Estimators for Target Tracking". *IEEE Transactions on Robotics,* ***31***(1), Feb, pp. 85–103.

[51] Dandach, S. H., Fidan, B., Dasgupta, S., and Anderson, B. D. O., 2006. "Adaptive source localization by mobile agents". In Proceedings of the 45th IEEE Conference on Decision and Control.

[52] Saúde, J., and Aguiar, A. P., 2009. "Single Beacon Acoustic Navigation for an AUV in the presence of unknown ocean currents". *IFAC Proceedings Volumes,* ***42***(18), pp. 298 – 303. 8th IFAC Conference on Manoeuvring and Control of Marine Craft.

[53] Clark, J. M. C., Kountouriotis, P. A., and Vinter, R. B., 2011. "A gaussian mixture filter for range-only tracking". *IEEE Transactions on Automatic Control,* ***56***(3), March, pp. 602–613.

[54] Mandić, F., Mišković, N., Palomeras, N., Carreras, M., and Vallicrosa, G., 2016. "Mobile beacon control algorithm that ensures observability in single range navigation". *IFAC-PapersOnLine,* ***49***(23), pp. 48–53.

[55] Hermann, R., and Krener, A., 1977. "Nonlinear controllability and observability". *IEEE Transactions on Automatic Control,* ***22***(5), oct, pp. 728–740.

[56] Antonelli, G., Arrichiello, F., Chiaverini, S., and Sukhatme, G. S., 2010. "Observability analysis of relative localization for AUVs based on ranging and depth measurements". In 2010 IEEE International Conference on Robotics and Automation, pp. 4276–4281.

[57] Batista, P., Silvestre, C., and Oliveira, P., 2011. "Single range aided navigation

and source localization: Observability and filter design". *Systems & Control Letters,* ***60***(8), pp. 665 – 673.

[58] Bayat, M., and Aguiar, A. P., 2012. "Observability analysis for AUV range-only localization and mapping measures of unobservability and experimental results". *IFAC Proceedings Volumes,* ***45***(27), Sept., pp. 325–330.

[59] Crasta, N., Bayat, M., Aguiar, A. P., and Pascoal, A. M., 2013. "Observability analysis of 2D single beacon navigation in the presence of constant currents for two classes of maneuvers". *IFAC Proceedings Volumes,* ***46***(33), Sept., pp. 227–232.

[60] Crasta, N., Bayat, M., Aguiar, A. P., and Pascoal, A. M., 2014. "Observability Analysis of 3D AUV Trimming Trajectories in the Presence of Ocean Currents using Single Beacon Navigation". *IFAC Proceedings Volumes,* ***47***(3), Aug., pp. 4222–4227.

[61] Crasta, N., Bayat, M., Aguiar, A. P., and Pascoal, A. M., 2015. "Observability analysis of 3D AUV trimming trajectories in the presence of ocean currents using range and depth measurements". *Annual Reviews in Control,* ***40***, pp. 142 – 156.

[62] Olson, E., Leonard, J. J., and Teller, S., 2006. "Robust range-only beacon localization". *IEEE Journal of Oceanic Engineering,* ***31***(4), oct, pp. 949–958.

[63] Indiveri, G., Palma, D. D., and Parlangeli, G., 2016. "Single Range Localization in 3-D: Observability and Robustness Issues". *IEEE Transactions on Control Systems Technology,* ***24***(5), Sept, pp. 1853–1860.

[64] Indiveri, G., 2009. "An entropy-like estimator for robust parameter identification". *Entropy,* ***11***(4), pp. 560–585.

[65] Lekkas, A. M., Candeloro, M., and Schjølberg, I., 2015. "Outlier rejection in underwater acoustic position measurements based on prediction errors". *IFAC-PapersOnLine,* ***48***(2), pp. 82 – 87. 4th IFAC Workshop on Navigation, Guidance and Control of Underwater Vehicles NGCUV 2015.

[66] Emami, M., and Taban, M. R., 2017. "A customized H-infinity algorithm for

underwater navigation system: With experimental evaluation". *Ocean Engineering,* ***130***, pp. 611 – 619.

[67] Bahr, A., Leonard, J. J., and Fallon, M. F., 2009. "Cooperative localization for autonomous underwater vehicles". *The International Journal of Robotics Research,* ***28***(6), may, pp. 714–728.

[68] Pedro, M., 2014. "A range-based navigation system for autonomous underwater vehicles". Master thesis, Universidade de Lisboa, Instituto Superior Técnico, Dec.

[69] Rui, G., and Chitre, M., 2010. "Cooperative positioning using range-only measurements between two AUVs". In OCEANS 2010 IEEE - Sydney, pp. 1–6.

[70] Fallon, M. F., Papadopoulos, G., Leonard, J. J., and Patrikalakis, N. M., 2010. "Cooperative AUV navigation using a single maneuvering surface craft". *The International Journal of Robotics Research,* ***29***(12), pp. 1461–1474.

[71] Webster, S. E., Walls, J. M., Whitcomb, L. L., and Eustice, R. M., 2013. "Decentralized extended information filter for single-beacon cooperative acoustic navigation: Theory and experiments". *IEEE Transactions on Robotics,* ***29***(4), Aug, pp. 957–974.

[72] Parlangeli, G., and Indiveri, G., 2014. "Single range observability for cooperative underactuated underwater vehicles.". *IFAC Proceedings Volumes,* ***47***(3), Aug., pp. 5127–5138.

[73] Parlangeli, G., and Indiveri, G., 2015. "Single range observability for cooperative underactuated underwater vehicles". *Annual Reviews in Control,* ***40***, pp. 129 – 141.

[74] Moreno-Salinas, D., Pascoal, A. M., and Aranda, J., 2013. "Optimal sensor placement for multiple target positioning with range-only measurements in two-dimensional scenarios". *Sensors,* ***13***(8), pp. 10674–10710.

[75] Pedro, M., Moreno-Salinas, D., Crasta, N., and Pascoal, A., 2015. "Underwater single-beacon localization: Optimal trajectory planning and minimum-energy estimation". *IFAC-PapersOnLine,* ***48***(2), pp. 155–160.

[76] Moreno-Salinas, D., Crasta, N., Ribeiro, M., Bayat, B., Pascoal, A., and Aranda, J., 2016. "Integrated motion planning, control, and estimation for range-based marine vehicle positioning and target localization". *IFAC-PapersOnLine,* ***49***(23), pp. 34 – 40. 10th IFAC Conference on Control Applications in Marine Systems CAMS 2016.

[77] Crasta, N., Moreno-Salinas, D., Bayat, M., Pascoal, A., and Aranda, J., 2016. "Optimal motion planning for range-based marine vehicle positioning in the presence of unknown currents". *IFAC-PapersOnLine,* ***49***(23), pp. 41 – 47. 10th IFAC Conference on Control Applications in Marine Systems CAMS 2016.

[78] Balampanis, F., Maza, I., and Ollero, A., 2017. "Area partition for coastal regions with multiple UAS". *Journal of Intelligent & Robotic Systems*, Apr., pp. 1–16.

[79] Balampanis, F., Maza, I., and Ollero, A., 2017. "Coastal areas division and coverage with multiple uavs for remote sensing". *Sensors,* ***17***(4), pp. 1–25.

[80] Dukan, F., and Sørensen, A. J., 2013. "Integration filter for APS, DVL, IMU and pressure gauge for underwater vehicles". *IFAC Proceedings Volumes,* ***46***(33), pp. 280–285. 9th IFAC Conference on Control Applications in Marine Systems.

[81] Bayat, M., Crasta, N., Aguiar, A. P., and Pascoal, A. M., 2016. "Range-based underwater vehicle localization in the presence of unknown ocean currents: Theory and experiments". *IEEE Transactions on Control Systems Technology,* ***24***(1), Jan, pp. 122–139.

[82] Batista, P. T. M., 2010. "Sensor-based navigation and control of autonomous vehicles". Ph.D. thesis, Universidade de Lisboa, Instituto Superior Técnico.

[83] Batista, P., Silvestre, C., and Oliveira, P., 2010. "A sensor-based long baseline position and velocity navigation filter for underwater vehicles". *IFAC Proceedings Volumes,* ***43***(14), pp. 302 – 307. 8th IFAC Symposium on Nonlinear Control Systems.

[84] Batista, P., 2015. "Long baseline navigation with clock offset estimation and discrete-time measurements". *Control Engineering Practice,* ***35***, pp. 43 – 53.

[85] Indiveri, G., and Parlangeli, G., 2013. "Further results on the observability analysis and observer design for single range localization in 3D". *CoRR*.

[86] Hespanha, J. P., 2009. *Linear Systems Theory*. Princeton University Press.

[87] Frazzoli, E., 2001. "Robust Hybrid Control for Autonomous Vehicle Motion Planning". PhD thesis, MIT.

[88] Schaft, A. J., 1986. "On realization of nonlinear systems described by higher-order differential equations". *Mathematical Systems Theory,* ***19***(1), dec, pp. 239–275.

[89] Ülle Kotta, Moog, C. H., and Tõnso, M., 2018. "Minimal realizations of nonlinear systems". *Automatica,* ***95***, sep, pp. 207–212.

[90] Alcocer, A., 2009. "Positioning and navigation systems for robotic underwater vehicles". Ph.D. thesis, Universidade Técnica de Lisboa, Instituto Superior Técnico.

[91] Morgado, M., Batista, P., Oliveira, P., and Silvestre, C., 2012. "Attitude estimation for intervention-AUVs working in tandem with autonomous surface craft". *European Journal of Control,* ***18***(5), jan, pp. 485–495.

[92] Hajiyev, C., Cilden, D., and Somov, Y., 2016. "Gyro-free attitude and rate estimation for a small satellite using SVD and EKF". *Aerospace Science and Technology,* ***55***, aug, pp. 324–331.

[93] C., K., and Ozger, E., 2018. "Attitude and airdata estimation". *IFAC-PapersOnLine,* ***51***(1), pp. 431–436.

[94] Garcia, R., Pardal, P., Kuga, H., and Zanardi, M., 2019. "Nonlinear filtering for sequential spacecraft attitude estimation with real data: Cubature Kalman Filter, Unscented Kalman Filter and Extended Kalman Filter". *Advances in Space Research,* ***63***(2), jan, pp. 1038–1050.

[95] Vetrella, A. R., Fasano, G., and Accardo, D., 2019. "Attitude estimation for cooperating UAVs based on tight integration of GNSS and vision measurements". *Aerospace Science and Technology,* ***84***, jan, pp. 966–979.

[96] Huang, H., Chen, X., Zhang, B., and Wang, J., 2017. "High accuracy navigation information estimation for inertial system using the multi-model EKF fusing adams explicit formula applied to underwater gliders". *ISA Transactions,* ***66***, jan, pp. 414–424.

[97] Stepanov, O. A., Toropov, A. B., Loparev, A. V., Vasiliev, V. A., and Basin, M. V., 2018. "Polynomial filtering algorithm for single-beacon navigation problem". *IFAC-PapersOnLine,* ***51***(32), pp. 619–623.

[98] Costanzi, R., Fenucci, D., Caiti, A., Micheli, M., Vermeij, A., Tesei, A., and Munafò, A., 2018. "Estimation filtering for deep water navigation". *IFAC-PapersOnLine,* ***51***(29), pp. 299–304.

[99] Blok, P. M., van Boheemen, K., van Evert, F. K., IJsselmuiden, J., and Kim, G.-H., 2019. "Robot navigation in orchards with localization based on Particle filter and Kalman filter". *Computers and Electronics in Agriculture,* ***157***, feb, pp. 261–269.

[100] Mahato, S., and Chakraborty, A., 2016. "EKF based parameter identification of LTI system from seismic response measurements". *Procedia Engineering,* ***144***, pp. 360–365.

[101] Wang, J., Zhang, J., Wang, Y., Fang, X., and Zhao, Y., 2018. "Nonlinear identification of one – stage spur gearbox based on pseudo – linear neural network". *Neurocomputing,* ***308***, sep, pp. 75–86.

[102] Davis, A. F., and Fabien, B. C., 2018. "Systematic identification of drag coefficients for a heaving wave follower". *Ocean Engineering,* ***168***, nov, pp. 1–11.

[103] Shariati, H., Moosavi, H., and Danesh, M., 2019. "Application of particle filter combined with extended kalman filter in model identification of an autonomous underwater vehicle based on experimental data". *Applied Ocean Research,* ***82***, jan, pp. 32–40.

[104] Daosud, W., Hussain, M. A., and Kittisupakorn, P., 2017. "EKF-NN based hybrid estimator for ethylene polymerization process". In *Computer Aided Chemical Engineering*. Elsevier, pp. 1459–1464.

[105] Krämer, D., and King, R., 2017. "A hybrid approach for bioprocess state estimation using NIR spectroscopy and a sigma-point kalman filter". *Journal of Process Control*, nov.

[106] Markana, A., Padhiyar, N., and Moudgalya, K., 2018. "Multi-criterion control of a bioprocess in fed-batch reactor using EKF based economic model predictive control". *Chemical Engineering Research and Design,* ***136***, aug, pp. 282–294.

[107] Höckerdal, E., Frisk, E., and Eriksson, L., 2010. "Model based engine map adaptation using EKF". *IFAC Proceedings Volumes,* ***43***(7), jul, pp. 697–702.

[108] Höckerdal, E., Frisk, E., and Eriksson, L., 2011. "EKF-based adaptation of look-up tables with an air mass-flow sensor application". *Control Engineering Practice,* ***19***(5), may, pp. 442–453.

[109] Valiente, D., Gil, A., Fernández, L., and Reinoso, Ó., 2014. "A comparison of EKF and SGD applied to a view-based SLAM approach with omnidirectional images". *Robotics and Autonomous Systems,* ***62***(2), feb, pp. 108–119.

[110] Modalavalasa, N., Rao, G. S. B., Prasad, K. S., Ganesh, L., and Kumar, M., 2015. "A new method of target tracking by EKF using bearing and elevation measurements for underwater environment". *Robotics and Autonomous Systems,* ***74***, dec, pp. 221–228.

[111] D'Alfonso, L., Lucia, W., Muraca, P., and Pugliese, P., 2015. "Mobile robot localization via EKF and UKF: A comparison based on real data". *Robotics and Autonomous Systems,* ***74***, dec, pp. 122–127.

[112] Bouaziz, M., Rachedi, A., and Belghith, A., 2017. "EKF-MRPL: Advanced mobility support routing protocol for internet of mobile things: Movement prediction approach". *Future Generation Computer Systems*, dec.

[113] Yu, F., Mao, Z., Yuan, P., He, D., and Jia, M., 2017. "Recursive parameter estimation for hammerstein-wiener systems using modified EKF algorithm". *ISA Transactions,* ***70***, sep, pp. 104–115.

[114] Lin, C., Gong, X., Xiong, R., and Cheng, X., 2017. "A novel h ∞ and EKF joint estimation method for determining the center of gravity position of electric

vehicles". *Applied Energy,* ***194***, may, pp. 609–616.

[115] Xile, D., Caiping, Z., and Jiuchun, J., 2018. "Evaluation of SOC estimation method based on EKF/AEKF under noise interference". *Energy Procedia,* ***152***, oct, pp. 520–525.

[116] Johansen, T. A., and Fossen, T. I., 2016. "The eXogenous kalman filter (XKF)". *International Journal of Control,* ***90***(2), apr, pp. 161–167.

[117] Kalman, R. E., and Bucy, R. S., 1961. "New results in linear filtering and prediction theory". *Journal of Basic Engineering,* ***83***(1), p. 95.

[118] Popescu, O., Rose, C., and Popescu, D. C., 2004. "Maximizing the determinant for a special class of block-partitioned matrices". *Mathematical Problems in Engineering*, pp. 49–61.

[119] MathWorks, T., 2019. Global Optimization Toolbox: Genetic Algorithm.